HIGHWAY RESEARCH RECORD

Number 362 | Pavement Systems
10 Reports

Subject Areas

25 Pavement Design
26 Pavement Performance
62 Foundations (Soils)
63 Mechanics (Earth Mass)

HIGHWAY RESEARCH BOARD
DIVISION OF ENGINEERING NATIONAL RESEARCH COUNCIL
NATIONAL ACADEMY OF SCIENCES—NATIONAL ACADEMY OF ENGINEERING
Washington, D.C. 1971

ISBN 0-309-01976-1

Price: $3.80

Available from

Highway Research Board
National Academy of Sciences
2101 Constitution Avenue
Washington, D.C. 20418

SPONSORSHIP OF THIS RECORD

GROUP 2—DESIGN AND CONSTRUCTION OF TRANSPORTATION FACILITIES
John L. Beaton, California Division of Highways, Sacramento, chairman

Committee on Rigid Pavement Design
B. F. McCullough, Department of Civil Engineering, University of Texas at Austin, chairman
Henry Aaron, Kenneth J. Boedecker, Phillip P. Brown, John E. Burke, B. E. Colley, Donald K. Emery, Jr., Wallace J. Liddle, Phillip L. Melville, Lionel T. Murray, L. Frank Pace, Robert G. Packard, Thomas J. Pasko, Jr., Frank H. Scrivner, M. D. Shelby, Don L. Spellman, W. T. Spencer, T. C. Paul Teng, William Van Breemen

Committee on Flexible Pavement Design
Stuart Williams, Federal Highway Administration, U.S. Department of Transportation, chairman
John A. Bishop, W. H. Campen, Robert A. Crawford, James M. Desmond, W. B. Drake, Charles R. Foster, John M. Giffith, Frank B. Hennion, John W. Hewett, William S. Housel, Roger V. LeClerc, Wallace J. Liddle, R. E. Livingston, Alfred W. Maner, Chester McDowell, Carl L. Monismith, William M. Moore, Frank P. Nichols, Jr., Donald R. Schwartz, George B. Sherman, Eugene L. Skok, Jr., Richard L. Stewart, B. A. Vallerga, Anwar E. Z. Wissa

Committee on Surface Properties—Vehicle Interaction
W. E. Meyer, Transportation Center, Pennsylvania State University, University Park, chairman
M. D. Armstrong, Glenn G. Balmer, F. Cecil Brenner, A. D. Brickman, W. F. R. Briscoe, William C. Burnett, A. Y. Casanova III, Blaine R. Englund, William Gartner, Jr., Ralph C. G. Haas, Douglas I. Hanson, Robert N. Janeway, David C. Mahone, B. F. McCullough, Robert B. McGough, Paul Milliman, A. B. Moore, Desmond F. Moore, E. W. Myers, F. William Petring, Bayard E. Quinn, John J. Quinn, F. A. Renninger, Rolands L. Rizenbergs, Hollis B. Rushing, Richard K. Shaffer, Elson B. Spangler, W. E. Teske, M. Lee Webster, Ross G. Wilcox, Dillard D. Woodson

Committee on Pavement Condition Evaluation
Karl H. Dunn, Wisconsin Department of Transportation, Madison, chairman
Frederick E. Behn, W. B. Drake, Malcolm D. Graham, Leroy D. Graves, Ralph C. G. Haas, William S. Housel, W. Ronald Hudson, C. S. Huges, III, James W. Lyon, Jr., Alfred W. Maner, Phillip L. Melville, Alfred B. Moe, Bayard E. Quinn, G. Y. Sebastyan, Foster A. Smiley, Elson B. Spangler, Bertram D. Tallamy, W. E. Teske, Allan P. Whittemore, Eldon J. Yoder

Committee on Theory of Pavment Design
W. Ronald Hudson, Department of Civil Engineering, University of Texas at Austin, chairman
Richard G. Ahlvin, Ernest J. Barenberg, Richard D. Barksdale, Santiago Corro Caballero, Roberto Sosa Garrido, Eugene Y. Huang, William J. Kenis, Sr., Fred Moavenzadeh, Carl L. Monismith, Thomas D. Moreland, Robert G. Packard, William H. Perloff, Robert L. Schiffman, G. Y. Sebastyan, James F. Shook, Aleksandar S. Vesic, Ernest B. Wilkins, Mike Womack, Nai C. Yang

L. F. Spaine, Highway Research Board staff

The sponsoring committee is identified by a footnote on the first page of each report.

FOREWORD

The development of a truly optimal system of pavement design is an evolutionary, block-at-a-time construction process. Some contributions toward the developmental process are farsighted to the degree that they are mainly useful in the support of further research effort; others are immediately useful to the practicing engineer. This RECORD contains reports of contributions of both types. Researchers and theoreticians in the field of pavement design will be the principal beneficiaries of certain of the reports; pavement designers seeking immediate opportunities to improve their design processes will benefit from others.

Within the context of a systematic analysis of highway pavement systems, the concept of reliability as a design quantity is presented by Lemer and Moavenzadeh. Reliability is defined as a measure of the probability that a pavement will provide satisfactory service to the user throughout its design life. A mathematical statement of reliability is discussed, and some methods of application are suggested. In particular, Monte Carlo simulation and Markov models are presented as examples of useful methods.

Kher, Hudson, and McCullough present a conceptual rigid pavement system that formalizes into a series of mathematical models the many variables that must be considered in rigid pavement design. A computer program that solves the various models required to analyze the problem is discussed. The optimum solution is selected based on minimum cost from among the solutions obtained. The program utilizes 115 input variables. Output includes not only thickness design but also type of subbase material, jointing systems, and pavement reinforcement. A maintenance program and service life are also predicted for the selected design.

McCullough presents a summary of research on rigid pavement terminal anchorage installations conducted by the Texas Highway Department during a 3½-year period. A total of 152 anchorage systems on jointed concrete pavement and 186 units on continuously reinforced concrete pavement were included in the analysis. An empirical equation expressing movement in terms of pavement length, temperature change, pavement grades, subgrade coefficient, and number of lugs is presented. McCullough believes that this equation, considering the boundary conditions, could be used as a design equation. An experimental installation in connection with this project has shown the feasibility of connecting the terminal of a continuous pavement directly to a bridge structure.

The paper by Ghosh, Lal, and Vijagaraghaven presents the results of theoretical and experimental studies to determine the additional dynamic deflection of a rigid pavement resulting from the movement of a wheel load over a low spot in the corner region of the slab. The authors account for geometry of the low spot, load velocity, and elastic reaction modulus of the slab depending on support conditions. Graphs and formulas are presented to permit easy determination of the additional deflection. Good correlation is reported between theoretically and experimentally determined values.

Vaswani undertook to determine whether the properties of the deflected basins that occur in Dynaflect and Benkelman beam measurements make it possible to evaluate the subgrade and its overlying pavement separately. He reports on a theoretical analysis that he considers to show that the basin properties are a function of the modulus of elasticity of the subgrade, the average modulus of elasticity of the pavement over the sub-

grade, and the thickness index of the overlying pavement. A general chart that correlates maximum deflection and spreadability with the subgrade strength, the average pavement strength, and the thickness index of the pavement was developed based on the findings. Field test results are reported to have been encouraging.

Pretorius and Monismith report on an attempt to form an analytical procedure for predicting shrinkage stresses and cracking in pavements containing soil-cement bases. The approach utilizes the creep characteristics of all of the materials in the pavement structure together with the shrinkage and strength characteristics of the soil-cement in an incremental axisymmetric finite-element solution. An example is presented to illustrate the procedure. The authors consider the results to indicate that crack spacing can be approximated in a pavement containing a soil-cement base, provided that the actual distribution of shrinkage strains in the pavement is shown. A hope is expressed that others will apply this approach, or a similar approach, to other types of soil-cement mixes for comparisons.

A number of thickness design methods make use of traffic analysis procedures based on equivalent 18-kip single-axle load applications. Shook and Lepp, using results of truck weight and loadometer data from 47 states, found that equivalent 18-kip load applications correlate well with the number of heavy trucks but that the correlation coefficients vary considerably among states. In a similar study using only ADT, they found that considerable variation exists among states and highway class within a given state. The most useful relationship, and the highest correlation of all those investigated, was found among 18-kip load applications, legal axle load limit, average heavy truck weight, and number of heavy trucks.

A report of an investigation by Hammitt concerning the development of a structural design procedure for unsurfaced roadway shoulders, roads, and airfields is offered in abridged form. Data from 78 full-scale tests conducted by the U.S. Army Engineer Waterways Experiment Station were used in a multiple regression analysis that led to prediction equations that the author considers to be usable in design where soil is used as a surfacing layer.

The paper by Darlington describes an evaluation of the General Motors surface dynamics road profilometer by the Michigan Department of State Highways. The power spectral density approach is concluded to be of most interest for highway work. The profilometer was found not to return a survey type of elevation profile because long-wave features must be filtered out. For this reason, profiles furnished by the device must be viewed as correct in the frequency domain but incorrect in the spatial domain. The author suggests that an inertial guidance system capable of recording long-wave features could solve the problem.

The paper by Walker and Hudson describes an investigation of some practical uses of power spectral and coherence analyses of data obtained from the surface dynamics road profilometer. A brief description of spectral and coherent analyses is provided, and some practical examples of their use are given. The first application concerns an inexpensive replacement road-following wheel for the standard wheel that comes with the profilometer. The second example involves construction control and identification of differences between 2 methods for laying asphaltic base materials. The methods appear to be practical uses of spectral techniques that theretofore have been elusive. The authors believe that extensions may provide the best approach yet available to adequate road profile specifications and construction control.

—John E. Burke

CONTENTS

RELIABILITY OF HIGHWAY PAVEMENTS

A. C. Lemer and F. Moavenzadeh, Department of Civil Engineering,
Massachusetts Institute of Technology

In a context of systematic analysis of highway pavement systems, the concept of reliability as a design quantity is presented. Reliability is a measure of the probability that a pavement will provide satisfactory service to the user throughout its design service life. The prediction of reliability and its use in providing economically efficient pavements requires consideration of all aspects of service life. A mathematical statement of reliability is discussed for its meaning to pavement design and management, and some methods of application are suggested to demonstrate reliability computation as an operable and useful technique. In particular, Monte Carlo simulation and Markov models are used as examples of useful methods to be applied.

•A PROPERLY designed highway pavement should exhibit satisfactory performance throughout its design service life. Satisfactory performance is defined by the requirements of the transportation system of which the pavement is a part and must be achieved subject to constraints on scarce resources.

In its simplest and, historically speaking, its earliest form, performance was understood primarily as a pavement's ability to support a particular load without showing excessive deflection or cracking. Many current design procedures still use this criterion as a basis. More recently, however, work such as that done by AASHO (1) and the Canadian Good Roads Association (2) has recognized that riding qualities and users' comfort and safety are important in performance evaluation.

Performance may be expressed in terms of 3 principal measures (3) of effectiveness: serviceability, reliability, and maintainability. Serviceability is a measure of the degree to which the pavement provides satisfactory service to the user. Here the term "user" is understood to include not only the direct highway user but also the broad range of recipients of transport benefits. Reliability is a measure of the probability that serviceability will be at an adequate level throughout the design service life. The future behavior of an engineering system is essentially uncertain. Maintainability is a measure of the degree to which effort may be required during the service life to keep serviceability at a satisfactory level. There are 2 aspects of maintenance: normal maintenance, including the regularly scheduled actions directed toward prevention of failure, and repair maintenance, including the actions required to restore adequate serviceability given that a serious loss has occurred or may soon do so.

Reliability is important in the pavement system because of the uncertainty involved in all aspects of the pavement process: planning, design, construction, operation, and maintenance. Uncertainty arises from lack of information and inability to predict the future. It is embodied in the assumptions that must be made to derive analytical models, the limited amount of data available from tests, and the variable quality of the real-world environment (Fig. 1). An unusually heavy rainstorm or a poorly mixed batch of concrete can upset all of the careful planning that went into a pavement.

Traditionally, the uncertainty of prediction of the future behavior of constructed facilities is accounted for by including safety factors in designs. The effectiveness of these safety factors varies with the degree of variation of the parameters they modify.

Sponsored by Committee on Theory of Pavement Design and presented at the 50th Annual Meeting.

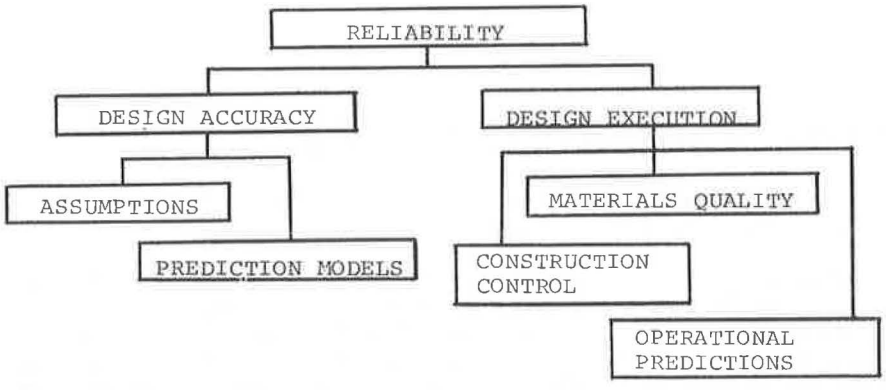

Figure 1. Components of reliability.

The use of higher safety factors when one is less certain (or when the consequences of loss are greater) is an implicit recognition of this fact. In many cases, however, there can be substantial overdesign and misallocation of resources because of safety factors too large for the actual uncertainties involved.

For example, if one is designing concrete and uses a safety factor of 1.2 to obtain 1,000 psi strength (i.e., design a mix with 1,200 psi mean strength), the assumption of a normal distribution of strength will indicate a 5 percent chance that strength will be below 1,000 psi if the coefficient of variation is 10 percent. If the coefficient of variation is 20 percent, the chance of strength being less than 1,000 psi is roughly 20 percent; whereas if the coefficient of variation is only 5 percent, the chances fall to less than 1 percent.

Obviously then, factors that affect the degree of variation in system parameters have a significant effect on reliability. Quality control in construction is a notable case in point. Beyond construction, there are uncertainties of operation and maintenance that are rather removed from the designer's consideration.

Very little attempt is generally made to evaluate and account for the uncertainties of service behavior. More important is the failure to recognize that these uncertainties are of serious consequences for future resources needs. Premature failure may cause the allowances for future service growth to be inadequate.

It would seem logical that adequate performance could best be provided by consideration of the pavement's characteristics throughout its design life. Both the trends of serviceability, as is currently the case, and the pavement's reliability must be predicted. A level of maintainability may be set such that satisfactory service is provided with a high degree of reliability and in an economically efficient manner.

This paper will discuss reliability as a design parameter and will show through an example how this parameter may be used to evaluate the uncertainties in pavement systems. A framework for analysis will first be presented, and techniques for implementing analysis within the framework will be described. The analysis will then be applied to a hypothetical pavement-decision problem to show how reliability considerations will interact with those of economics to influence decision-making.

Reliability Measurement

Reliability is the probability of success or, rather, the probability that the pavement will resist the loads applied to it throughout its design life. To evaluate the pavement's reliability, one must be aware of what the system's possible modes of failure are and, to some extent, how they occur. In general, for each failure mode i, there will be an environmental load D_i placed on the pavement and a capacity R_i of the pavement to resist that load. The loads D_i are determined by a set of environmental qualities (e_1, e_2, ..., e_L). The pavement's response is determined by a set of system characteristics

$(c_1, c_2, \ldots, c_M)$. Then, if there are N possible failure modes, failure is the condition in which one or more of the following inequalities is not satisfied:

$$D_1(e_1, e_2, \ldots, e_L) \leq R_1(c_1, c_2, \ldots, c_M)$$
$$D_2(e_1, \ldots, e_L) \leq R_2(c_1, \ldots, c_M)$$
$$\vdots \qquad\qquad \vdots$$
$$D_N(e_1, \ldots, e_L) \leq R_N(c_1, \ldots, c_M)$$

That is, if the demand on the system exceeds the ability of the system to resist that mode of failure, such failure will occur.

For example, a highway pavement might fail through loss of safety or through substantial structural failure (loss of structural integrity). Loss of safety would perhaps be described in terms of skid resistance through statistical correlations with observed accidents. Structural failure might mean loss of subgrade support. There would then be 2 failure modes. The pertinent environmental qualities, e_L, might include a number of loadings, temperature, and vehicle speeds. System capabilities, c_M, would include material strengths, subgrade modulus, and surface-course aggregate qualities.

For each failure mode, a model—theoretical or empirical or some combination thereof—is needed to determine how this failure would occur, i.e., how the pavement behaves under load. Theories of stress distribution in pavement systems are examples of such models for deformation, as are the equations produced by the AASHO Road Test for subjective evaluations of ride. That is, these models give a functional relationship between service loads and a parameter that is important to service quality, which is in these cases service deflection or riding quality. It is then possible to describe failure in terms of some maximum or minimum acceptable value of the parameter, which in turn defines the service load that is most likely to result in that value.

The application of these models (which may be uncertain) to data on the system environment characteristics that are probabilistic (and which are uncertain) permit the calculation of the reliability R, which is the probability that all of the previous inequalities are true. Thus, $R = P \text{ (no failure)} = P(D_i \leq R_i)$, where $i = 1, \ldots, N$.

A major task is then to analyze the probabilities that individual failure modes will occur and then to combine these failure modes to compute reliability. It is difficult to attain the initial estimates of failure probabilities because of the complexity of the physical processes involved. It is often impossible to arrive at closed-form mathematical statements of the probabilities involved, and so simulation methods become the only feasible approach.

In simulation techniques (particularly the Monte Carlo method), input data are supplied in probabilistic form. These data often consist of statistical information gathered by experimentation. The computerized description of the behavior model is used to compute many samples to build up a statistical description of output. For example, if the model of interest is the standard elastic stress-strain relationship $\epsilon = \sigma/E'$ where E is an experimentally measured random variable, the probability distribution of E is sampled many times, and a corresponding value of ϵ is computed for each (with constant σ). This procedure gives an estimation of the probability distribution of ϵ as a function of E. In complex situations, this simulation method is the only way of obtaining this probabilistic estimate of output.

TIME EFFECTS AND SERVICE LIFE

Reliability will generally be a time-dependent parameter; an obvious example is the failure of a material through fatigue. The events that lead up to the occurrence of a failure are distributed over a period of time. It is often possible to observe certain facility features that imply a deteriorating quality. For example, fine cracks in a rigid pavement may cause no loss in riding quality, but they do warn that water will have access to base materials. That is, pumping and loss of subgrade support are strong possibilities in the near future.

Realistically, then, reliability will be computed by using stochastic models of a facility's service behavior. Stochastic models are generally time-dependent probabilistic representations of physical processes. A facility may be viewed as having a number of possible serviceability states or conditions that it may occupy. Age, use, and renovation are then represented as transitions between states. The previously described models of how failure modes occur are useful for computing the probabilities of particular interstate transitions (Fig. 2).

One particular type of stochastic model that shows promise for use in analyzing pavement behavior is the Markov process. The special feature of the Markov process is that the future state of the process is dependent only on the current state. That is, predictions of the probability that the process will be in any particular state at some future time may be based on observation of the current state. The model has no memory of its past history. If $\rho(n)$ is the probability vector describing the probabilities that the process is in any one of the several possible states at time n, and if $\underset{\sim}{P}$ is the matrix of 1-step transition probabilities, then

$$\rho(n + 1) = \rho(n)\underset{\sim}{P}$$

Because of the lack of memory, it may be shown through regressive application of this formula that

$$\rho(n) = \rho_0 P^n$$

where ρ_0 is the initial state probability vector. These simple statements describe a Markov process.

For the simple Markov process, the $\underset{\sim}{P}$ matrix is constant. A continuous time process is produced when time-varying functions are introduced into the matrix elements. This modification is often a more accurate, but usually a more difficult to compute, representation of physical behavior.

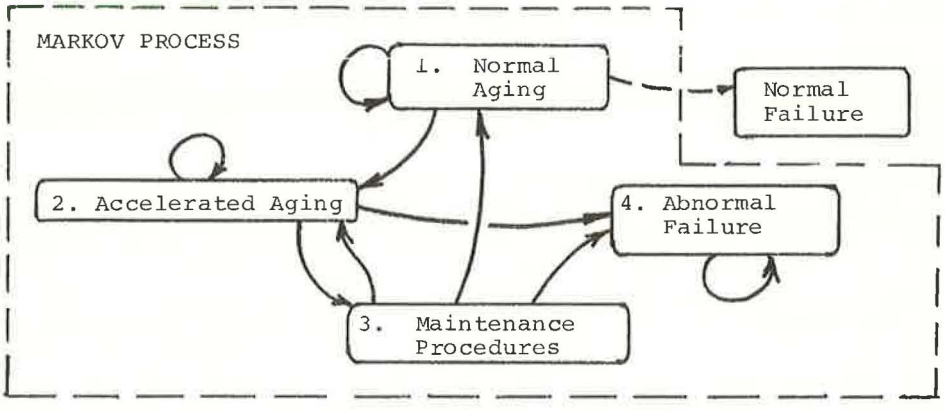

Transition Matrix

$$\begin{bmatrix} p_{11} & p_{12} & 0 & 0 \\ 0 & p_{22} & p_{23} & p_{24} \\ p_{31} & p_{32} & 0 & p_{34} \\ 0 & 0 & 0 & p_{44} \end{bmatrix}$$

Figure 2. Use of Markov process to analyze changes during pavement service life.

One difficulty is the lack of memory in a simple Markov process. Future predictions depend only on the present. An appropriate counter example in the field of pavements is the memory effect in viscoelastic materials. This feature must be kept in mind when such a model is used.

In spite of this difficulty, there are 2 primary justifications for using a Markov process to analyze pavement reliability and service life behavior. First, for the periods of time considered by the analyst for planning and design, the Markov process may provide reasonable models of pavement behavior. That is, any memory the facility might have of how it reached its present state will often have faded by the time a measurably new state is predicted. Second, in a context of statistical decision theory, a Markov process may serve as a first estimate that is to be modified as more data become available. With this point of view, the Markov model may serve to test initial operation and maintenance policies and check how they interact with design.

To use a Markov model, one must first describe the service behavior of the facility in terms of states and possibly interstate transitions, then estimate the values of probabilities in the P matrix, and with this information present the entire process in the transition matrix (Fig. 2).

APPLICATIONS

The applicability of reliability analysis and of Monte Carlo and Markov simulation models in this analysis may best be illustrated by an example. For this example, a pavement for a low-volume highway is considered. Two pavement sections were designed for the expected traffic and are shown in Figure 3. The asphalt and concrete

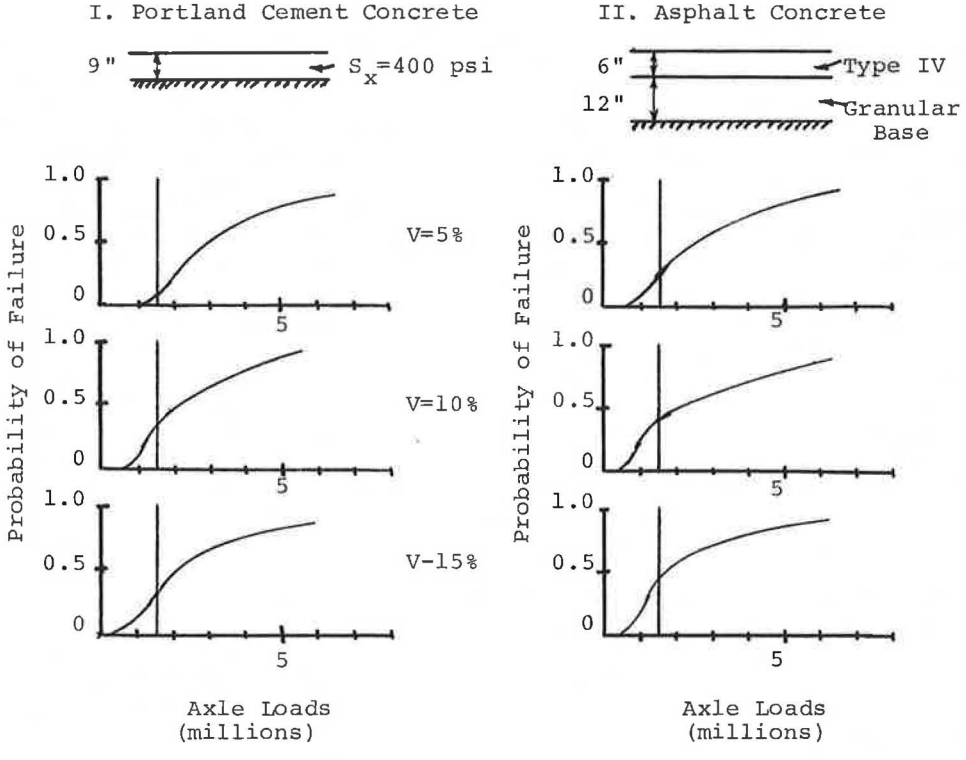

Figure 3. Design alternatives: initial daily traffic, 200 VPD (equivalent 18-kip loads); traffic growth rate, 4 percent per year; design life, 15 years; soil (subgrade) - CBR = 3, k = 100 pci.

sections were designed according to The Asphalt Institute (4) and extended AASHO (5) formulas respectively. Soil conditions and traffic predictions (in this case, total number of loads) were taken as external constraints not subject to change.

It has been suggested (3) that serviceability for highway pavement is measured by 3 components—rideability, safety, and structural integrity. Rideability applies to the quality of ride experienced by people and goods traveling the road and is analogous to the original AASHO serviceability concept. Safety applies to the likelihood of accidents and is related to skidding and to road hazards. Structural integrity describes gross load-bearing characteristics of the pavement.

Failure could then occur through loss of any one or more of these qualities. That is, the pavement could become rough and bumpy, causing the user dissatisfaction with riding qualities; the pavement could become slippery or develop large potholes; or, finally, large-scale subsidence or large deformations under a heavy vehicle might occur.

The statement of failure modes for reliability computation would then have 3 basic inequalities. Failure in the first of these, which is adequate rideability, is assumed to be due solely to the cumulative effects of axle-load repetitions and is the basis for the designs shown in Figure 3. This mode will be referred to as normal failure because, according to the design assumptions, this mode is the only one that may occur.

The distribution of probability of normal failure as a function of axle load repetitions was found for each of the pavements and for a variety of assumptions regarding construction quality control by using Monte Carlo simulation of the design equations. Where the initial designs were developed by using fixed expected values of the pertinent parameters such as strength, these parameters were now input as probability distributions. Quality control was characterized by the coefficients of variation of the materials strength parameters. Examples of distributions so derived are shown in Figure 3.

It is interesting to note that decreased construction control may lead to higher mean values of loads to failure. This is because the looser control leads to more spread in the strength distributions, which leads in turn to higher probabilities of very high values of strength as well as low values of strength. Thus, the mean value of the computed factor may rise, but the overall distribution spreads out considerably and reliability falls. In the analysis, losses of safety and of structural integrity are considered, in this case, to be abnormal failures. Because something may happen during the life of the pavement to cause such failures, they must be considered in analysis. Based on such considerations, the service life of the pavement in this example might be partially modeled by a 4-state Markov process. This model is partial because it is linked with a normal failure model for rideability losses (Fig. 2).

Four states will be used in the Markov model. Normal aging (1) is the condition that leads to normal failure. Load applications cause slow and steady deterioration of rideability. Accelerated aging (2) is a state caused, for example, by the initiation of cracking or surface polishing. Such conditions will represent accelerated losses of serviceability because they could precede losses of structural integrity or safety respectively. Maintenance procedures (3) will be initiated when the accelerated aging conditions are detected and can be successful by returning the pavement to normal aging. Abnormal failure (4) will eventually occur if maintenance efforts fail or are never undertaken. Design decisions determine the probabilities of aging and maintenance activities.

The probability matrices for the Markov process must now be formulated. That is, transition probabilities must be assigned to the arrows shown in Figure 3. Table 1 gives several alternative plans that might be considered. It should be noted that terms such as "high maintenance" in the plan descriptions signify greater maintenance activity and, thus, higher probability of going from the accelerated aging state to the maintenance state.

The probabilities are postulated for 6-month computation periods. That is, each probability refers to the state in which the process might be in 6 months, given knowledge of the present state. The normal failure distributions refer to a 15-year design life, so probabilities in the Markov "subprocess" must be computed for 30 transitions. The reliability values given in Table 2 were computed as the probability that neither normal nor abnormal failure states occur in the 15-year design service life.

TABLE 1

OPERATING AND MAINTENANCE POLICIES AS A MARKOV SUBMODEL

Policy No.	Policy Description	P-Matrix
I	Standard operating policies	$P_I = \begin{Vmatrix} 0.95 & 0.05 & 0 & 0 \\ 0 & 0.40 & 0.20 & 0.40 \\ 0.60 & 0.30 & 0 & 0.10 \\ 0 & 0 & 0 & 1 \end{Vmatrix}$
II	High maintenance activity, standard quality	$P_{II} = \begin{Vmatrix} 0.95 & 0.05 & 0 & 0 \\ 0 & 0.40 & 0.50 & 0.10 \\ 0.60 & 0.30 & 0 & 0.10 \\ 0 & 0 & 0 & 1 \end{Vmatrix}$
III	Standard maintenance activity, high quality	$P_{III} = \begin{Vmatrix} 0.95 & 0.05 & 0 & 0 \\ 0 & 0.40 & 0.20 & 0.40 \\ 0.80 & 0.10 & 0 & 0.10 \\ 0 & 0 & 0 & 1 \end{Vmatrix}$
IV	High maintenance activity, high quality	$P_{IV} = \begin{Vmatrix} 0.95 & 0.05 & 0 & 0 \\ 0 & 0.40 & 0.50 & 0.10 \\ 0.80 & 0.10 & 0 & 0.10 \\ 0 & 0 & 0 & 1 \end{Vmatrix}$

The reliability calculations give the probabilities of no failure in a 15-year design period. It should be pointed out that the differences in reliability between concrete and asphalt pavements are due more to the form of the equations used than to any other factor. Fewer variables in the equation lead to greater effect of variations in each variable on the final result. Hence, quantitative measurements are most valid within a single design type. Only relative evaluations may be made between different designs.

An alternative type of information one might want would be a description of possible failure age. Because the failure depends on traffic volume, failure age will depend on the growth rate of traffic. Figure 4 shows these data for the concrete pavement and standard operating conditions. Data such as these would be useful in the planning stage for making construction staging and financing decisions. An attempt could be made to choose an optimal design life, based on possible traffic growth and costs of service.

TABLE 2

RELIABILITY VALUES

Design Type	Construction Quality (percent)	Operating Policy	Reliability
Asphalt	15	I	0.24
		II	0.46
		III	0.25
		IV	0.48
	10	I	0.25
		II	0.48
		III	0.26
		IV	0.50
	5	I	0.30
		II	0.57
		III	0.31
		IV	0.60
Concrete	15	I	0.31
		II	0.61
		III	0.33
		IV	0.64
	10	I	0.34
		II	0.66
		III	0.36
		IV	0.70
	5	I	0.35
		II	0.67
		III	0.37
		IV	0.71

The standard way these results would be used is with respect to cost data. A balance between cost and reliability would be struck to achieve a good design. For example, similar results in this case, not of similar magnitude but of improved reliability, are obtained for the concrete pavement by improving maintenance with constant quality control or by improving quality control with constant maintenance activity. The former alternative would require higher initial outlay of funds, whereas the latter would represent deferred outlays. In terms of net costs and timing, it is likely that one of these 2 alternatives would be preferred, given that the increased reliability is desirable.

By taking another point of view, one might decide that the greater expected lifetime of a concrete pavement with reliability equal to that of a comparable asphalt pavement might justify an increased construction cost. On the other hand, lower expected

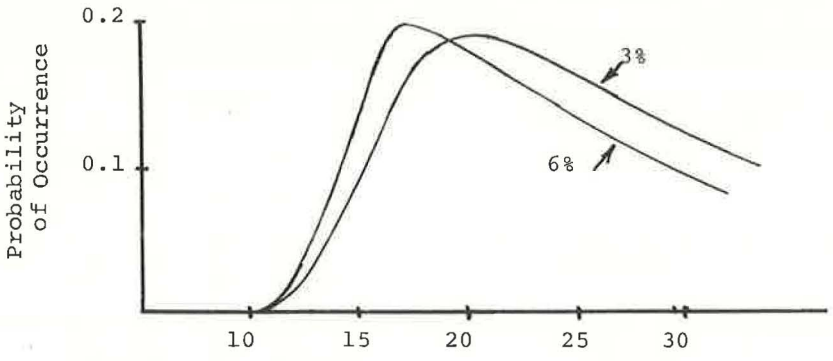

Figure 4. Distribution of failure age as a function of traffic growth rate.

life might be preferred as a means of obtaining flexibility in an urban system.

SUMMARY AND CONCLUSIONS

The previous discussion illustrates how the concept of reliability may be used in pavement analysis and decision to account for uncertainty. It is felt that the traditional use of safety factors is inadequate on 2 counts. First, the safety factor has no clear relation to the true uncertainty in the system. The use, for example, of a single standard load factor on all Interstate roads makes no allowance for the fact that traffic growth patterns could differ substantially with patterns of regional economical development. Second, safety factors that represent overdesign are wasteful of economic resources and can be a cause of loss to society just as premature failure would be.

The use of reliability is a practical means of overcoming these 2 inadequacies. Techniques such as Monte Carlo simulation and Markov modeling are suggested to demonstrate how one might implement reliability analysis. In a context of systematic analysis of highway pavements, reliability is an important factor.

ACKNOWLEDGMENT

The computational work that forms the basis for the example in this paper was performed at the M. I. T. Information Processing Center on an IBM 360-65 system. The work was supported by a grant from the Sloan Fund for Basic Research.

REFERENCES

1. The AASHO Road Test: Report 5—Pavement Research. HRB Spec. Rept. 61E, 1962.
2. Canadian Good Roads Association. Pavement Evaluation Studies in Canada. Internat. Conf. on the Structural Design of Asphalt Pavements, Ann Arbor, 1962.
3. Lemer, A. C., and Moavenzadeh, F. The Analysis of Highway Pavement Systems. Dept. of Civil Eng., M. I. T., Cambridge, Mass., Prof. Paper P69-12, 1969.
4. Maner, A. W. Progress in Asphalt Pavement Thickness Design. Civil Engineering, March 1970, pp. 39-42.
5. Hudson, W. R., and McCullough, B. F. An Extension of Rigid Pavement Design Methods. Highway Research Record 60, 1964, pp. 1-14.

COMPREHENSIVE SYSTEMS ANALYSIS FOR RIGID PAVEMENTS

Ramesh K. Kher, W. Ronald Hudson, and B. Frank McCullough,
Center for Highway Research, University of Texas at Austin

Design of portland cement concrete pavements is a complex soil-structure interaction problem involving evaluation and analysis of numerous variables. Many of these variables within the broad categories of loads, environments, material properties, structural maintenance, progressive failure, and economics must be considered in an ideal design procedure. Concrete pavement and overlay types, reinforcement selection, joint detailing, and selection of subbase materials are other factors increasing the complexity of design. Various methods of design have been presented in the past, but no procedure is accepted in general because of the limited nature of problem analysis. The complexity of the problem demands that a procedure be evolved for analyzing various parts and assembling them in a coordinated effort called systems analysis. A conceptual rigid pavement system is presented that formalizes the myriad of interrelated variables into a series of mathematical models. A method is developed in the form of a computer program to solve the various models, some of which are developed as part of this work and others of which are adopted from the state of the art. The program utilizes over 100 input variables and analyzes numerous possible solutions generated within the boundaries defined by the constraints. The output is a set of pavement design strategies based on present worth of overall costs. Details with respect to selection of thickness, materials, reinforcement, and joints, as well as overlay patterns and predicted life, are presented for each design.

•THE ANALYSIS of rigid pavements (1, 2) has previously centered around concrete stress, which is a principal indicator of failure by the distress mechanism of cracking in the slab. In turn, concrete pavement thickness has been determined by a single criterion; that is, the attempt to avoid the formation of such cracks by holding the level of stress below a specified allowable value. The basic model in such analyses has been the theory of elasticity with various assumptions to present the concepts in simple and usable forms.

Empiricism has been used to analyze and design for special cases and to modify theory. Since the early 1900's, many empirical and semi-empirical formulas of rigid pavement design have been used (3). The empirical nature of the methods has been due in part to the limited knowledge of material behavior and failure mechanisms and in part to limitations of analytical techniques.

From time to time, the knowledge of material behavior and failure mechanisms has been extended by theoretical analysis and observations on controlled road tests, laboratory experiments, and prototype pavements (4, 5, 6, 7). However, these research efforts have generally been oriented to cover 1 aspect of this specific subject, and there has always been a lack of coordination among various phases of design. As a result, these efforts have not improved the design procedures to a form general enough to be extrapolated for the many design conditions, materials, and environmental factors involved.

Sponsored by Committee on Theory of Pavement Design and presented at the 50th Annual Meeting.

Rigid pavements not only should be designed by the prevalent approach of making them structurally adequate with respect to concrete thickness but also should be analyzed as investments based on economics. The combinations of money and materials should be analyzed by using the concepts of systems analysis to provide optimum resource allocations. Such an approach has been used to formulate a working systems model called Rigid Pavement System 1 (RPS1). Various submodels are combined into an overall computer program. Available research dealing with various parts of the system are used. Certain other models pertinent to a successfully coordinated system are developed by using mathematical and statistical techniques.

The program utilizes various material properties, traffic data, performance variables, stochastic parameters, and cost inputs to analyze a large number of design strategies within the constraints specified. The program output consists of a wide variety of design strategies to choose from.

The objectives of this research are (a) to achieve a complete problem description within a systems framework, (b) to develop a rigid pavement design method using existing knowledge in the best way, and (c) through sensitivity analysis, to point out the areas of urgently needed research after the first 2 objectives are achieved.

SYSTEMS APPROACH

Systems concepts are composed of basic ideas that help to accomplish an operational process in the most efficient manner through organizing an integrated approach rather than a piecemeal synthesis of technological features. Such a piecemeal synthesis has been adopted in the existing design procedures that have, in general, been oriented toward emphasizing certain important features of design and neglecting certain others (8). Figure 1 shows the formulation of the current design procedures in a systems framework.

In these procedures, the load and its volume and intensity have been the main inputs to the system, and the guiding decision criteria of design have been to limit the level of stresses in the corner, edge, or interior of the slab. The design criteria have been refined by successive cycles of designing new pavements and observing the performance

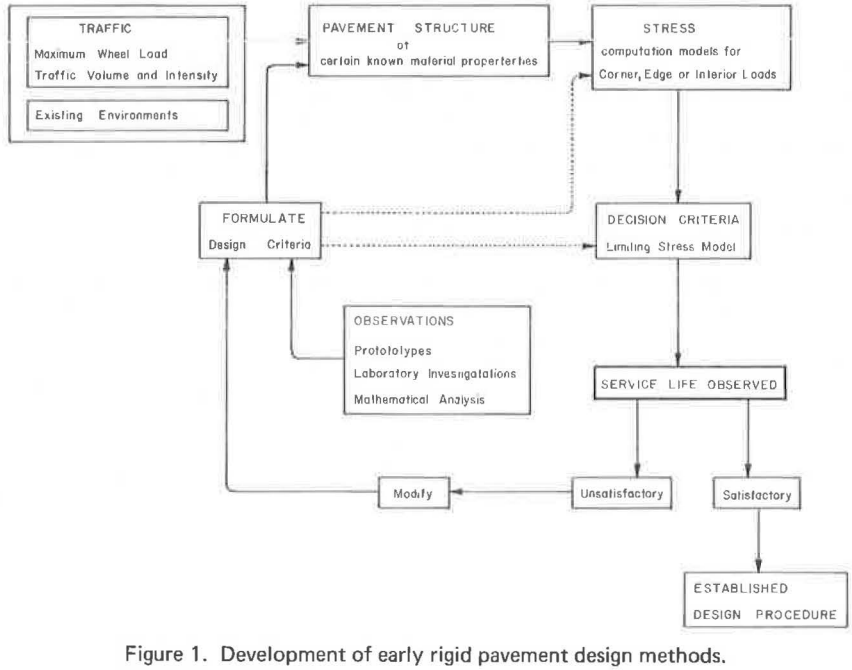

Figure 1. Development of early rigid pavement design methods.

of the designed pavements. Pavements have often been termed satisfactory or unsatisfactory. Satisfactory designs have established those procedures by which they were designed, whereas the designs that performed poorly have added to the knowledge to develop new design criteria. Experimental observations and mathematical analyses have helped in the development of such criteria.

Technological development has enhanced the realization that the specific aspects such as stress analysis or thickness design are not the only criteria for design of rigid pavements. There are various kinds of inputs, responses, and decision criteria to be considered in an ideal design procedure. The other areas of consideration for a rational design procedure are pavement and overlay construction, reinforcement selection, joint detailing, selection of subbase material, stage construction, and, above all, a valid optimization among alternative pavement strategies.

It is, therefore, realized that a good description of the problem, a new insight into the complexity, and an optimization of techniques considering various economic criteria may lead to a rational pavement design procedure. The formulation of such an approach will be achieved through the applications of the concepts of systems engineering.

A system can be described as a device, procedure, or scheme behaving according to some description to accomplish an operational process (9). Thus, rigid pavement can be defined as a system obeying physical laws to transform the effects of input variables into various responses characterized by a wear-out function. Design of such a system needs a coordinated set of procedures to detail the use of money and materials in the most economical combinations. Such a procedure of resource allocation is defined as a system and should be carried out by the application of classical economic concepts.

The coordinated approach called systems analysis, when applied to the design of rigid pavements, offers several advantages. The development of a complete problem description provides new insight and perspective into the complexity of the problem, including the feedbacks and interactions involved. This insight, in turn, provides a structure for coordinating and utilizing research from many sources and rapidly points out the areas of weakness and, consequently, the areas of urgently needed research. A coordinated approach to the problem helps in the understanding and development of those functions and theories that can determine optimal choices of solutions in the face of various judgment criteria and weighting functions. The analysis permits the use of various techniques in optimization and operations research to solve the problem. Finally, in the process of developing an overall optimal solution, immediate benefits are gained by the use of current knowledge in the systems framework until better techniques of analysis are developed. The principles of systems engineering are used to formulate a conceptual rigid pavement design system that is discussed in the following sections.

FORMULATION OF CONCEPTUAL SYSTEM

According to system definition, a comprehensive formulation of the design process characterizing various technical and economic aspects is needed before a more realistic working pavement design system can be formulated for immediate use involving state-of-the-art information. Figure 2 shows many of the factors involved in the conceptual rigid pavement design system.

Physically, the pavement system can be defined as an operator that, when acted on by the excitation functions, converts itself to give responses. The responses are generally characterized immediately by a mechanical state defined by stresses, strains, deflections, and surface properties and eventually by the time-dependent, accumulated effects of these primary responses in the forms of rupture, distortion, disintegration, and decreasing skid resistance.

System Inputs

System excitation variables, often termed as system inputs, have been a matter of a great amount of research with respect to their effects on the system and its responses.

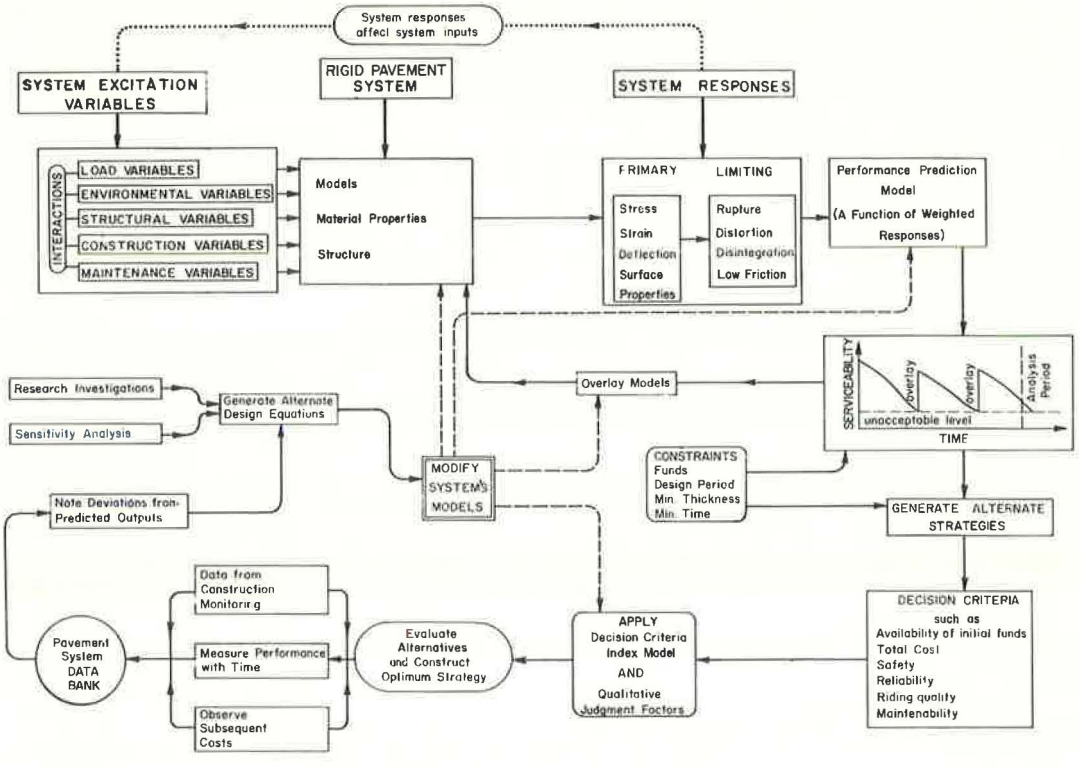

Figure 2. Conceptual rigid pavement design system.

An example in this context includes the various models developed in the past to compute the effects of loads applied on the system. The effect of loads or traffic is to create a certain mechanical state in the pavement. The materials in the system respond to this mechanical state in various ways. Main load effects are due to (a) magnitude; (b) distribution with respect to time, such as frequency, rate, and duration; (c) total accumulated applications; and (d) distribution with respect to placement.

An excessive magnitude of load can produce a well-known distress mode called rupture through overstress, whereas the repeated applications of stress to the pavement materials produce system distortion and rupture through phenomena such as fatigue and creep in concrete and other support materials. Magnitude of load and repeated applications also produce physical disturbances in subbases and subgrades with respect to the macroscopic reorientations of the material structures resulting in densification, distortion, and failure.

Environmental inputs are varied and cyclic. Among them are temperature, moisture, humidity, and rainfall. Temperature variations and their magnitudes, frequencies, and durations cause warping, expansion, and contraction and produce stresses in the pavement structure. Moisture and humidity variations in concrete slabs produce stresses in much the same manner as temperature. Rainfall affects the groundwater conditions that may produce physical results such as pumping and loss of support.

Maintenance is also an external input to the system, but its intended effect, contrary to other inputs, is to increase the life of the system by improving the system responses as well as riding quality.

There is frequent interaction involved among various inputs to the system. Environments, for example, may affect the volume of traffic or the amount of maintenance required, or the presence of moisture may affect the amount and distribution of heat in and beneath the pavement slab.

The System

The physical system is characterized by material properties, material arrangements, amount of materials and the shape given to them, and quality of construction. The system as constructed and especially the material properties generally described by various engineering characteristics are very important parameters of the system. The basic properties of materials are complex physical functions dependent on numerous parameters. The significant basic properties, for engineering purposes, are defined as functions that quantify material responses to one or more external inputs and are necessary to compute responses of the pavement system.

The materials are nonlinear and viscoelastic in nature, and their properties are never constant over time. Inputs such as loads and environments are the main reasons why basic properties of the materials provided in the system change with time. Excessive load and its repeated applications, in addition to producing a mechanical state, change load-deformation characteristics of pavement materials; densification and consolidation of support materials affect their engineering characteristics; thermal and moisture variations in concrete change its properties; moisture variations in subgrade stimulate its swelling characteristics; and traffic changes the skid characteristics of paving materials.

System Responses

Pavement system responses consist of 2 types—primary and limiting. A primary response is defined by the mechanical state of the system, whereas a limiting response is obtained by the progressive effects produced as a result of the repetitive or continued existence of the state of primary response. The limiting response is the actual criterion of failure of pavements.

It may be noted that limiting responses interact with inputs like loads and maintenance. For example, the roughness of a pavement at any time influences the dynamic magnitude of the traffic loads and the maintenance required.

The progressive deterioration of the system caused by its limiting responses is of great importance in the systematic design. Discomfort to the rider is the ultimate measure of pavement deterioration. The vibrations of vehicles moving on a pavement determine this discomfort and are functions of factors such as suspension characteristics of vehicles, vehicle speeds, and pavement roughness (10, 11).

The average of these human responses characterizes the serviceability of a pavement, i.e., the extent to which the traveling public is served. Serviceability and age histories of pavements are very essential to evaluate the cost implications of the system.

Development of mathematical theory to compute an index to evaluate pavement distress will require a comprehensive set of models for input assessment, material behavior, primary and limiting outputs, and, finally, human responses to the motions generated because of these outputs. As an alternate, the AASHO Road Test, in a very simplified version, helped develop a concept to bypass these required models and directly predict the pavement serviceability by correlating the subjective ratings of pavements to their objective characteristics.

Solution Generation and Evaluation

This part of the system involves generation of potential alternative strategies and their evaluation for the selection of the best. A strategy is defined as a set of resource allocations for a design to last the required life, according to specifications laid down. Possible strategies are evaluated for obtaining the optimum by invoking various decision criteria shown in Figure 2. Each decision criterion has to be quantified and weighted to define a function that can be called a decision criteria index. Such a function is another complex formulation in the system. In the past, this function has always been used in its simplest form; i.e., by subjective evaluation of various factors such as riding quality, safety, and availability of funds.

Implementation, Storage, and Feedback

Implementation and feedback are the long-range planned objectives of any management system. A pavement management system involving these fulfills the requirements of a self-sufficient system.

The system models, when continuously synthesized by feedback from various sources, improve the system and its capabilities. The feedbacks consist of analysis of deviations from predicted capabilities, research investigations, and sensitivity analysis of the existing system.

The pavement system data bank is an important part of the feedback subsystem. It consists of, among other things, the performance evaluations of the optimal strategies constructed in the past. Data from construction monitoring, measurements of performance over time, and observations of subsequent expenditures are the important characteristics to be observed from the implemented strategies.

OPERATIONAL RIGID PAVEMENT SYSTEM

A comprehensive formulation of the rigid pavement design process using the integration of technological and economical considerations, as discussed previously, is the ultimate goal and will be achieved through cycles of model formulations, implementations, and feedback. It will involve a large amount of research over a number of years. However, immediate payoffs can be obtained by coordinating the existing state of the art in a meaningful way inside the broader framework of the comprehensive system. Such a systems approach was first presented in 1968 for the design of flexible pavements (12, 13). The same basic approach led to the formulation of an operational rigid pavement system. The development of this working system can be described by the following: objectives, inputs, constraints and options, decision criteria, and output.

Objectives

Much research has been done in the past on various individual models or groups of models defining various parts of the comprehensive system discussed previously. A large payoff can be obtained from this research while the ultimate design system and its models are being developed.

Therefore, it was planned to go through the available research literature, analyze the significant models, and formulate the first version of rigid pavement design system utilizing every model that is available in the existing state of the art and that can be fitted efficiently into the system. Such models, which are important links in the system and for which the research is not available, are mathematically developed.

Inputs

System inputs dictated by various models used in the system consist of about 115 parameters and can be described in the following general groupings.

Performance Variables—These variables define the levels of initial and terminal serviceabilities for an initial or an overlaid structure. Swelling nature of clays is also partially defined by one of the performance variables. These variables are used in system performance models to determine the life of an initial design or the overlaid structure when its serviceability index is allowed to drop from its initial value to a certain level specified as the minimum allowable for the facility under design.

Traffic Volume, Growth, and Distribution Variables—These inputs are used to determine the loads that the pavement will have to carry during its analysis period. They are divided into 2 main parts: (a) initial traffic volume data, and (b) traffic growth with time and distribution over space.

Traffic Delay Variables—This set of variables is used to analyze the economic costs of overlay construction incurred due to the inconvenience of persons delayed in traffic. These costs at times become as significant as any other part contributing to the total cost of the system. The present design system considers such inconvenience by mathematically calculating the costs of traffic delays and operating time losses (13).

Material Properties—These variables are required by various models of the system for analyzing the pavement structures. All properties are utilized, directly or indirectly, for the prediction of the life of an initial design or the overlaid structure. These are generally the engineering properties of the materials and can be determined in a laboratory or in the field, with the exception of some that are theoretically defined. Various properties of the subgrade, subbases, concretes, reinforcements, and overlays are the inputs of the system.

Stochastic Parameters—For the nonhomogeneous materials used in pavements, the material properties change from point to point and are also functions of time and environments. Such variations can be taken into account by using the dispersion data of the laboratory tests conducted to determine these properties. A design value can be found by specifying a certain level of confidence desired for the design with respect to any particular property. The standard deviation determined from the dispersion data of that property will be an input to the system. The present design system uses this concept for 2 important variables of design: (a) flexural strength of concrete, and (b) modulus of subgrade reaction or Texas triaxial class of subgrade.

Cost Inputs—The criterion of total overall cost in terms of present value is used for this working system to indicate the preference of any design over another. The overall cost is the sum of the costs of materials, construction, maintenance, and other operations. A number of cost inputs are, therefore, used by the working system for its evaluation of different design strategies.

For rational economic analysis and decision-making in the case of a public enterprise such as a highway, it is decided that an interest rate be built to properly evaluate the future investments with respect to current revenues. A salvage value of the pavement at the end of the analysis period is also used to enhance the rationalization of economic analysis.

Dimensional Inputs—These inputs are for the overall dimensions such as number of lanes of the facility to be designed and their widths.

Miscellaneous Parameters—Certain inputs do not fall in any of the preceding categories. They are used to aid in other inputs and in the computer program.

Constraints and Options

This set of variables enforces different restraints on the working system. A set of specified constraints generates the overall number of possible designs that are then analyzed and checked against a number of other constraints located at various places in the working system. Designs are accepted or rejected at these checks. They are, therefore, defined in the 2 following categories:

1. Inputs that define the minimum and maximum thicknesses of the materials to be provided and that determine the overall number of possible designs that will be considered; and
2. Inputs that reject certain designs designating them to be infeasible and that select the feasible designs out of all the possible designs generated in the preceding.

The computer program has 3 main options, with respect to the types of designs desired, to create maximum flexibility in design. The system can be restrained to design one or all of the following:

1. Pavement type—jointed and continuously reinforced concrete pavements;
2. Overlay type—asphalt concrete and portland cement concrete overlays; and
3. Reinforcement type—wire mesh and deformed bar reinforcement.

In general, system constraints and options are the designer's decisions to generate a reasonable type and number of solutions; but, at certain times, they can be the actual physical limitations advocated by the special conditions of design and construction.

Decision Criteria

Total overall cost is chosen as the prime decision criterion for the selection of the optimal and nearly optimal pavement strategies. Availability of initial funds is another

decision criterion that also acts as a restraint. Safety is controlled by the provision of seal coats and by specifying the minimum serviceability level. Riding quality and maintainability are controlled again by minimum specified serviceability level.

Output

The decision criteria included in the present working system are not comprehensive enough for making final judgments; this is left to the decision-maker. It is very difficult to quantify, with current knowledge, the relative importance a decision-maker will ascribe to various economic, social, and experience values. The solution output, therefore, is arranged in a way that does not deprive the designer of his judgment toward decision-making. An ordered set of alternative design strategies and pertinent information for each are produced in the form of a summary table based on increasing order of the present worth of total overall costs.

DESCRIPTION OF THE WORKING SYSTEM

Computer program RPS1 is written to solve various performance, structural, and cost models. The solution results in arrays of design strategies and their pertinent information. The strategies are stored and scanned for optimization by various techniques built into the program.

A summary flow chart for the working system is shown in Figure 3. The design process in general can be broadly divided into the following major parts:

1. Reading data, checking against invalid inputs, and printing input data;
2. Generating possible initial designs;
3. Selecting feasible initial designs;
4. Designing subbases, reinforcements, and joints;
5. Developing overlay strategies for feasible initial designs;
6. Analyzing cost of all strategies;

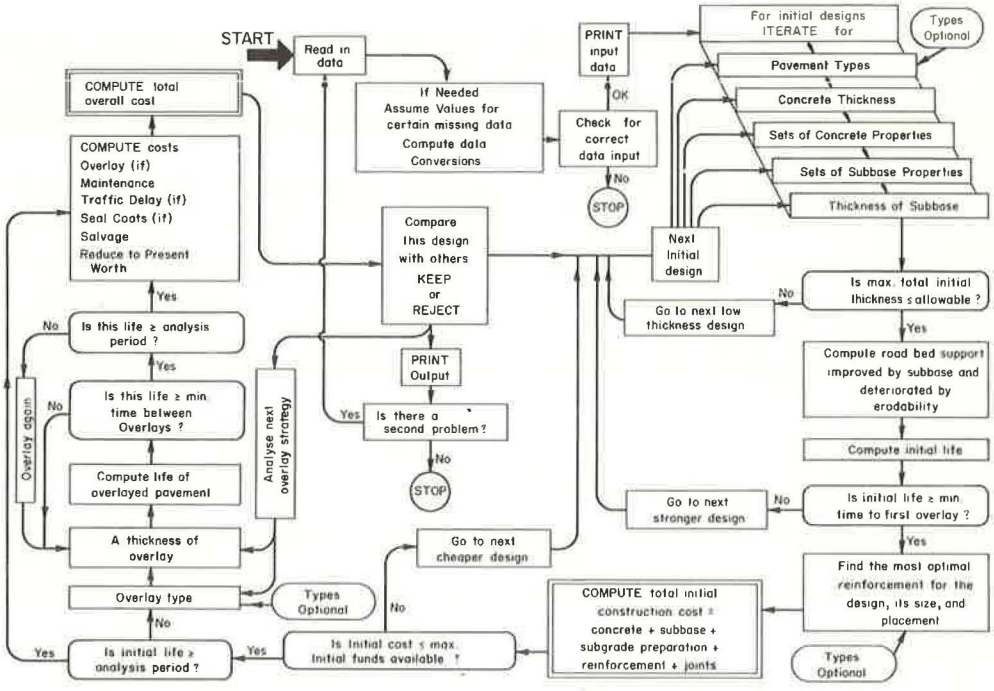

Figure 3. Summary flow diagram of Rigid Pavement System 1.

7. Storing, optimizing, and scanning; and
8. Printing output.

The overlay strategies are developed for those initial designs that reach the minimum specified serviceability levels in times less than the analysis period. These designs are overlaid with portland cement concrete or asphalt concrete overlays, as specified.

Figure 4 shows the general overlay performance patterns built into the program. Figure 4 also shows a relative difference in the designed performance patterns of structurally strong, medium, and weak initial designs (these designs illustrate the technique and do not represent actual problems).

Various structural and economic models are fitted together in this computer program to function as a most efficient total working system. A complete description of procedures and models is rather elaborate and is out of the scope of this paper. However, a brief summary of the structural models used in RPS1 is given in the following:

1. Serviceability loss due to traffic, which is an extension of an AASHO Road Test equation (14).
2. Serviceability loss due to swelling nature of clays, as developed by Scrivner et al. (13) and modified elsewhere (15).
3. Traffic distribution over time, as provided by the Texas Highway Department.
4. Increased foundation support due to subbases, which is developed by using layer elastic theory (15).
5. Reduction in roadbed support over the lifetime, which is developed by the analysis of slabs using discrete-element programs (15).
6. Asphalt concrete overlay design, which is developed by using layer elastic theory (15).
7. Portland cement concrete overlay design, as developed by the U.S. Army Corps of Engineers (16).
8. Correlations among material properties, which are developed by using the available data (15).

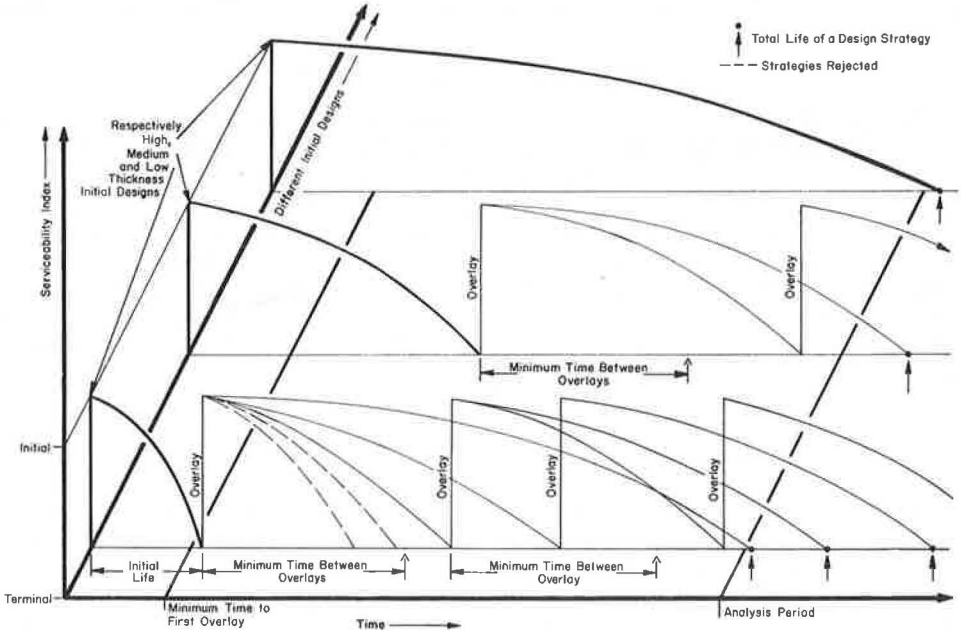

Figure 4. Illustrative performance patterns of overlays in Rigid Pavement System 1.

9. Stochastic variations of the material properties, which are developed by using statistics (15).

SYSTEMS ANALYSIS OF EXAMPLE PROBLEMS

The solutions given by the working system are illustrated by the following example (15, 17): A facility on the Interstate system is to be designed to carry high-speed traffic. The facility is in a rural area and will carry about 10,000 initial average daily traffic with a 5 percent yearly growth. The total of 5 million 18-kip equivalent axle loads will be carried during a lifetime of 20 years.

Serviceability index values after an initial and overlay construction will be 4.2 and 4.0 respectively. Minimum serviceability index of 2.5 will be maintained at all times. The facility passes through an area of moderate swelling clays.

Available initial funds restrict the possibility of relatively very thick initial construction. Also, it has been specified that the pavement will not be overlaid for at least 5 years after the initial construction and for 6 years after any overlay construction.

During an overlay construction, traffic will be disturbed over ½ mile of road length. Five percent of the vehicles will be stopped because of construction. An average of 48 percent of the average daily traffic will arrive during the 8-hour working period every day. There are 2 lanes in each direction. One lane will be overlaid while traffic is diverted to the second lane.

Subgrade has a mean modulus value of 100 pci with a standard deviation of 15 pci. A low-strength and a high-strength concrete are available with flexural strengths of 450 and 650 psi and standard deviations of 40 and 60 pci respectively. Two subbases, granular and cement-treated, are available with modulus values of 20,000 and 900,000 psi respectively. A granular subbase is observed to create a mild loss of support during its service life, whereas a cement-treated subbase remains very stable. Two types of deformed bars for each longitudinal, transverse, and tie-bar steel are available. One type of wire mesh is also available. Asphalt concrete for overlays has a modulus value of 200,000. For portland cement concrete overlays, the same concrete as used in the initial construction is to be provided.

It is also specified that the design should have a confidence level of 95 percent with respect to each of the material properties—subgrade modulus and concrete flexural strength. Adequate maintenance should be provided.

DISCUSSION OF SYSTEMS ANALYSIS

Within the specified combinations of concrete and subbase thicknesses, there are 196 initial possible designs out of which several designs are rejected by the program because of constraints such as nonavailability of initial funds or initial life being less than the minimum specified time. The remaining 79 initial designs gave rise to 751 design strategies out of which 652 were feasible within the program limitations. The first 20 designs consisted of jointed and continuously reinforced pavements with subsequent asphalt concrete overlays. Present worth of the total cost varied from $5.43 to $5.65 per square yard. The optimal design for this problem (problem 1) is shown in Figure 5. A comparison of the effects of 2 important input parameters was obtained by also solving for 2 alternate conditions (Fig. 5b and c).

DISCUSSION OF DESIGNS

Most optimal designs in each of the 3 problems discussed in the foregoing required either 1 or 2 overlays during their service lives. In the past, this concept of stage construction has never been favored for rigid pavements, mainly because of inadequate analytical techniques and partly because of limited knowledge of the various aspects of composite pavements. Such initial designs have always been attempted and were contemplated to last their design lives without overlays.

In each of the example cases described previously, the designs without overlays were estimated to have higher total overall costs than those chosen by the program. This is not a recommendation for overlays, but merely a recognition in the design program that many typical portland cement concrete pavements require overlays in less than 20 years.

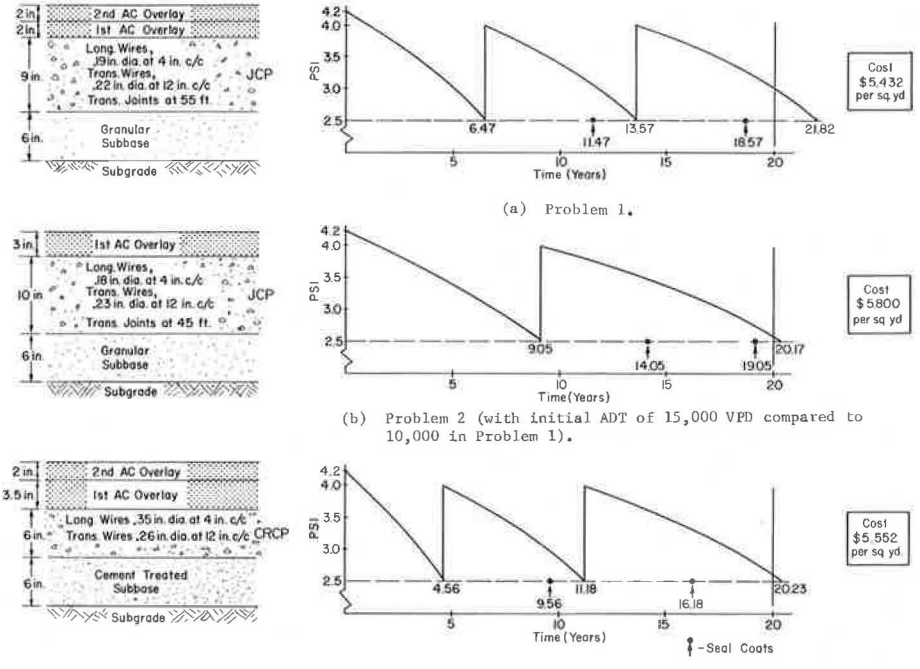

Figure 5. Systems analysis of example problems.

Figure 5b clearly shows an interesting decision from the system. The program has favored a design with higher initial thickness and cost and only 1 thick overlay during the lifetime of the facility. The program makes this selection to avoid the higher costs that would be incurred for traffic delays during overlay constructions (in this problem, average daily traffic is 15,000). However, this problem has a cost of $5.80 per square yard for the minimum cost design, whereas problem 1 has a cost of $5.432 per square yard. This is a direct result of carrying more traffic.

The effect of a restriction when enough funds are not available for initial construction is shown in Figure 5c. A thinner slab is provided in the initial construction, and the structure is overlaid shortly thereafter. Total thickness of overlays is higher in this problem than they are in problem 1. However, a cost of $5.552 per square yard for the optimal design results in problem 3, compared to a cost of $5.432 per square yard in problem 1. This is a direct result of having a restriction on available money for initial construction.

CONCLUSIONS

This paper presents a brief discussion of a complex detailed working systems analysis program. It is impossible to present all the details here. They are given elsewhere (15, 17). No inferences should be drawn from the example problems; they are given merely for illustration. The following conclusions are based on the detailed program and research:

1. The problem of designing a rigid pavement is not solved by analyzing a small number of initial design. A successful solution demands using economy and other decision criteria in the analysis of various possible design strategies and searching for the optimum design based on cost factors.
2. Such a solution process can be evolved in a systems framework and is difficult to handle ad hoc. This method is feasible and is shown to be very successful in RPS1.

3. Each design parameter has a definite effect on the overall cost and design of the pavement. The magnitude of these effects varies for different parameters as illustrated. A comprehensive sensitivity study is now under way on this program to order the factors by effect.
4. The RPS1 program must be put into use by highway departments and the results implemented and continually upgraded if the efforts of this project are to reach fruition.

ACKNOWLEDGMENTS

This investigation was conducted at the Center for Highway Research, the University of Texas at Austin. The authors wish to thank the sponsors, the Texas Highway Department and the Federal Highway Administration.

The opinions, findings, and conclusions expressed in this publication are those of the authors and not necessarily those of the Federal Highway Administration.

REFERENCES

1. Timoshenko, S., and Woinowshy-Krieger, S. Theory of Plates and Shells, 2nd Ed. McGraw-Hill, New York, 1959.
2. Westergaard, H. M. Stresses in Concrete Pavements Computed by Theoretical Analysis. Public Roads, Vol. 7, No. 2, 1926, pp. 25-35.
3. State of the Art: Rigid Pavement Design, Research on Skid Resistance, Pavement Condition Evaluation. HRB Spec. Rept. 95, 1968.
4. Spangler, M. G. Stresses in the Corner Region of Concrete Pavements. Eng. Exp. Station, Iowa State College, Ames, Bull. 157, 1942.
5. Kelley, E. F. Applications of the Results of Research to the Structural Design of Concrete Pavements. Public Roads, Vol. 20, No. 5-No. 6, July 1939, pp. 83-126.
6. Pickett, G., Raville, M. E., Janes, W. C., and McCormick, F. J. Deflections, Moments and Reactive Pressures for Concrete Pavements. State Eng. Exp. Station, Kansas State College, Pittsburg, Bull. 95, Oct. 1951.
7. The AASHO Road Test. HRB Spec. Rept. 61, 1961-1962, 7 reports.
8. Thickness Design for Concrete Pavements. Concrete Information, Portland Cement Assn., 1966.
9. Hudson, W. R., Finn, F. N., McCullough, B. F., Nair, K., and Vallerga, B. A. Systems Approach to Pavement Design, Systems Formulation, Performance Definition and Materials Characterization. Materials Research and Development, Inc., NCHRP Project 1-10, Interim Report, March 1968.
10. Hutchinson, B. G., and Haas, R. C. G. A Systems Analysis of the Highway Pavement Design Process. Highway Research Record 239, 1968, pp. 1-24.
11. Haas, R. C. G., and Hudson, W. R. The Importance of Rational and Compatible Pavement Performance Evaluation. HRB Spec. Rept. 116, 1971, pp. 92-111.
12. Hudson, W. R., McCullough, B. F., Scrivner, F. H., and Brown, J. L. A Systems Approach Applied to Pavement Design and Research. Texas Highway Department, Texas Transportation Institute, Texas A&M Univ., and Center for Highway Research, Univ. of Texas at Austin, Res. Rept. 123-1, March 1970.
13. Scrivner, F. H., Moore, W. M., McFarland, W. F., and Carey, G. R. A Systems Approach to the Flexible Pavement Design Problem. Texas Transportation Institute, Res. Rept. 32-11, 1968.
14. Hudson, W. R., and McCullough, B. F. An Extension of Rigid Pavement Design Methods. Highway Research Record 60, 1964, pp. 1-14.
15. Kher, R. K. A Systems Analysis for Rigid Pavement Design. Univ. of Texas at Austin, PhD dissertation, 1970.
16. Engineering and Design Rigid Airfield Pavements. U.S. Army Corps of Engineers, Manual EM 1110-45-303, Feb. 3, 1958.
17. Kher, R. K., Hudson, W. R., and McCullough, B. F. A Systems Analysis of Rigid Pavement Design. Texas Highway Department, Texas Transportation Institute, Texas A&M Univ., and Center for Highway Research, Univ. of Texas at Austin, Res. Rept. 123-5, Nov. 1970.

EVALUATION OF TERMINAL ANCHORAGE INSTALLATIONS ON RIGID PAVEMENTS

B. F. McCullough, Center for Highway Research and Department of Civil Engineering, University of Texas at Austin

This paper explores the problem of cyclic movement with continuously reinforced concrete pavement. The growth and pushing outward effect, resulting from environmental changes, causes ruptures of abutment walls and is responsible for other undesirable pressure. It was hypothesized that the same type of anchorage system used on jointed pavements could be used on continuous pavements, thus solving the expansion problem. Anchorages were installed on continuous pavements in much the same manner as they had previously been installed on jointed pavements. The anchor lugs were placed in the ground transversely across the pavement and were attached to an anchor slab. Long-term observations and measurements were performed on 186 existing terminal anchorage systems on continuous concrete pavements. After several years of observation, it was found that no adverse movement or pavement growth took place. The terminal movement was found to be directly related to pavement length of up to 1,000 ft and temperature change and indirectly related to pavement grade, subbase coefficient, and number of lugs. An empirical equation expressing movement in terms of these variables is derived in this study. This equation, considering the boundary conditions, could be used as a design equation.

•AN ALARMING AMOUNT of pavement growth was experienced in the late 1950's in numerous jointed concrete pavements (JCP) on the Texas highway system especially along the coastal area. As a result of concrete pavement growth, internal forces are built up in the slab and produce an outward push toward the free ends that closes the expansion joint at the bridge ends, ruptures the abutment walls, and applies an undesirable amount of pressure on the bridge or structure. In an effort to check this pavement growth problem, the Houston District constructed the first terminal anchorage system in Texas in March 1959. The satisfactory performance obtained with these initial installations consequently resulted in terminal anchorages being installed at a number of structures throughout the state.

At about the same time that these anchorage installations were being installed on jointed concrete pavement, the Texas Highway Department initiated the use of continuously reinforced concrete pavement (CRCP) on a widespread scale throughout the state. Logically transposing the experience with the growth problem of jointed concrete pavements to continuous pavements resulted in the decision that continuous pavements would also require an extensive anchorage system. Figure 1 shows the details of the anchorage system developed for CRCP.

DESIGN

In their treatise on terminal anchorages, Shelby and Ledbetter enumerated the basic concepts and assumptions used in designing the terminal anchorage system that was initially used by the Texas Highway Department (1). Basically, the anchorage system for

Sponsored by Committee on Rigid Pavement Design and presented at the 50th Annual Meeting.

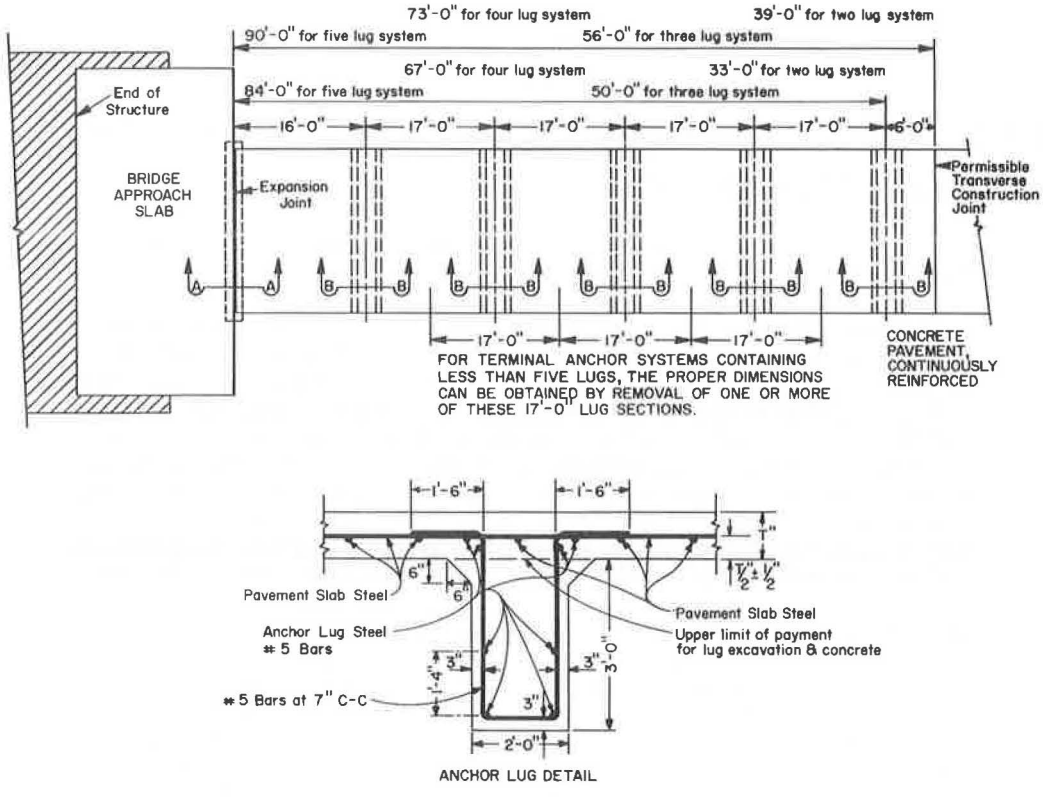

Figure 1. Typical lug design of continuously reinforced concrete pavement.

jointed concrete pavement consists of 2 anchor lugs, 3 ft deep and 2 ft wide, at each pavement terminal. The terminal anchorages are heavily reinforced to provide a stiff and rigid resistance member. The design concept of the anchorage system is to transfer the pavement growth forces to the soil mass through the passive bearing and shear resistance of the subsoil. It was felt that the critical elements were the bearing area of the lugs and the shear plane along the bottom of the lugs as well as along the face of a Coulomb wedge.

The design for the anchorage system on continuous pavements was basically the same as the design for jointed pavements with the exception that 5 anchor lugs were used, and this resulted in a longer anchor slab (90 ft).

The nomenclature of various components of the anchorage system may be enumerated at this point. The slab placed on top of the base or on top of the subsoil is defined as the anchor slab. The members extending vertically into the ground are defined as lugs; the one nearest the structure is considered the front lug.

PERFORMANCE

After 1959 the terminal anchorage systems of the types illustrated were installed on both jointed concrete pavements and continuously reinforced concrete pavements. During the early part of 1963, several cases of terminal anchorage failure were reported in the Houston area on jointed concrete pavements. A preliminary survey indicated that a number of the terminal anchorage systems had experienced cracking in the anchor slab, closing of the joints between the anchor slab and the bridge approach slab, and faulting of the abutment walls. During the same period, all of the terminal anchorage systems on CRCP were performing satisfactorily, and in no case was adverse move-

ment occurring. The only disadvantage associated with CRCP anchorage systems was the excessive cost required to construct them at each pavement terminal. As a result of these 2 facts, a research project was initiated in March 1963 to evaluate terminal anchorage installations on rigid pavements.

OBJECTIVE OF STUDY

The objective of this study was to perform the field observations necessary to re-evaluate the lug anchorage designs. In addition, long-term observation and measurements were performed on 186 existing terminal anchorage systems on continuous concrete pavements.

EXPERIMENT DESIGN AND DISCUSSION OF DATA

The first phase of this study consisted of an appraisal of the factorial arrangement of test sections. On the basis and availability of other continuously reinforced concrete pavements throughout the state, sections were added as necessary to make as full a fractorial as possible. At the same time, sections were added in the northern part of Texas so that a comparison of environmental conditions could be made. The areas from which field data were obtained are shown in Figure 2. Locations could not be selected any farther south than shown because concrete pavements are not constructed in that area of the state. Data were taken as before on all sections for an additional year and were then analyzed.

Layout of Experiment

Figures 3 and 4 show the factorials of sections for 8 different subbase types including cement-stabilized, asphalt-stabilized, surface-treated, crushed sandstone, river gravel, rounded river gravel, crushed limestone, and lime-stabilized subbases. These experi-

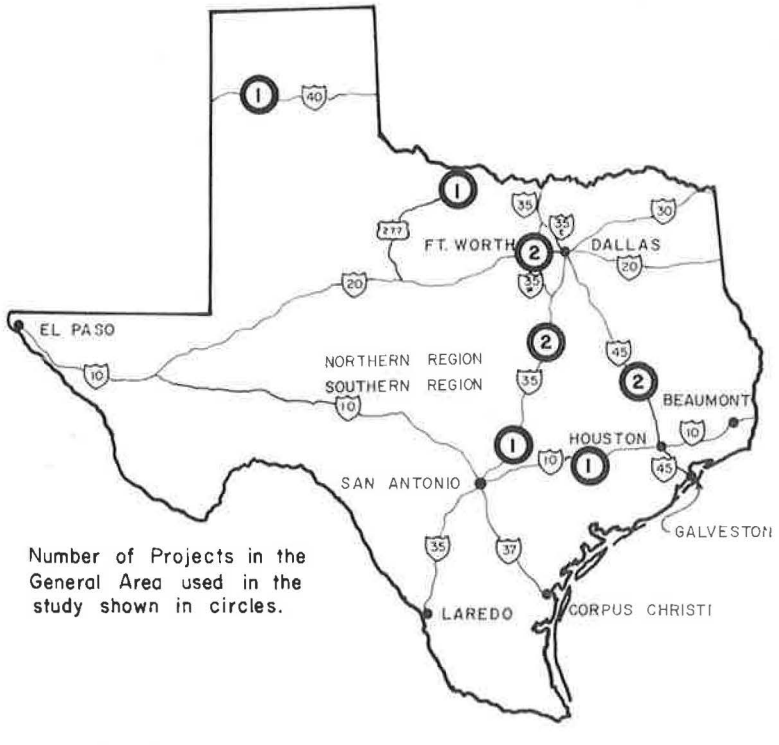

Figure 2. Division of the state on the basis of weather conditions.

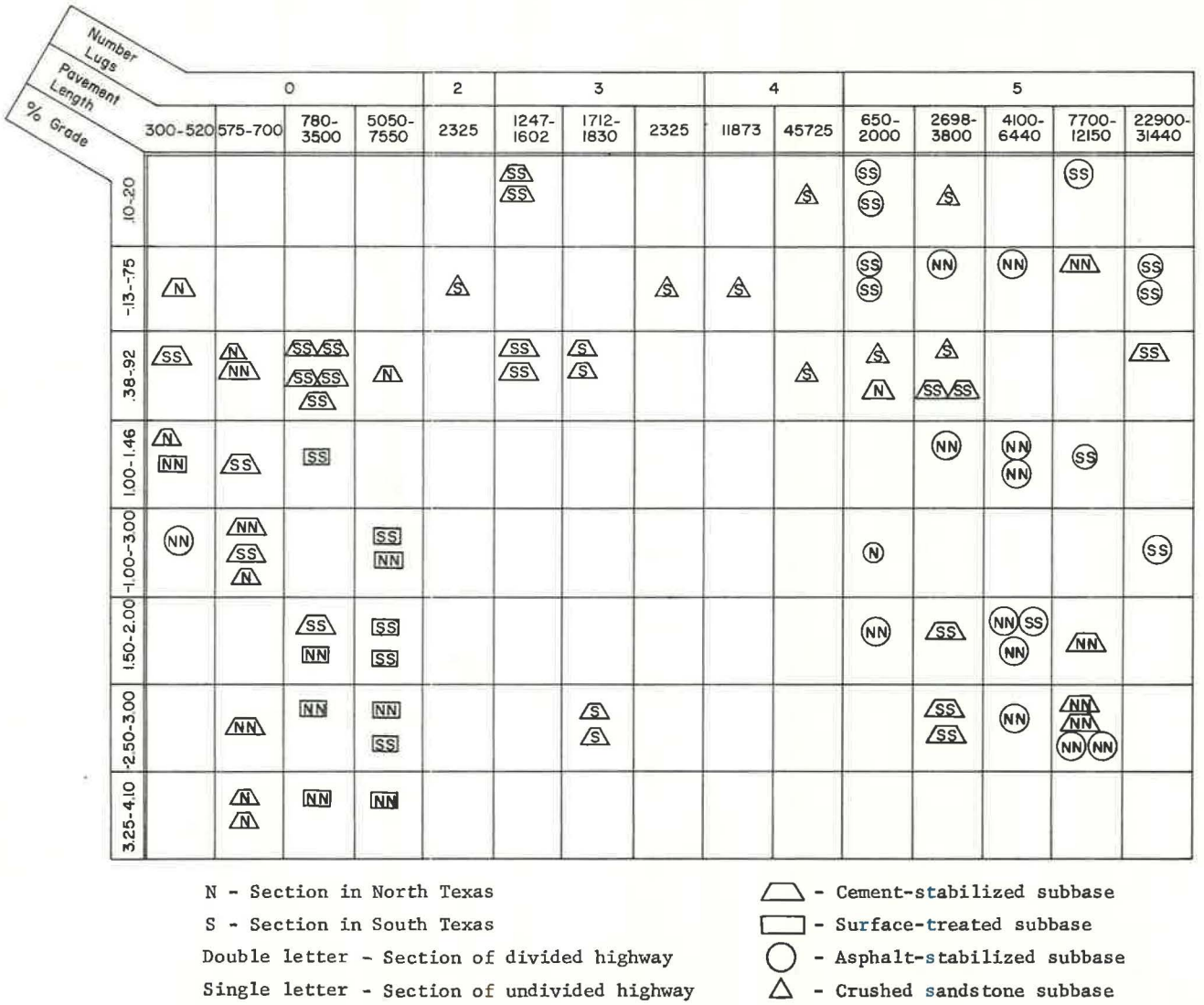

Figure 3. Factorial of lugs, length, and grade for pavements having cement-stabilized, surface-treated, asphalt-stabilized, and crushed sandstone subbases.

(a)

NUMBER OF LUGS / SLAB LENGTH / % GRADE	0	5	
	700	2600	3250
+1.96	NN	NN	
−1.96	NN		
+2.50		NN	
+4.00			NN

(b)

NUMBER OF LUGS / SLAB LENGTH / % GRADE	5		
	2000	4900	5200
−.50		NN	
+.57		N	
+2.30			N
+3.00	NN		

(c)

NUMBER OF LUGS / SLAB LENGTH / % GRADE	0			
	1225	2800	5900	12300
+.10				NN
−.28		NN		
+1.17			NN	
−2.48			NN	
+3.00	NN			
−3.00	NN			

(d)

NUMBER OF LUGS / SLAB LENGTH / % GRADE	0				
	2700	3085	4030	4750	9594
+1.77		N			
+1.85		N			
+2.20					NN
+2.70				NN	N
+3.00		NN	NN	NN	N
+3.50	NN				

NOTE: N – Sections in North Texas S – Sections in South Texas

Figure 4. Factorial of lugs, length, and grade, and for pavements having (a) crushed river gravel subbase, (b) rounded river gravel subbase, (c) crushed limestone subbase, and (d) lime-stabilized subbase.

ment designs are for CRCP only and are presented to give an indication of the data used.

Sections in north Texas were also added to the factorials of 3 subbase types for the weather environment study (Fig. 3). These sections were chosen so that variables such as number of lugs, slab length, and percentage of grade for both northern and southern sections would be approximately the same.

The sections in south Texas with a 1-course surface treatment on the subbase and a crushed sandstone subbase were used to study the age factor (Fig. 3). These sections were chosen because data had been taken on them for a period of approximately 7 years.

Data Analysis

Data analysis for this paper was carried out first by obtaining cyclic end movement per degree of temperature for each section and second by using these as a basis for comparison. In this manner, temperature was eliminated as a variable, and the factorial arrangement of the test sections could be used to study the effect of pavement age, length, percentage of grade, number of lugs, environmental location, and subbase type.

Pavement Age—The main concern with pavement age is the possibility of pavement growth due to the infiltration of foreign material into the shrinkage cracks. It would seem plausible that any growth of the pavement end would show up as a permanent change in the distance between gage plugs (placed at 10-in. centers) at a given temperature. Furthermore, any major change in thermal coefficient would affect the cyclic end movement per degree of temperature change.

Figure 5 shows gage plug reading versus air temperature for a typical section used in the age study. All points are close to the line passed through the data, and, because

these points represent data taken at random intervals during a period of 5 years, it can be said that pavement age has not affected the cyclic end movement or gage plug distance at zero degree temperature for this section. Similar plots for all other sections of the age study have shown the same relationship.

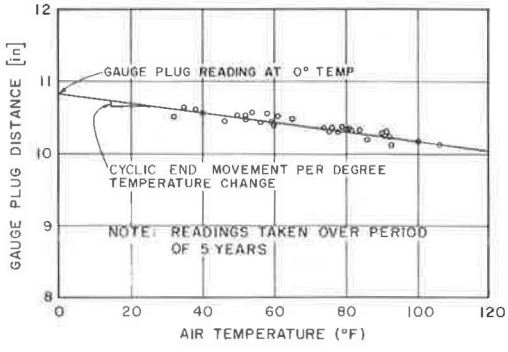

Figure 5. Effect of pavement age on end movement.

Effect of Slab Length on End Movement—Earlier research on this project revealed that a pavement length of more than 1,000 ft does not influence end movement more than a length of 1,000 ft (2). From this it may be concluded that a maximum length of 500 ft contributes to movement on each end of the pavement slab. In pavements longer than 1,000 ft, the center portion of the slab is restrained by the frictional force from the subbase.

Environmental Location—A study of the effect of weather conditions on end movement has to exclude temperature so that northern and southern sections can be compared. Cyclic end movement for northern sections can be plotted versus replicated southern sections that have equal parameters such as subbase type, percentage of grade, length of slab, and number of lugs. Ideally, if there were no difference between northern and southern sections, the points would result in a 45-deg line. Figure 6 shows a plot of this type. It should be noted that all sections with slab lengths of more than 1,000 ft are considered equal, as far as slab length is concerned, on the basis of the preceding discussion. Also, all grades lower than 0.30 percent were considered equal because it was felt that grades lower than this would be inconsequential.

Although the points in Figure 6 do not fall exactly on the 45-deg line, there is approximately equal division. Therefore, on the basis of this study, it will be assumed that there is no appreciable difference in end movement characteristics resulting from environmental location within the state.

Length and Grade Percentage—The following relationship was found to exist between the cyclic end movement, slab length, and percentage of grade while other variables are held constant:

$$\text{Log } b = \log A_5 + A_4 \log \left(\frac{L}{|G| + 1} \right) \quad (1)$$

where

b = cyclic end movement, in./deg F;
L = length of slab contributing to end movement, ft;
|G| = absolute value of grade percentage;
A_4 = arbitrary constant; and
A_5 = constant dependent on subbase type and number of lugs.

Here again cyclic end movement is used so that temperature as a variable may be excluded from the study.

Because a purpose of this paper is to verify an equation format previously developed (2), Eq. 1 will be used as a starting point for analysis. Figure 7, in which each point represents 1 section, shows log b

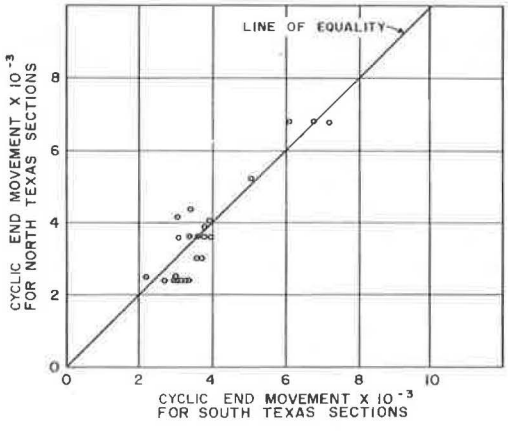

Figure 6. End movement in south Texas versus end movement in north Texas.

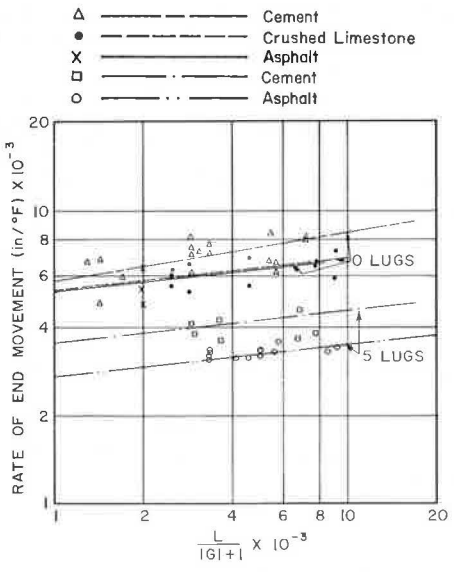

Figure 7. Cyclic end movement versus term for pavement length and percentage of grade for asphalt-stablized, cement-stabilized, and crushed limestone subbases.

TABLE 1

DIFFERENCE IN END MOVEMENT CHARACTERISTICS DUE TO NUMBER OF TERMINAL LUGS AND SUBBASE TYPE

Subbase	Number of Lugs	$A_5 \times 10^{-3}$
Surface treated	0	2.90
Cement stabilized	0	5.75
Cement stabilized	3	4.30
Cement stabilized	5	3.70
Asphalt stabilized	0	5.30
Asphalt stabilized	5	2.68
Crushed river gravel	0	5.50
Crushed river gravel	5	4.40
Crushed limestone	0	5.50
Rounded river gravel	5	3.40
Lime stabilized	0	4.50
Crushed sandstone	2	9.40
Crushed sandstone	3	7.70
Crushed sandstone	4	7.20
Crushed sandstone	5	7.00

plotted versus $\log \left(\frac{L}{|G| + 1} \right)$ for different subbase types and number of lugs.

The A_5 intercept changes with subbase type and with number of lugs (Fig. 7, 0 lug), whereas A_4 is approximately equal for both. Therefore, it may be stated that A_4 is an arbitrary constant not dependent on any of the other variables, whereas A_5 is dependent on both subbase type and number of lugs. Thus, these data bear out the original equation format as given in Eq. 1.

Subbase Coefficient and Number of Lugs—Table 1 gives A_5 for each subbase type and number of lug combinations in this experiment. It was found that the following relationship existed between A_5, subbase coefficient of friction, and number of lugs:

$$\text{Log } A_5 = A_1 + A_2 \log C + A_3 \log (N + 1) \qquad (2)$$

where

A_1, A_2, and A_3 = arbitrary constants,
C = subbase coefficient of friction, and
N = number of rigid lugs.

A literary search was conducted, and a value for each subbase coefficient or friction was obtained. These values were assumed values of subbase coefficient of friction, and A_5 was correlated in terms of these values. However, a more thorough study of this relationship indicates that the subbase part of A_5 may be a combination of effects and not just coefficient of friction. For example, the type of subbase may influence the cyclic end movement because of different types of soil masses acting against the lug surfaces. Therefore, it is felt that the part of A_5 determined by the subbase might be more appropriately called subbase coefficient C.

Based on this assumption, values of subbase coefficient of friction, as such, could not be used for final correlation; and, because A_5 is different for each subbase type with the same number of lugs, some arbitrary scale had to be set up and values obtained for the subbase coefficient so they could be correlated with A_5.

Values of subbase coefficients were obtained by making a linear relationship between C, for the different subbase types, and A_5. This was done by selecting random numbers to represent C for the subbase with the lowest cyclic end movement (surface-treated

subbase) and the highest cyclic end movement (crushed sandstone subbase). A value of 2.65 was chosen for surface treatment and 1.35 for crushed sandstone. This then makes values of C, for the other subbase types, fall between 1.35 and 2.65.

To obtain these values, Eq. 2 was used. This equation contains 3 unknown constants. Therefore, by use of 3 simultaneous equations of this form, the coefficients A_1, A_2, and A_3 can be determined. These 3 equations are obtained by use of the A_5 constants given in Table 1 for sections with surface-treated and crushed sandstone subbases and their respective number of lugs. The equations used were as follows:

$$\text{Log } (2.9 \times 10^{-3} \text{ in./deg F}) = A_1 + A_2 \log (2.65) + A_3 \log (0 + 1) \quad (3)$$

$$\text{Log } (9.4 \times 10^{-3} \text{ in./deg F}) = A_1 + A_2 \log (1.35) + A_3 \log (2 + 1) \quad (4)$$

$$\text{Log } (7.0 \times 10^{-3} \text{ in./deg F}) = A_1 + A_2 \log (1.35) + A_3 \log (5 + 1) \quad (5)$$

After solving the equations for A_1, A_2, and A_3, Eq. 2 was used to calculate C-values for each of the other subbases given in Table 1 by using A_5 and the respective number of lugs. Table 2 gives the calculated C-values for all sections in Table 1.

Verification of Equation Format

Substitution of Eq. 2 into Eq. 1 yields the following relationship:

$$\text{Log } b = A_1 + A_2 \log C + A_3 \log (N + 1) + A_4 \log \left(\frac{L}{|G| + 1} \right) \quad (6)$$

On the basis of these data, the empirical relationship between end movement and the enumerated parameters is the same.

EMPIRICAL DESIGN EQUATION

On the basis of data taken on this project, it was found that Eq. 6 is valid and, furthermore, that no factor should be added to compensate for environmental location or pavement age. Therefore, a multiple regression correlation was run on this equation to determine the coefficient for each term. Then the equation could be used as a predictor of end movement in terms of the parameters contained in the equation.

Regression Analysis

The correlation of constants A_1, A_2, A_3, and A_4 of Eq. 6 was determined by a multiple regression technique using the values of the parameters of each end system and the values (1) of the subbase coefficient previously determined (Table 2). The following results of this regression analysis are $A_1 = -1.902$, $A_2 = -2.027$, $A_3 = -0.312$, $A_4 = 0.107$, and $R^2 = 0.71$, and standard error = 0.0008 in./deg F. The resulting empirical design equation is as follows:

TABLE 2

SUBBASE COEFFICIENTS FOR USE IN EMPIRICAL DESIGN EQUATION

Subbase	Subbase Coefficient of Friction
Surface treated	2.65
Lime stabilized	2.13
Asphalt stabilized	1.96
Rounded river gravel	1.95
Crushed river gravel	1.93
Crushed limestone	1.93
Cement stabilized	1.90
Crushed sandstone	1.35

$$\Delta X = \frac{0.01253 \left(\frac{L}{|G| + 1} \right)^{0.107} (\Delta T)}{C^{2.027} (N + 1)^{0.312}} \quad (7)$$

where

ΔX = total movement for a given temperature change experienced at an expansion joint, in.; and

ΔT = change in air temperature for a given period, deg F.

Evaluation of Equation

The standard error given in the preceding paragraph means that Eq. 7 would predict an expected end movement for a given temperature change within ±0.0008 in./deg F. However, all of this error is not due to equation fit. A standard deviation analysis was run on all replicate sections, and the analysis indicated that an error of 0.00041 in./deg F of that measured could be expected from 2 sections under equal conditions. This replicate error is probably due to random variation in sampling and the existence of unknown variables.

Although the coefficients found by regression analysis are slightly different from the ones found in a previous study (probably due to more available data for each variable), the standard error in this study is much less. Therefore, it is felt that these coefficients fit the actual conditions much better and the resulting equations will be much more reliable as a design guide.

CONCLUSIONS AND RECOMMENDATIONS

On the basis of this research project conducted by the Texas Highway Department during a period of 3½ years, the following conclusions are warranted:

1. The cyclic terminal movement of an 8-in. CRCP is directly related to pavement length and temperature change and indirectly related to pavement grade, subbase coefficient, and number of lugs. An empirical expression indicating movement in terms of these variables is presented here and may be used as a basis for design.
2. The cyclic terminal movement of an 8-in. CRCP with and without terminal anchorages was found to be independent of pavement age and environmental location.
3. The study assumed that a maximum of 500 ft of CRCP contributes to end movement experienced at an expansion joint.
4. Care should be taken in using the empirical equation derived here for design purposes. Parameters should not be used that are outside the limits of these data. Close observation of the values found to represent different types of bases indicates that these values may include more than just coefficient of friction because the values do not follow what might logically be expected. There is a possibility that some of the values derived here are partially due to the type of soil mass acting against the lug as well as the imposing force of surface friction. Because the equation is of an empirical form, no further distinction can be made at this time. However, it is felt that the values derived for each type of subbase apply to this empirical design equation.
5. With certain combinations of subbase coefficient and grade percentage, the number of terminal lugs for CRCP can be reduced to zero. A satisfactory performance during a period of 7 years and, in 1 case, 15 years verifies this.

ACKNOWLEDGMENT

This research was sponsored by the Texas Highway Department and the Federal Highway Administration. The opinions, findings, and conclusions expressed are those of the authors and not necessarily those of the sponsors.

REFERENCES

1. Shelby, M. D., and Ledbetter, W. B. Experience in Texas With Terminal Anchorage of Concrete Pavement. HRB Bull. 332, 1962, pp. 26-39.
2. McCullough, B. F., and Sewell, T. F. Parameters Influencing Terminal Movement on Continuously Reinforced Concrete Pavement. Texas Highway Department, Res. Rept. 39-2, Aug. 1964.
3. Graybill, F. A. An Introduction to Linear Statistical Models, Vol. I. McGraw-Hill, New York, 1961, pp. 195-220.
4. McCullough, B. F. A Field Survey and Exploratory Excavation of Terminal Anchorage Failures on Jointed Concrete Pavement. Texas Highway Department, Res. Rept. 39-1, March 1965.
5. McCullough, B. F., and Herber, F. A Report on Continuity Between a Continuously Reinforced Concrete Pavement and a Continuous Slab Bridge. Texas Highway Department, Res. Rept. 39-3, Aug. 1966.

IMPACT EFFECT ON RIGID PAVEMENT CORNER HAVING LOW SPOTS

R. K. Ghosh, Ram Lal, and S. R. Vijayaraghavan, Rigid Pavement Research Division, Central Road Research Institute, India

An approximate analysis has been made of the additional deflection that occurs in a rigid pavement corner because of the impact of a moving wheel over a low spot in the region. Analytical solutions for both supported and unsupported conditions of the corner have been presented. When there is a low spot, the dynamic deflection of the corner increases very rapidly with the speed of the vehicle up to a certain limiting speed, depending on the characteristics of the slab and support condition. In the case of thin slabs, the increase may be as high as 90 percent above the static value. In comparison, when no low spot is present, the dynamic deflection decreases with the vehicle speed and is lower than the static value. Experiments conducted for some selected cases show that the comparison between analytical and experimental values of additional dynamic deflection is satisfactory within the limitation of the investigation.

•IN RIGID PAVEMENT, surface irregularities such as low spots are sometimes observed near joints and corners. These are a result of either bad workmanship or improper maintenance. In the latter case, expulsion of sealing compound from the joints results in concentrating the stresses and impacts. The resulting localized disintegration of concrete under vehicular traffic forms depresssions or low spots. These depressions not only affect the riding quality of the pavement but also induce additional heavy impact loads on the pavement, such as the impact when a wheel travels over the low spots.

A solution for the case when the low spot is away from a joint may be obtained from Timoshenko's analysis (3). The effect of a low spot at a joint or a corner, where it is discontinuous, is covered here. The wheel load has been assumed to be concentrated at a point, and the joint has been assumed to be doweled.

FULLY SUPPORTED FORWARD SLAB

For the assumed configuration of a low spot spread over 2 diagonally opposite corners of adjacent slabs (Fig. 1), the following equation may be written with reference to the coordinates (origin O) shown in Figure 2:

$$\eta = (\lambda/2)\{1 + \cos[(2\pi x)/\iota]\} \quad (1)$$

where η is the variable depth of low spot, λ is its maximum depth at the center, and ι is its total length spread equally over both the slabs.

Reaction Due to Inertia

The effect of inertia may be neglected because the slab is fully supported and any vibration will be very much damped.

Sponsored by Committee on Flexible Pavement Design.

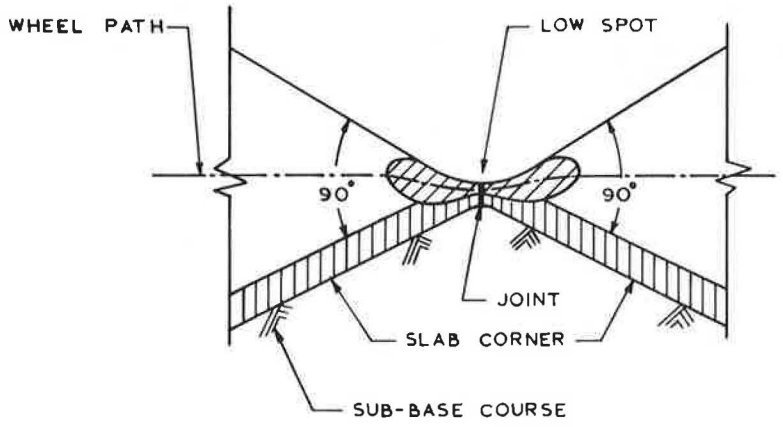

Figure 1. Low spot at adjacent slab corners of a concrete pavement.

Vertical Inertial Force of Load

If a is acceleration caused by point load W that causes additional dynamic deflection y, then

$$a = [d^2 (y + \eta)]/dt^2 \tag{2}$$

The vertical inertial force due to this acceleration is

$$F = (W/g) \{[d^2 (y + \eta)]/dt^2\} \tag{3}$$

Resisting Force Due to Elasticity

The resisting force due to the elasticity of the slab and its subgrade support is

$$R = - k \cdot y \tag{4}$$

where k is the elastic reaction modulus of the pavement system in the corner region.

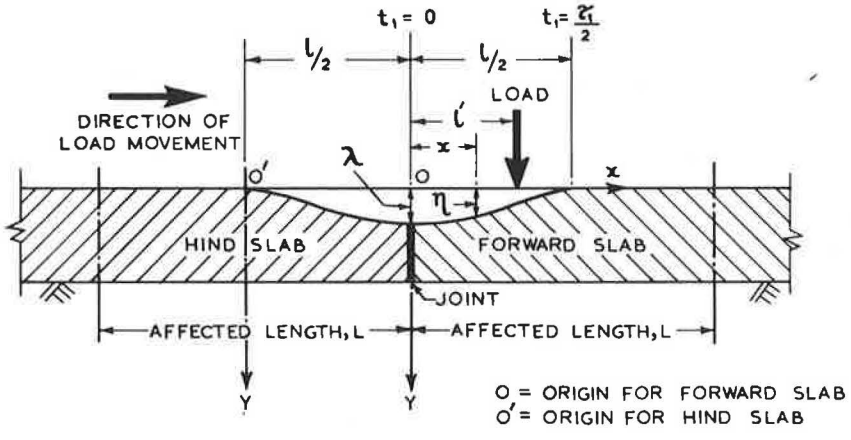

Figure 2. Section of slabs through low spot along the bisector of the corner angle.

Forced Vibration

From Eqs. 3 and 4, the equation for forced vibration due to the load moving on the low spot may be obtained as

$$(W/g)\ \{[d^2\ (y + \eta)]/dt^2\} = -k \cdot y$$

or

$$(W/g)\ (d^2y/dt^2) + ky = -(W/g)\ (d^2\eta/dt^2) \tag{5}$$

Reckoning the time from the instant the load is at x = 0 (Fig. 2) and denoting the velocity of load by υ so that $x = \upsilon \cdot t$, we obtain the following from Eq. 1:

$$\eta = (\lambda/2)\ [1 + \cos\ (2\pi\upsilon t/\iota)] \tag{6}$$

Substituting the value of η in Eq. 5, we get

$$(d^2y/dt^2) + (kg/W)\ y = (2\lambda\pi^2\upsilon^2/\iota^2)\ \cos\ (2\pi\upsilon t/\iota)$$

Denoting $kg/W = p^2$, where p is the angular frequency of free vibration, we get

$$\ddot{y} + p^2 \cdot y = (2\lambda\pi^2\upsilon^2/\iota^2)\ \cos\ (2\pi\upsilon t/\iota) \tag{7}$$

Additional Deflection

For initial conditions of y = 0 and $\dot{y} = 0$ at t = 0, the solution of Eq. 7 is obtained from Dehmul's integral (4) as

$$y = (2\lambda\pi^2\upsilon^2/p\iota^2) \int_0^{t_1} \cos\ (2\pi\upsilon t/\iota)\ \sin\ p\ (t_1 - t)\ dt$$

or

$$y = \left(\lambda/\{2[1 - (\iota^2/\upsilon^2)\ (p^2/4\pi^2)]\}\right)\ [\cos\ pt_1 - \cos\ (2\pi\upsilon/\iota)\ t_1] \tag{8}$$

Denoting $\tau_1 = \iota/\upsilon$ = total time taken by the load to cross the low spot and $\tau = 2\pi/p$ = period of free vibration, we reduce Eq. 8 to

$$y = \{\lambda/[2(1 - \tau_1^2/\tau^2)]\}\ [\cos\ (2\pi t_1/\tau) - \cos\ (2\pi t_1/\tau_1)] \tag{9}$$

For any position of the load along the low spot (Fig. 2), Eq. 9 is further modified as

$$y/\lambda = \{1/[2(1 - \tau_1^2/\tau^2)]\}\ \{\cos\ [(2\pi\iota'/\iota)\ (\tau_1/\tau)] - \cos\ (2\pi\iota'/\iota)\} \tag{10}$$

The values of y expressed in terms of λ have been calculated from Eq. 10 for different values of the ratio, τ_1/τ, corresponding to the 3 positions of load at $\iota' = \iota/4$, $3/8\ \iota$, and $\iota/2$ along the low spot. These are shown in Figure 3. Figure 3 shows that, for all values of ι', the additional deflection reaches maximum when τ_1/τ approaches zero. τ_1/τ tends to zero when the velocity of load is very high. The overall maximum occurs when ι' approaches $\iota/2$. The deflection becomes negative at locations corresponding to the values of τ_1/τ between 1 and 3.0.

Reaction Modulus

If W denotes the load (spring-borne weight), k is the elastic reaction modulus at the triangular corner, and Δ_{max} is the maximum static deflection, we get

$$k = W/\Delta_{max} \tag{11}$$

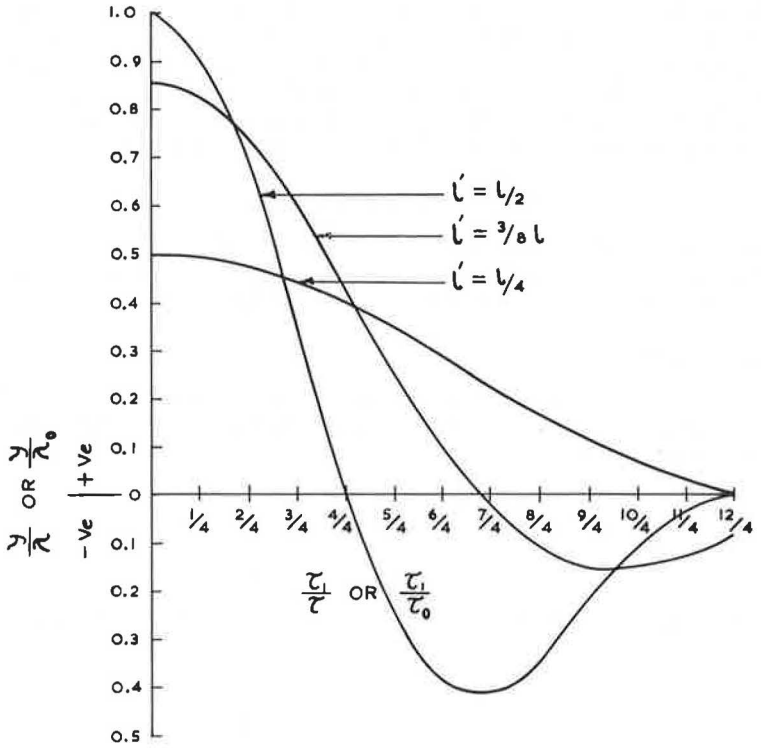

Figure 3. Additional dynamic deflection for forward slab under fully supported (y/λ vs τ_1/τ) and unsupported (y/λ_0 vs τ_1/τ_0) conditions.

The value of Δ_{max} may be computed from the following Westergaard equation (5):

$$\Delta_{max} = (W/K\iota_S^2)\,[1 \cdot 1 - (\sqrt{2} \cdot r/\iota_S)\,(0 \cdot 88)] \tag{12}$$

where K is the modulus of subgrade reaction; ι_S is the radius of relative stiffness given by $[Eh^3/12\,(1 - \mu^2)K]^{1/4}$, in which E and μ are respectively modulus of elasticity and Poisson's ratio of the slab material, and h is the slab thickness; and r is the radius of equivalent circle of tire imprint.

Neglecting r for a point load, we obtain

$$\Delta_{max} = [(1 \cdot 1\ W)/K\,\iota_S^2] \tag{13}$$

Example

If we take a particular example with W = 9,000 lb, K = 400 pci, $E = 4 \times 10^6$ psi, h = 8 in., and $\mu = 0.2$, Δ_{max} works out to be 3.78×10^{-2} in. Considering 25 percent load transfer at doweled joint, $\Delta_{max} = 0.75 \times 3.78 \times 10^{-2}$ in. The reaction modulus is $k = W/\Delta_{max} = 9{,}000/(0.75 \times 3.78 \times 10^{-2}) = 323{,}000$ lb/in. Because $p^2 = kg/W$, by substitution we get

$$p = \tfrac{1}{2\pi}\,[(323{,}000 \times 32 \times 12)/9{,}000]^{1/2} = 18.63 \text{ cps}$$

Therefore, $\tau = 1/p = {}^1/_{18.63}$ sec, and the ratio

$$\tau_1/\tau = (\iota/\upsilon)/\tau = 18.63\ \iota/\upsilon \tag{14}$$

For ι = 4, 6, and 8 in. and v ranging from 20 to 73 ft/sec (i.e., 14 to 50 mph), the values of τ_1/τ have been calculated. $(y/\lambda)_{max}$ may then be obtained from either Eq. 10 or the data shown in Figure 3. The variation of $(y/\lambda)_{max}$ with v is shown in Figure 4. It is evident that the additional downward (positive) deflection increases with the load velocity for a particular length of low spot. However, for a constant velocity, the additional downward deflection decreases with an increase in the length of low spot.

UNSUPPORTED FORWARD SLAB

In the case of an unsupported corner, the additional dynamic deflection due to a low spot being traversed by a moving load will be governed, among other factors, by the inertia of the slab, the effect of which will be appreciable.

Reaction Due to Inertia

The geometry of an unsupported corner as a cantilever slab in the form of an isosceles triangle of uniform thickness is shown in Figure 5. If the width of an elemental strip dx at a distance x from the support is

$$b_x = b\,[1 - (x/L)] \tag{15}$$

the mass of the strip is

$$w = (b_x \cdot dx \cdot h \cdot \gamma)/g \tag{16}$$

where b is the breadth of the cantilever at the support, h is the uniform slab thickness,

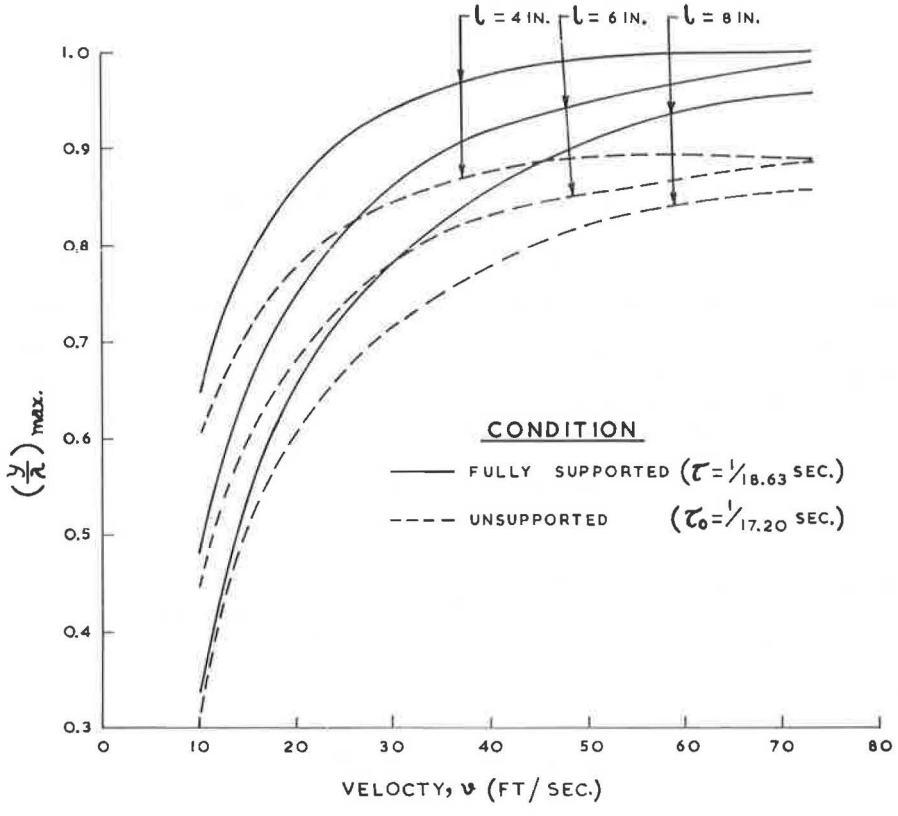

Figure 4. Maximum additional downward deflection for forward slab for different velocities of load.

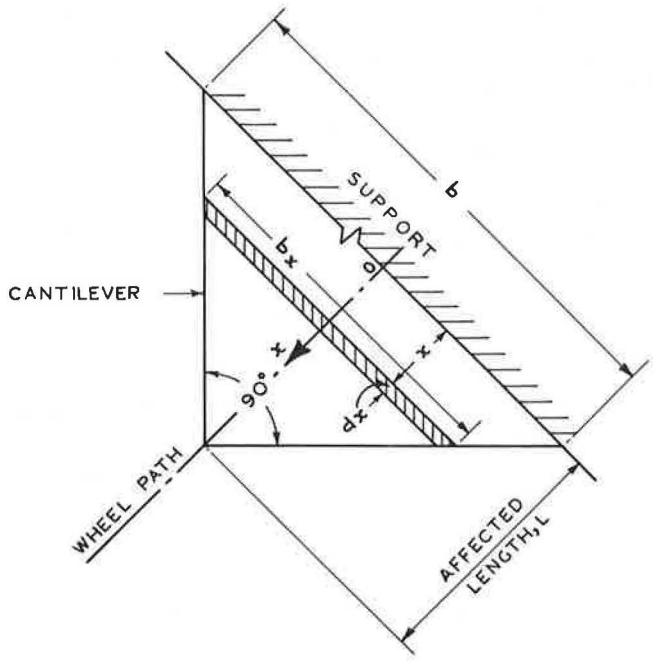

Figure 5. Unsupported corner of forward slab.

L is the unsupported effective span length of the slab, g is the acceleration due to gravity, and γ is the unit weight of slab material. Because of continuity of the cantilever over the support, the zone of influence of the load extends beyond the actually unsupported length. From tests conducted by the authors (1), it was observed that the effective length of the overhang was about 90 percent more than the actually unsupported length under both static and dynamic conditions of loading.

Because acceleration of the unit mass is equal to d^2y/dt^2, the inertial force of the strip may be obtained from

$$s_x = w(d^2y/dt^2) = [(b_x \cdot dx \cdot h \cdot \gamma)/g] (d^2y/dt^2)]$$

or

$$s_x = \left(\{b [1 - (x/L)] dx \cdot h \cdot \gamma\}/g\right) (d^2y/dt^2) \quad (17)$$

The total inertial force of the whole cantilever is, therefore,

$$S = (bh\gamma/g) (d^2y/dt^2) \int_0^L [1 - (x/L)] dx$$

or

$$S = (bh\gamma L/2g) (d^2y/dt^2) \quad (18)$$

Denoting $bh\gamma L/2 = M$, we obtain the following reaction due to inertia:

$$S = - (M/g) (d^2y/dt^2) \quad (19)$$

Vertical Inertial Force of Load

If we use the same low spot configuration as shown in Figure 2, the equation for inertial force F of the load W is

$$F = (W/g)\,\{[d^2\,(y + \eta)]/dt^2\} \tag{20}$$

Resisting Force Due to Elasticity

If we assume that the cantilever is an elastic spring, the resisting force due to its elasticity is, as before,

$$R = -\,k \cdot y \tag{21}$$

Forced Vibration

From Eqs. 19, 20, and 21, the expression for forced vibration produced by a load moving on a low spot may be obtained as

$$(W/g)\,\{[d^2\,(y+\eta)]/dt^2\} = -\,(M/g)\,(d^2y/dt^2) - k \cdot y$$

or

$$[(W + M)/g]\,(d^2y/dt^2) + k \cdot y = -\,(W/g)\,(d^2\eta/dt^2) \tag{22}$$

Applying Eq. 6 to Eq. 22, we get

$$(d^2y/dt^2) + [kg/(W + M)]\,y = [W\lambda/(W + M)]\,(2\pi^2 v^2/\iota^2)\,\cos\,(2\pi vt/\iota) \tag{23}$$

Denoting $kg/(W + M) = p_0^2$, where p_0 represents the angular frequency of free vibration and $W\lambda/(W + M) = \lambda_0$, we then transform Eq. 23 to

$$\ddot{y} + p_0^2 \cdot y = (2\lambda_0 \pi^2 v^2/\iota^2)\cos\,(2\pi vt/\iota) \tag{24}$$

Additional Deflection

For the same initial conditions as those for fully supported case, the solution of differential Eq. 24 yields

$$y = (2\lambda_0 \pi^2 v^2/p_0\,\iota^2) \int_0^{t_1} \cos\,(2\pi vt/\iota)\,\sin\,p\,(t_1 - t)\,dt$$

or

$$y = \left(\lambda_0/[2\,[1 - (\iota^2/v^2)\,(p_0^2/4\pi^2)]]\right)\,[\cos\,p_0 t_1 - \cos\,(2\pi vt_1/\iota)] \tag{25}$$

If we denote $\iota/v = \tau_1$ (as before) and $\tau_0 = 2\pi/p_0$, Eq. 25 becomes

$$y = \{\lambda_0/[2\,(1 - \tau_1^2/\tau_0^2)]\}\,[\cos\,(2\pi t_1/\tau_0) - \cos\,(2\pi t_1/\tau_1)] \tag{26}$$

For any position of load along the low spot (Fig. 2), Eq. 26 may be further modified as

$$y/\lambda_0 = \{1/[2\,(1 - \tau_1^2/\tau_0^2)]\}\,\{\cos[(2\pi\iota'/\iota)\,(\tau_1/\tau_0)] - \cos\,(2\pi\iota'/\iota)\} \tag{27}$$

Equation 27, deduced in the foregoing, is of the same form as Eq. 10. If the variation of y/λ_0 with τ_1/τ_0 for 3 positions of load (i.e., $\iota' = \iota/4$, $^3/_8\iota$, and $\iota/2$) is drawn, an exactly similar set of curves as those shown in Figure 3 would be obtained.

Reaction Modulus

As before, $\Delta_{max} = W/k$. Except for cantilever overhang (1),

$$\Delta_{max} = WL^3/2EI_0 \tag{28}$$

where I_0 represents moment of inertia of the section of the cantilever at support. Therefore,

$$k = W/\Delta_{max} = 2EI_0/L^3 \tag{29}$$

Example

If we take the same example as that for the fully supported case, then W = 9,000 lb, L (effective) = 48 in., h = 8 in., I_0 = 2,896 in.^{4}, E = 4 × 10^6 psi, and Δ_{max} (from Eq. 28) = 4.296 × 10^{-2} in. With the 25 percent load transference at doweled joints reduced, Δ_{max} = 3.22 × 10^{-2} in. From Eq. 29, the reaction modulus k = 9,000/3.22 × 10^{-2} = 279,300 lb/in. Because M = bhγL/2, taking b = $\sqrt{2}$ × 48 in. and γ = 144 lb/cu ft, we get M = 1,086 lb. Because $p_0^2 = kg/(W + M)$, we get

$$p_0 = \tfrac{1}{2}\pi\ [(279{,}000 \times 32 \times 12)/(9{,}000 + 1{,}086)]^{1/2} = 17.20 \text{ cps}$$

Therefore, $\tau_0 = {}^1/_{17.20}$ sec. But because τ_1/υ, the ratio

$$\tau_1/\tau_0 = 17.20\ \iota/\upsilon \tag{30}$$

For ι = 4, 6, and 8 in. and υ varying between 10 and 73 ft/sec (i. e., 6.82 to 50 mph), the values of the ratio τ_1/τ_0 have been computed. The values of $(y/\lambda)_{max}$ may be obtained from Figure 3. The variation of $(y/\lambda)_{max}$ with υ for the present case has been worked out and is shown in Figure 4. The set of curves obtained is similar to that for the fully supported case.

FULLY SUPPORTED HIND SLAB

Because the low spot is situated at the confluence of 2 or more slabs (Fig. 1), the moving load while traversing the low spot is met with change in support and other conditions, such as discontinuity at joints between the hind and forward slabs and slope of the low spot. Thus, as soon as the load enters the low spot in the hind slab, it begins to accelerate because of the downward slope. On approaching the forward slab, however, the load experiences a retardation with corresponding increase in pressure on the slab and, hence, deflection.

For analysis of impact effect on the hind slab, the expression for the low spot configuration may be modified as follows with reference to the origin O′ (Fig. 2):

$$\eta = (\lambda/2)\ [1 - \cos\ (2\pi x/\iota)] \tag{31}$$

Forced Vibration

The equation for forced vibration from Eq. 5 is

$$(W/g)\ (d^2y/dt^2) + k \cdot y = -\ (W/g)\ (d^2\eta/dt^2) \tag{32}$$

Reckoning the time from the instant the load is at O′ and with υ as the load velocity so that x = υt, we find from Eq. 31 that

$$\eta = (\lambda/2)\ [1 - \cos\ (2\pi\upsilon t/\iota)] \tag{33}$$

Equation 32 can now be rewritten as

$$(d^2y/dt^2) + (kg/W)\ y = -\ (2\lambda\pi^2\upsilon^2/\iota^2)\cos\ (2\pi\upsilon t/\iota) \tag{34}$$

Additional Deflection

The solution of Eq. 34 yields additional deflection as

$$y = [\lambda/[2\ (1 - \tau_1^2/\tau^2)]]\ [\cos\ (2\pi t_1/\tau_1) - \cos\ (2\pi t_1/\tau)] \qquad (35)$$

For any position of load along the centerline of the low spot, Eq. 35 may be modified as

$$y/\lambda = \{1/[2\ (1 - \tau_1^2/\tau^2)]]\ \{\cos\ (2\pi\iota'/\iota) - \cos\ [(2\pi\iota'/\iota)\ (\tau_1/\tau)]\} \qquad (36)$$

where ι' represents the distance traveled by the load at any instant measured from O'. The values of y in terms of λ have been computed from Eq. 36 for different values of τ_1/τ, and 3 positions of load at $\iota' = \iota/4$, $^3/_8\iota$, and $\iota/2$ are shown in Figure 6. It may be seen that y is negative (upward deflection) when τ_1/τ is small, i. e., velocity is high. The overall maximum positive value of 0.42λ at $\tau_1/\tau = 1.65$ is attained for y as the load approaches the corner tip of the hind slab.

For the fully supported case, $\tau_1/\tau = 18.63\ \iota/\upsilon$ (see Eq. 14). Because positive additional deflection occurs for values of τ_1/τ greater than 1, the velocities chosen for analysis range from 2.0 to 12.4 ft/sec (i. e., 1.3 to 8.4 mph) for ι = 4, 6, and 8 in. The y/λ values may be obtained from Eq. 36. The variation of $(y/\lambda)_{max}$ with υ is sinusoidal in nature and is shown in Figure 7.

UNSUPPORTED HIND SLAB

Forced Vibration

Rewriting Eq. 22 for forced vibration by substituting the value of η from Eq. 33, we get

$$(d^2y/dt^2) + [kg/(W + M)]\ y = -\ [W\lambda/(W + M)]\ (2\pi^2\upsilon^2/\iota^2)\cos\ (2\pi\upsilon t/\iota) \qquad (37)$$

Additional Deflection

Using the usual notations and solving Eq. 37, we obtain

$$y/\lambda_0 = \{1/[2\ (1 - \tau_1^2/\tau_0^2)]]\ \{\cos\ (2\pi\iota'/\iota) - \cos\ [(2\pi\iota'/\iota)\ (\tau_1/\tau_0)]\} \qquad (38)$$

Comparing Eqs. 38 and 36 shows that they are exactly alike. Therefore, the curves shown in Figure 6 representing Eq. 36 would also be valid for Eq. 38.

For the present case, the ratio $\tau_1/\tau_0 = 17.20\ \iota/\upsilon$ (see Eq. 30). For the same range of values of ι, υ, and τ_1/τ_0 as in the previous case, the maximum positive values of the ratio y/λ have been computed. The values of $(y/\lambda)_{max}$ for different values of υ are shown in Figure 7.

EXPERIMENTAL INVESTIGATION

This section discusses experimental verification of some of the analytical findings obtained previously. The experiments cover only the fully supported corner case with and without low spot.

Low Spot

Two adjacent corners at an expansion joint between concrete pavement slabs in the internal road system of the Institute were selected for the investigation. An artificial low spot, as shown in Figure 2, was prepared by grinding the concrete surface near the corners and by applying 1:1 cement-sand mortar over the ground surface. Figure 8 shows the low spot. The width and total length of the low spot were 4 and 8 in. respectively. The maximum depth, λ, was measured to be 0.10 in. at its center. Because the width of the expansion joint was $^3/_4$ in., the low spot spread over a length of $3^5/_8$ in. on each corner. The sealing compound at the joint was chamfered to conform to the general shape of the low spot.

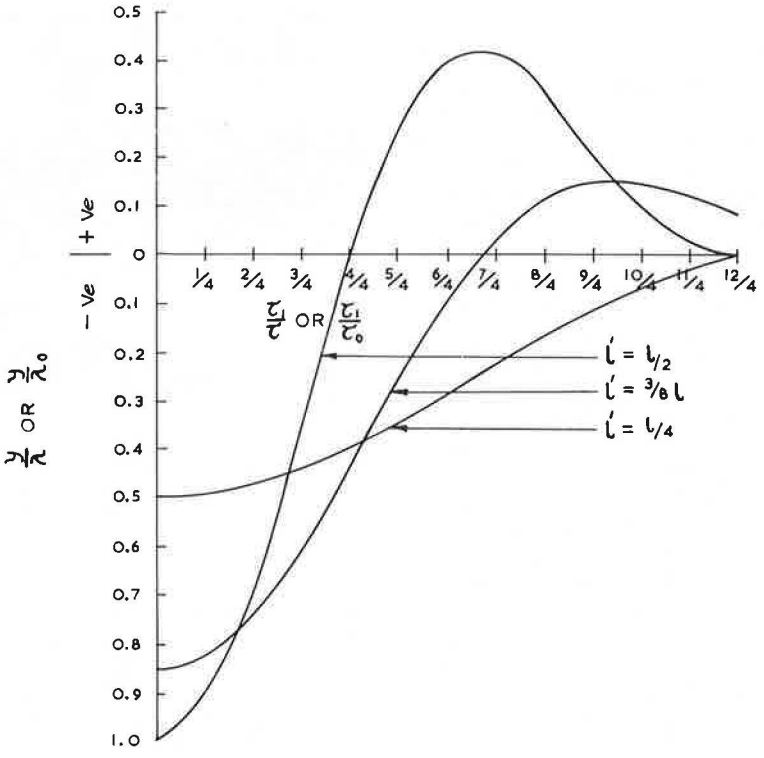

Figure 6. Additional dynamic deflection for hind slab under fully supported (y/λ vs τ_1/τ) and unsupported (y/λ_0 vs τ_1/τ_0) conditions.

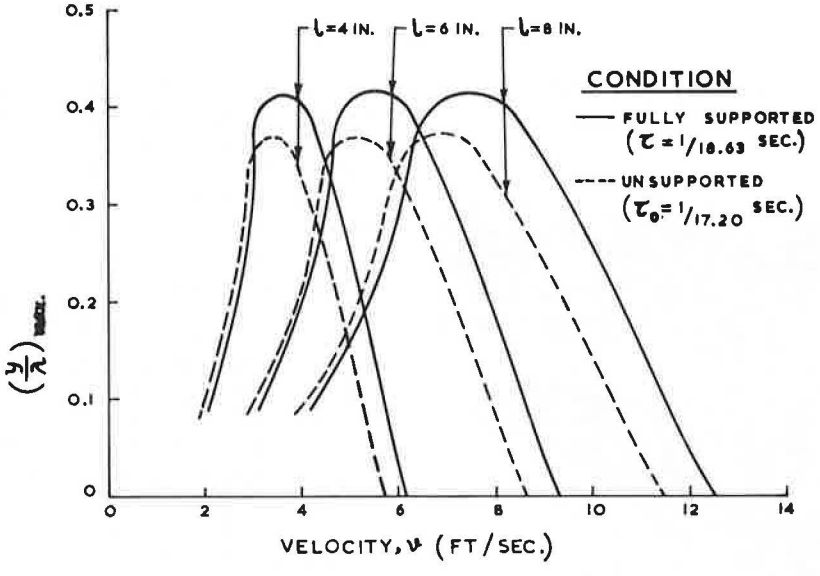

Figure 7. Maximum additional downward deflection for hind slab for different velocities of load.

Instrumentation

For measuring transient deflections caused by moving loads, a cantilever steel-strip deflectometer equipped with electrical resistance strain gages was used. Four strain gages of Hungarian Orion EMG type, each having a gage factor of 2.21 and a resistance of 120 ohms, were firmly bonded to the deflectometer, with 2 gages on each of the top and bottom surfaces at identical locations very close to the clamped end. The bridge was connected to the KWS/II-5 carrier frequency amplifier of German make (Hottinger Messtechnik). With the help of the amplifier, it was possible to have an indication of the static and dynamic responses from the movement of the recording needle. The static response could also be directly recorded through compensation by balancing the meter. The bridge-feeding was done by a 5,000 cps oscillator that also generated the switch voltage for the phase critical demodulator. The measuring voltage on the bridge output could be made visible by connecting it to a Phillips low-frequency oscilloscope. The maximum sensitivity of the oscilloscope was 2 mV/cm. The sweep time on the X-scale could be varied from 1 sec/cm to 5 μsec/cm. The vertical scale of the oscilloscope screen was calibrated for a known setting, and each small division corresponded to 0.0049 in. Figure 9 shows the general setup of the experiment.

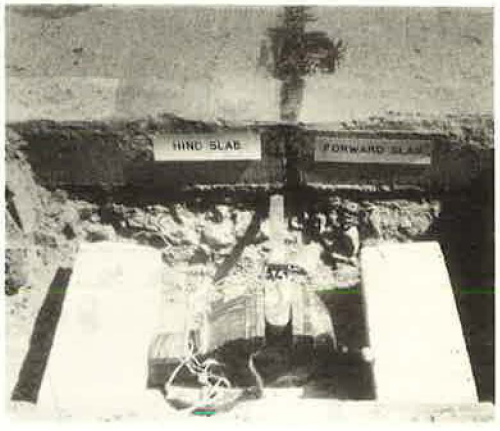

Figure 8. Test corners with low spot, with deflectometer pickup fixed under the hind slab 1 in. from center of expansion joint.

In the first series of experiments, the deflectometer tip was fixed at the bottom of the forward slab corner at a distance of 4 in. from the center of the expansion joint. In the second series, the deflectometer was placed under the hind slab corner, with its distance from the center of expansion joint being 1 in. The deflectometer assembly was protected from accidental damage during the test by being covered with a heavy steel plate.

Test Procedure

An empty Tata-Mercedes-Benz truck was used in the test. Its front and hind wheels on the right were made to traverse the test corners of 2 adjacent concrete slabs. Although the wheel load and tire pressure for both the front wheels were 2,352 lb and 82 psi respectively, those for the 2 dual-tire wheels in the rear were 2,464 lb and 84 psi respectively.

Figure 9. General setup of experiment, with amplifier and recording oscilloscope assembly shown on left.

The truck was operated to traverse the corners parallel to the longitudinal edge of the pavement at different speeds (4 to 37 mph). The static response was measured at crawl speeds of less than 1 mph. The correct position of the wheel from the edge was obtained from the tire imprint traced out by the tire on paper placed close to the corners.

The response of forward and hind slabs, with and without low spots, to a moving front wheel only was transmitted on an oscilloscope screen and photographed for each run. The dynamic deflections were computed from the photographic records

TABLE 1

LOAD TRANSFER AT JOINT UNDER STATIC LOADING CONDITION

Test	Slab That Wheel Is On	Deflection Under Load[a] (in.)	Deflection at Corner Tip of Adjacent Slab (in.)	Load Transferred (percent)
1	Forward	0.0539	0.0221	29.1
2	Forward	0.0539	0.0196	26.6
3	Forward	0.0539	0.0221	29.1
4	Hind	0.0515	0.0196	27.6
5	Hind	0.0515	0.0221	30.0
6	Hind	0.0515	0.0196	27.6
Avg				28.3

[a]When center of load is 4 in. from center of expansion point.

by measuring the peak ordinates for those runs in which the outward lateral deviation of the wheel from the longitudinal edge of the corners was 0 to 2 in. The exact speed of the truck for each run was computed from the distance between the front and rear wheels (14 ft) and the sweep time from oscilloscope records. The speedometer readings provided a rough check. Observations were also made for the static response of the forward slab corner when the front wheel was about to leave the hind slab but was still fully on it. In this position the center of load was 4 in. from the center of the expansion joint. Observations were also made of the hind slab corner with the wheel fully placed on the forward slab. From these observations, an average load transfer of 28.3 percent of wheel load at the joint could be calculated (Table 1). Responses were recorded for slabs with and without low spots.

Response of Forward Slab Without Low Spot

The maximum values of static deflection of the forward slab corner at crawl speed of the truck were recorded for different lateral positions of the front wheel. The variation in deflection for different positions of the wheel shown in Figure 10 indicated that

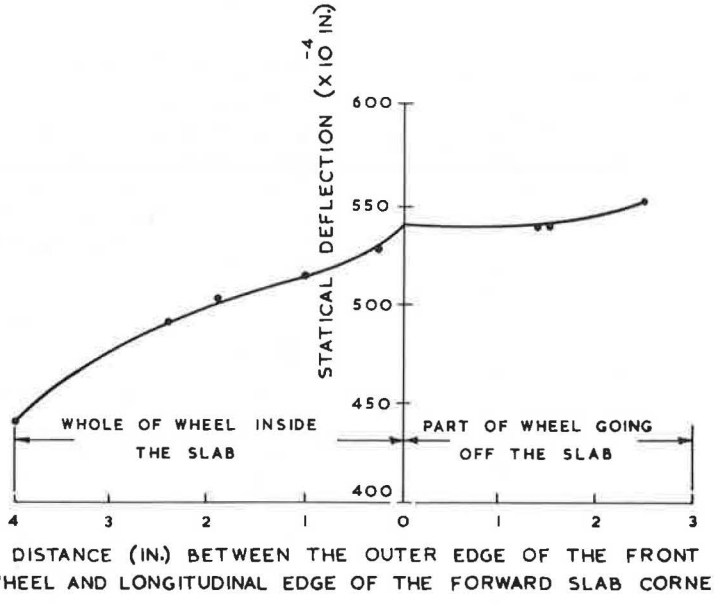

Figure 10. Variation in static deflection of the forward slab under front wheel resulting from lateral shift of latter.

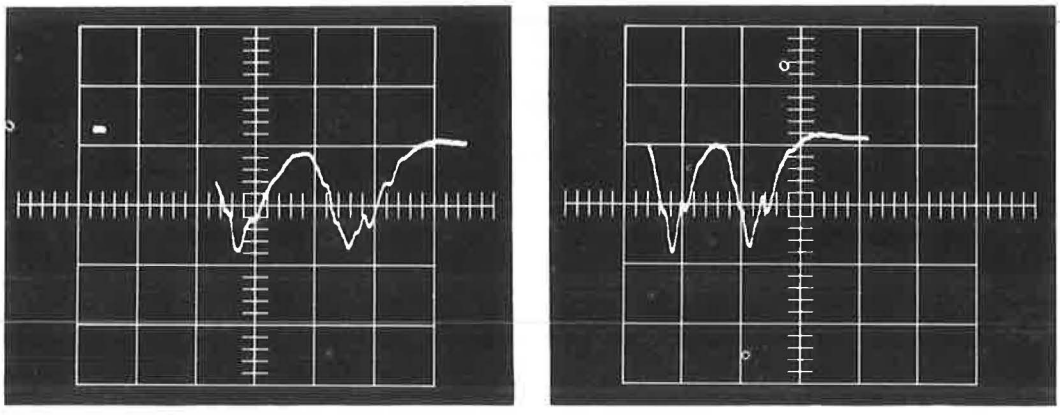

Figure 11. Kinetic response of forward slab corner without low spot: (a) speed = 39.0 ft/sec; and (b) speed = 51.5 ft/sec.

the deflection remained practically unaffected when the outer periphery of the wheel was off the edge up to 2 in. There was, however, a gradual decrease in deflection when the wheel was inside the slab but moving away from the edge.

Kinetic response of the forward slab corner was obtained by running the truck at different speeds ranging between 9.6 and 35 mph. Figure 11 shows typical photographic records of the response obtained for 2 speeds. The values of dynamic deflection for different speeds and lateral positions of the wheel are given in Table 2 and are shown in Figure 12.

Response of Forward Slab With Low Spot

In this case the truck was run at speeds between 11 and 37 mph. The typical photographic records of the responses for 2 speeds are shown in Figure 13. The test data are given in Table 2 and are shown in Figure 12.

TABLE 2

EXPERIMENTAL VALUES OF DYNAMIC DEFLECTION AT DIFFERENT SPEEDS

Slab	Test	Vehicle Speed (ft/sec)	Dynamic Deflection (in.)	Distance[a] (in.)
Forward without low spot	1	14.0	0.04655	-0.5
	2	27.5	0.04165	2.0
	3	35.0	0.04043	2.0
	4	36.8	0.03675	0.5
	5	39.0	0.03920	0.0
	6	51.5	0.03920	1.5
Forward with low spot	1	16.3	0.04900	2.0
	2	18.9	0.05390	2.0
	3	21.2	0.07105	1.0
	4	21.9	0.05880	0.0
	5	26.9	0.07350	0.0
	6	28.5	0.09065	0.5
	7	29.2	0.09310	2.0
	8	32.0	0.09675	1.0
	9	39.5	0.09675	0.0
	10	41.0	0.09800	0.0
	11	54.0	0.10535	-0.5
Hind with low spot	1	5.6	0.04655	0.0
	2	7.6	0.04900	1.0
	3	8.2	0.04900	2.0
	4	10.7	0.05390	0.5

[a]Distance of the outer periphery of the wheel from the longitudinal edge of the corner.

Response of Hind Slab

Photographic records of responses of the hind slab corner with and without low spots were obtained for speeds varying between 4 and 7 mph. A typical response record is shown in Figure 14. The results are given in Table 2 and are shown in Figure 15.

Comparison of Experimental Data With Theoretical Values

The experimental results of additional deflection were compared with the values obtained from theoretical analysis.

Reaction Modulus—For W = 2,352 lb, h = 3.7 in., K = 500 pci, μ = 0.2, and $E_{dyn} = 1.3 \times 4 \times 10^6$ psi under impact loading (30 percent increase assumed over the E_{stat} value, 2), Δ_{max} from Eq. 13 worked out to be 0.02419 in. when full load was transfered. However, because 28.3 percent of the load got transferred through

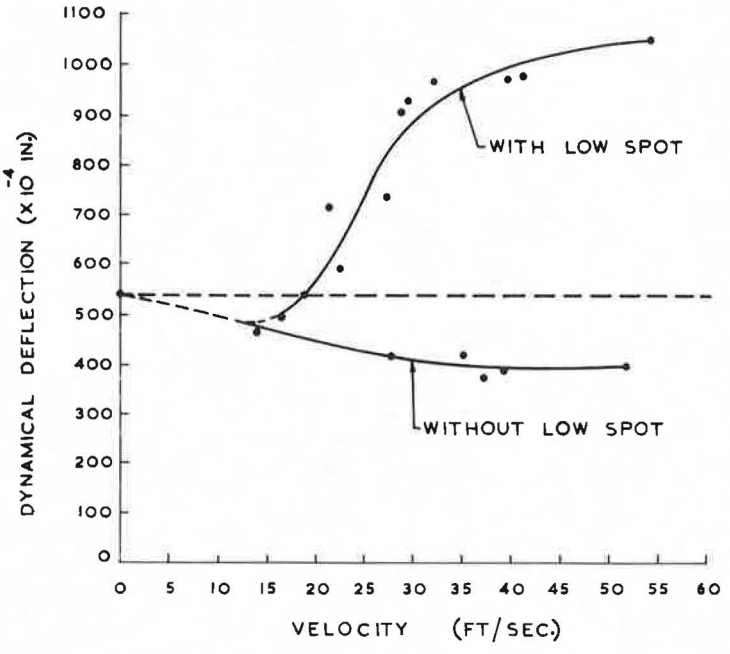

Figure 12. Experimental results of dynamic deflection of forward slab corner (at distance of 4 in. from center of expansion joint) with and without low spot for different load velocities.

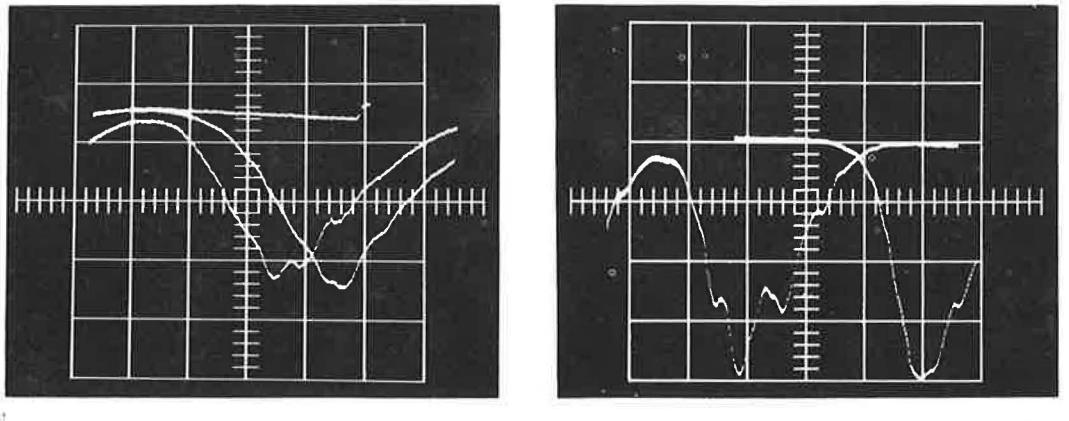

Figure 13. Kinetic response of forward slab corner with low spot: (a) speed = 26.9 ft/sec; and (b) speed = 41.0 ft/sec.

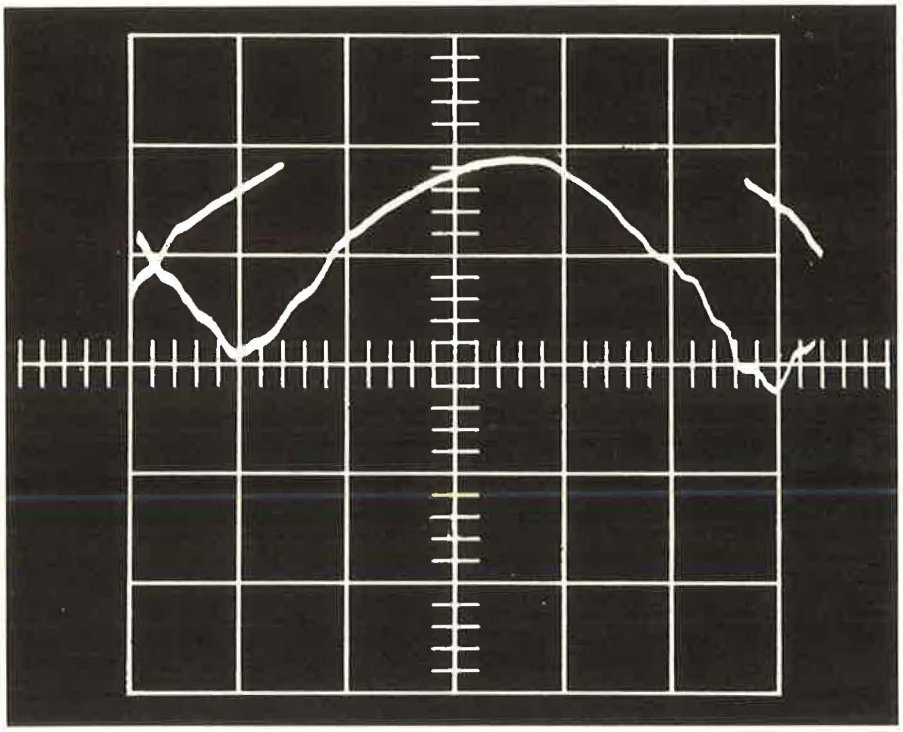

Figure 14. Kinetic response of hind slab corner with low spot (speed = 5.6 ft/sec).

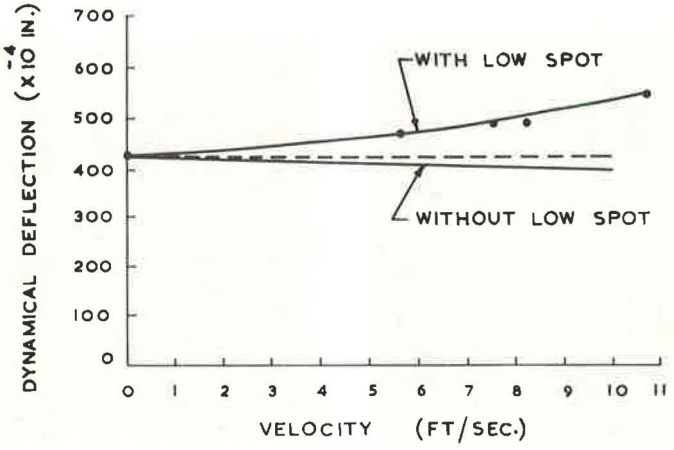

Figure 15. Experimental results of dynamic deflection of hind slab corner (at distance of 1 in. from center of expansion joint) with and without low spot for different load velocities.

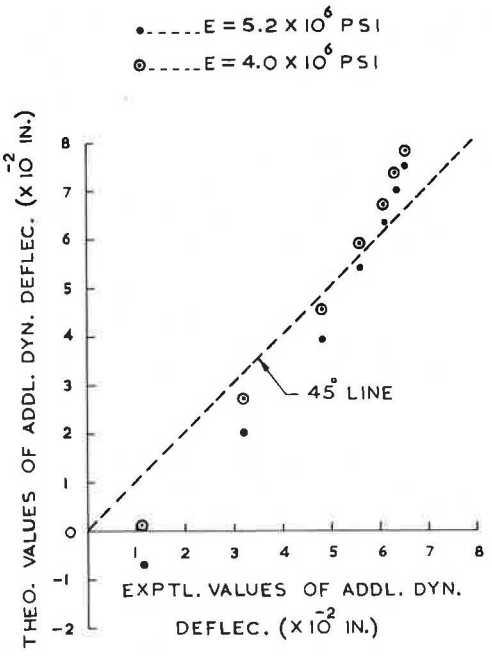

Figure 16. Comparison of theoretical and experimental values of additional dynamic deflection of forward slab.

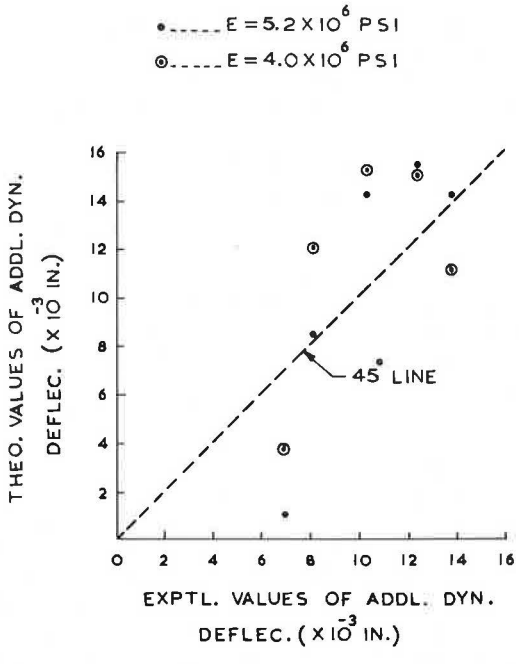

Figure 17. Comparison of theoretical and experimental values of additional dynamic deflection of hind slab.

the joint, Δ_{max} was equal to 0.717 × 0.02419 in. The value of k derived from Eq. 11 was 135,600 lb/in.

Free Period of Vibration—In the relationship $p^2 = kg/\bar{W}$, $\bar{W}$ is the amount of effective load in contact with the low spot causing additional dynamic deflection. With contact area of the front wheel and total area of low spot on the forward slab being 28.7 in.^{2} and 16 in.^{2} respectively, $\bar{W} = 2{,}352 \times {}^{16}/_{28.7} = 1{,}310$ lb. Hence,

$$p = {}^{1}/_{2\pi}\,[(135{,}600 \times 32 \times 12)/1{,}310]^{1/2} \text{ cps}$$

or p is equal to 31.8 cps. Therefore, τ is equal to ${}^{1}/_{31.8}$ sec.

Additional Deflection

Forward Slab—For $\tau = {}^{1}/_{31.8}$ sec, $\tau_1/\tau = 31.8\ \iota/\upsilon$. The values of τ_1/τ were calculated for $\iota = 8$ in. and $\upsilon = 20$ to 50 ft/sec. The values of y/λ and, hence, of y (with $\lambda = 0.10$ in.) could now be obtained either from Eq. 10 or more readily from values shown in Figure 3, taking $\iota' = \iota/2$. The theoretical and experimental values of y, the latter being obtained from the mean curve shown in Figure 12, were compared as shown in Figure 16, which also includes the values for E = 4.0 × 10^6 psi.

Hind Slab—For $\tau_1/\tau = {}^{1}/_{31.8}\ \iota/\upsilon$, $\iota = 8$ in., and $\upsilon = 6$ to 10 ft/sec, the values of τ_1/τ were calculated. From these, the values of y/λ and y could be computed either from Eq. 36 or more readily from values shown in Figure 6, for $\iota' = ({}^{3}/_{8})\ \iota$. The theoretical and experimental values of y are shown in Figure 17.

DISCUSSION AND SUMMARY

1. The objective of the investigation is to determine the additional dynamic deflection of rigid pavement from the impact of a wheel load movement over the low spot in the

corner region of the slab. Readily usable formulas and graphs, which are reported in the paper to determine additional dynamic deflection of both forward and hind slab corners for different conditions of support, allow an easy application of the findings. The theoretically determined values for some selected cases have been compared with the experimental results.

2. The additional deflection is proportional to the depth, length, and slope of low spot, load velocity, and elastic reaction modulus of the slab, depending on support condition. Even though the theoretical curves for additional deflection for both the support conditions (fully supported and unsupported) are similar for either hind or forward slab, those for hind and forward slabs are basically different. The maximum deflection for the forward slab is reached when the load is just leaving the low spot and the vehicle is traveling at high speeds. In the case of the hind slab, the maximum additional deflection at high speeds is always negative, i.e., upward in direction. Positive downward deflection of lower magnitude, however, occurs at lower speeds, and the maximum is induced when the load just leaves the hind slab.

3. For a low spot length over both the hind and forward slabs of 4 to 8 in., slab thickness of 8 in., and effective corner length of 48 in., the maximum positive additional deflections (theoretically determined) in the hind slab do not vary with the length of the low spot and are of the magnitude of 0.415λ and 0.372λ for fully supported and unsupported conditions respectively, where λ is the depth of the low spot. These occur at low speeds of 2.5 to 3.5 ft/sec, 4.5 to 5.5 ft/sec, and 6.5 to 7.5 ft/sec for the 4-, 6-, and 8-in. lengths of the low spot respectively.

4. For the same conditions as in the preceding, the maximum positive deflection (theoretically determined) of the forward slab occurs at a speed of about 70 to 75 ft/sec and approaches the values of 0.96 to 1.0λ and 0.86 to 0.89λ for fully supported and unsupported conditions respectively. The difference between the maximum values for fully supported and unsupported conditions is 0.10 to 0.11λ at high speeds, the deflection in the unsupported slab always being lower in magnitude. When the length of the low spot is increased from 4 to 8 in., the maximum positive deflection is reduced by only 3 to 4 percent.

5. The tests have been conducted on fully supported concrete pavement slabs of a 3.7-in. thickness laid over a W.B.M. subbase (K-value $\approx$ 500 pci). In all the cases within the purview of the tests, there is a gradual reduction in the dynamic deflection with increase in speed of the vehicle when there is no low spot. At a speed of 50 ft/sec (34 mph), the reduction is 27.5 percent when compared to the value at crawl speed (i.e., static condition). With a low spot, the dynamic deflection of the forward slab corner increases very rapidly with speed up to about 50 ft/sec (34 mph), after which the curve is asymptotic. At this speed, the additional positive dynamic deflection due to the low spot is 167 percent of the dynamic deflection when no low spot is present. This amounts to an increase of 94.5 percent in deflection over the static value.

6. The experiment further shows that the dynamic deflection of the hind slab corner also increases with speed of the vehicle when a low spot is present. The increase is 25 and 35 percent over the static condition and the case when no low spot is present respectively for a vehicle speed of 10 ft/sec (6.8 mph). Because, as indicated by theoretical analysis, at high speeds the dynamic deflection of the hind slab corner with a low spot is always lower than it is when no low spot is present, the experiment has been conducted only at low speeds.

7. The comparison of the values of theoretically determined and experimentally obtained additional dynamic deflection shows that they are in good agreement with each other. The agreement in the case of forward slab is, however, more satisfactory. The slight difference between the theoretical and experimental values may be attributed to inaccuracies in theoretical assumptions in the spread and nature of load, value of dynamic modulus of elasticity, K-value of the subbase, and the like. Although in reality the load is of a distributed nature, it has been assumed to be concentrated in the theoretical analysis. There is also the possibility that part of the vibrations of the wheel being transmitted to the body of the vehicle may cause an alteration of the vertical pressure of the springs on the axle. This may happen when the frequency of the wheel is not large in comparison to that of the body of the vehicle.

8. The analysis made in this paper serves to highlight the progressive detrimental effect of the surface irregularities such as low spots on rigid pavement under moving loads and to stress the necessity of exercizing adequate controls during construction of new pavements and proper maintenance of the existing pavement.

ACKNOWLEDGMENT

Acknowledgment is due to B. Subbaraju, Director of the Central Road Research Institute, New Delhi, for his keen interest in pursuit of this study. The paper is published with his permission.

REFERENCES

1. Ghosh, R. K., Lal, R., and Vijayaraghavan, S. R. An Approximate Analysis for Kinetic Response of Triangular Cantilever Overhang. Jour. Australian Road Research Board, Vol. 3, No. 2, June 1967.
2. Taylor, W. H. Concrete Technology and Practice, 2nd Ed. Angus and Robertson Ltd., 1967, p. 218.
3. Timoshenko, S., and Young, D. H. Vibration Problems in Engineering, 3rd Ed. D. Van Nostrand Co., Inc., New York, 1955.
4. Warburton, G. B. The Dynamical Behavior of Structures. Macmillan Co., New York, 1964.
5. Westergaard, H. M. Stresses in Concrete Pavements Computed by Theoretical Analysis. Public Roads, Vol. 7, No. 2, 1926, pp. 25-35.

METHOD FOR SEPARATELY EVALUATING STRUCTURAL PERFORMANCE OF SUBGRADES AND OVERLYING FLEXIBLE PAVEMENTS

Nari K. Vaswani, Virginia Highway Research Council

The structural evaluation of flexible pavements is now carried out mostly with deflection-measuring devices such as the Dynaflect or the Benkelman beam. The object of the investigation reported here was to determine whether the properties of the deflected basin measured by these devices on the pavement surfaces could make it possible to evaluate the subgrade and the overlying pavement together and separately. In this investigation it was found that, by means of theoretical and field studies, the maximum and other deflections in the deflected basin could be used to evaluate the strength of the subgrade before the pavement is laid over it, the strengths of the subgrade and pavement separately after the pavement is laid, and the change in strength of the subgrade and pavement due to seasonal changes or age. A general chart was developed that correlates maximum deflection and spreadability with the subgrade strength, the average pavement strength, and the thickness index of the pavement. This chart was tested for separate structural evaluations of the subgrade and its overlying pavement for projects in Virginia. Ten typical examples of the projects are given in the paper.

•AN INCREASE in the development of sophisticated equipment for use in evaluating the structural performance or strength of pavements occurred following publication of the WASHO Road Test results. In spite of the availability of this equipment, many states, including Virginia, have been unable to determine whether failures or changes in the structural behavior of flexible pavements are attributable to the subgrade only, the pavement over the subgrade, or both the subgrade and the pavement.

The surface deflections of a pavement have proved to be a very valuable indicator of the structural performance of the pavement as a whole, including its subgrade. Most states, including Virginia, have equipment for measuring these deflections. The commonly adopted apparatus is the Benkelman beam. The Dynaflect is being used in Virginia and in some other states. Both measure the maximum and other vertical displacements within the deflected basin. In this investigation, Dynaflect data were used to determine the contribution of the subgrade and the overlying layers to the structural behavior of the flexible pavement.

SCOPE AND PURPOSE

A theoretical evaluation was conducted in this investigation in which maximum deflection data and other available measurements of displacements in the deflected basin were used to evaluate the strength of the subgrade separately from the strength of the overlying pavement and, thus, to determine the amount of change in the strength of the subgrade separately from the change in the strength of the overlying pavement. The study was divided into 3 parts as follows:

1. Theoretical determination of the thickness-equivalency values of materials having different moduli of elasticity and Poisson's ratios;

Sponsored by Committee on Flexible Pavement Design and presented at the 50th Annual Meeting.

2. Development of a pavement evaluation chart that evaluates the subgrade strength separately from the pavement strength; and
3. Application of the pavement evaluation chart for evaluating the subgrade before the pavement is laid and the subgrade and overlying layers separately after the pavement is laid at any time of the year.

VARIABLES, CONSTANTS, AND ASSUMPTIONS

The dependent variables in this investigation were the maximum deflection of the deflected basin and the spreadability of the deflected basin. The spreadability is the average deflection in percent of the maximum deflection and, in this investigation, was taken as follows:

$$\frac{d_{max} + d_1 + d_2 + d_3 + d_4}{5\, d_{max}} \times 100 \text{ percent} \quad (1)$$

where

d_{max} = maximum deflection of the pavement, as measured in the field and d_o, when theoretically calculated; and
d_1, d_2, d_3, d_4 = deflections at 1, 2, 3, and 4 ft from the center of the applied load.

The Dynaflect equipment used in Virginia measures all the deflections of the basin at one setting. The correlation between the Dynaflect and the Benkelman beam as measured in Virginia is given by the relationship d_{max} of the Benkelman beam = 28.6 d_d of the Dynaflect (1).

In the theoretical evaluation, the materials in the layered system were assumed to be elastic, isotropic, and homogeneous, and it was assumed that there was a perfect bond between the adjacent layers. A Chevron computer program (2) was used for this evaluation. A maximum wheel load of 9,000 lb, as allowed in Virginia (3), was chosen for use in the investigation. The tire pressure was taken as 70 psi over a circular contact area having a radius of 6.4 in.

Pavement systems with layers of decreasing strength from the top of the pavement toward the subgrade were taken into consideration. Neither the sandwich layer system nor the case of weaker layers over stronger layers is included in the results because of their different behavior. This difference in behavior is reported from studies (4) conducted prior to this investigation.

THEORETICAL EVALUATION OF SUBGRADE PROPERTIES

Based on Boussinesq's and Terzaghi's (5) analyses, the following simple relationship for displacements in a deflected basin of the top horizontal surface has been drawn for a semi-infinite single-layer system:

$$d_r = \frac{P}{E_S} \cdot \frac{(1 - u_s^2)}{f(r)} = \frac{d_o}{f(r)} \quad (2)$$

where

d_r = deflection in the deflected basin at a distance r from the load center;
P = applied load;
u_s = Poisson's ratio of the subgrade material in the layer;
E_S = modulus of elasticity of the material in the layer; and
f (r) = function of r, the distance from the center of the applied load.

Based on Eq. 2, the deflection values in the deflected basin were calculated for various values of E_S, u_S, and P. It was found that, for all values of E_S and u_S, the deflections at any point in terms of the maximum deflection d_o were constant. The deflections for a 9,000-lb wheel load, a 70-psi tire pressure, and a 6.4-in. radius at 1, 2, 3, and 4 ft from the center of the applied load were found to be 0.277 d_o, 0.134 d_o, 0.089 d_o, and 0.067 d_o respectively.

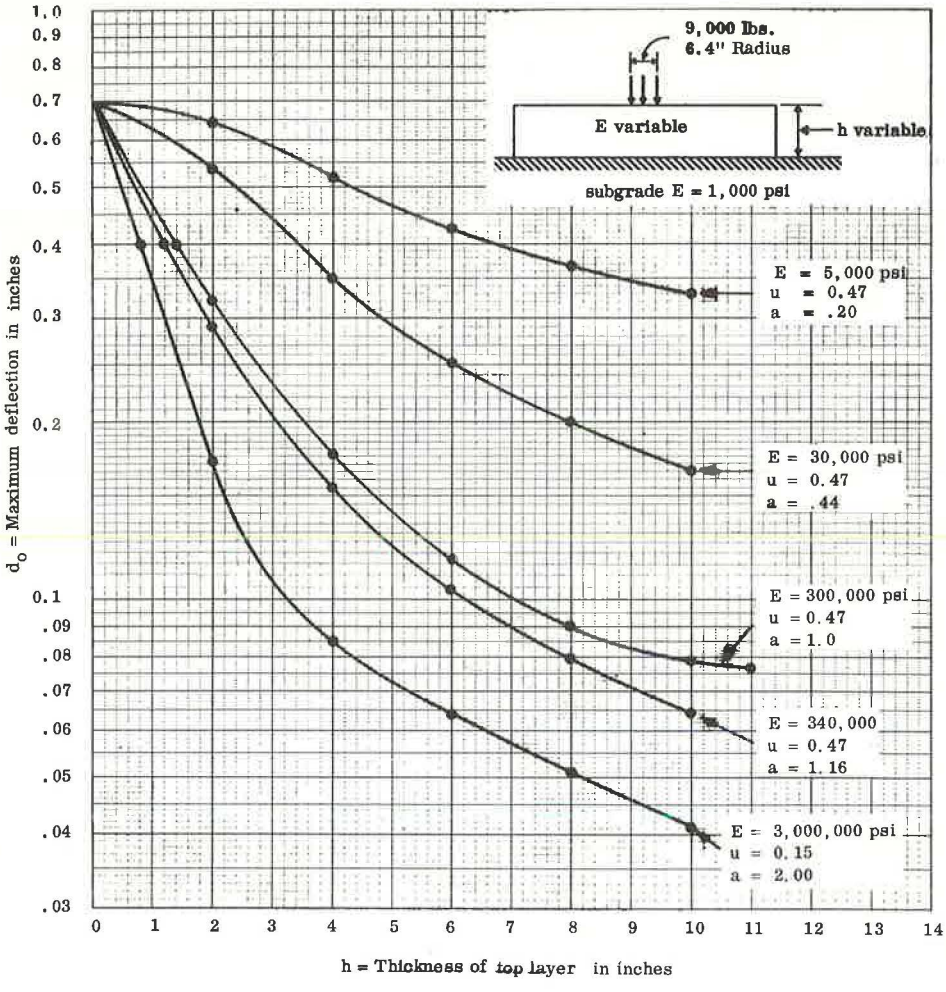

Figure 1. Evaluation of thickness-equivalency values.

The investigations carried out on projects in Virginia also showed that the deflection is a function not only of the strength of the pavement structure over the subgrade but also of the strength of the subgrade. A 1969 investigation (7) gave the following equation: $\log d_o + 0.043$ (D + subgrade factor) = 0.32. This equation could also be converted in the general equation to the form log d + a log (D + subgrade factor) = b, where a and b are constants. Figure 2 (main curves, left to right) shows how the subgrade strength contributes toward the decreased deflections.

INTERACTION OF SUBGRADE AND PAVEMENT OVER SUBGRADE WITH MAXIMUM DEFLECTION AND SPREADABILITY

For u = 0.47 and P = 9,000 lb it was found that Eq. 2 reduces to the form $E_S \times d_o$ = 700 lb/in. Based on this computation, the 2 horizontal scales shown in Figure 2 have been drawn along the base line to show the relationship between the modulus of elasticity of the subgrade (without an overlying layer, i.e., at D = 0) and the maximum deflection d_{max} or d_o. This figure shows that at the base line the spreadability of the subgrade is 31.35, irrespective of the modulus of elasticity of the subgrade, when D = 0.

Thus, the spreadability of a semi-infinite subgrade material for any value of E_S and u_S for a 9,000-lb wheel load was found to be constant as follows:

$$\text{Spreadability} = \frac{d_o + 0.277\,d_o + 0.134\,d_o + 0.089\,d_o + 0.067\,d_o}{5\,d_o} \times 100 = 31.35$$

The value of d_o varies with the values of E_S and u_S. If u_S is kept constant, the value of E_S will have to be proportionately changed to get the same value of maximum deflection d_o.

THICKNESS INDEX AND SUBGRADE FACTOR

In the AASHO Road Test, the resistance to deflection or the structural behavior of a pavement was defined by the following model equation:

$$\log d_{max} = a_0 + a_1h_1 + a_2h_2 + a_3h_3 + \ldots = a_0 + D \qquad (3)$$

where

a_0 = a constant;
a_1, a_2, a_3 = coefficients of relative strength and are termed thickness equivalencies in this investigation and could be defined as equivalent strengths per inch depth of the material in a given layer;
h_1, h_2, h_3 = thicknesses of the layers having thickness-equivalency values of a_1, a_2, and a_3 respectively; and
D = thickness index and is equal to $a_1h_1 + a_2h_2 + a_3h_3$.

The thickness equivalencies of the materials for given moduli of elasticity were theoretically determined by calculating maximum deflections with a top layer of a given modulus of elasticity resting over a subgrade with a modulus of elasticity of 1,000 psi. Figure 1 shows the relationship between the maximum deflection and the thicknesses of the top layers with given moduli of elasticity.

To determine the theoretical thickness equivalency of each of these materials required that the thickness equivalency of 1 material be assumed as unity. The thickness equivalency of the material with a modulus of elasticity E of 300,000 psi was assumed to be equal to 1.0. An example of evaluating the thickness equivalency of a material is as follows. In Figure 1, for $d_o = 0.35$, the thickness of the layer with E = 30,000 psi is 4 in., whereas the thickness of the layer with E = 300,000 psi for the same value of d_o is 1.8 in. Thus, the thickness equivalency of the material with E = 30,000 psi at $d_o = 0.35$ is equal to 1.8/4 = 0.45. In a similar manner, the thickness equivalency of the material having an E of 30,000 psi is determined for different values of d_o from Figure 1. An average of the thickness-equivalency values so obtained is considered as the thickness equivalency of the material having an E of 30,000 psi. It was found that there was very little difference between the thickness equivalencies obtained for the same material with varying amounts of deflections. The thickness equivalencies of the materials so determined are shown in Figure 1.

An evaluation was carried out to determine whether the thickness-equivalency values so determined would satisfy Eq. 3 given previously. This was done by evaluating 2- and 3-layer systems with varying thicknesses and moduli of elasticity of the layers overlying the same subgrade as shown in Figure 1. The correlation between log d_o and the log of the thickness index D was found to be good, with a correlation coefficient of 0.985 and a standard error of estimate of 0.098 in the equation $\log d_o + 0.92 \log D = -0.173$.

It may be pointed out that in 1968 a similar type of relationsip was developed from projects in Virginia. This relationship was $\log d_{max} + 0.068\,D = 2.06$ (6). The relationship could be converted in the general equation to the form $\log d_o + \bar{a} \log D = b$ as determined by the theoretical evaluation mentioned previously, where a and b are constants of the equation.

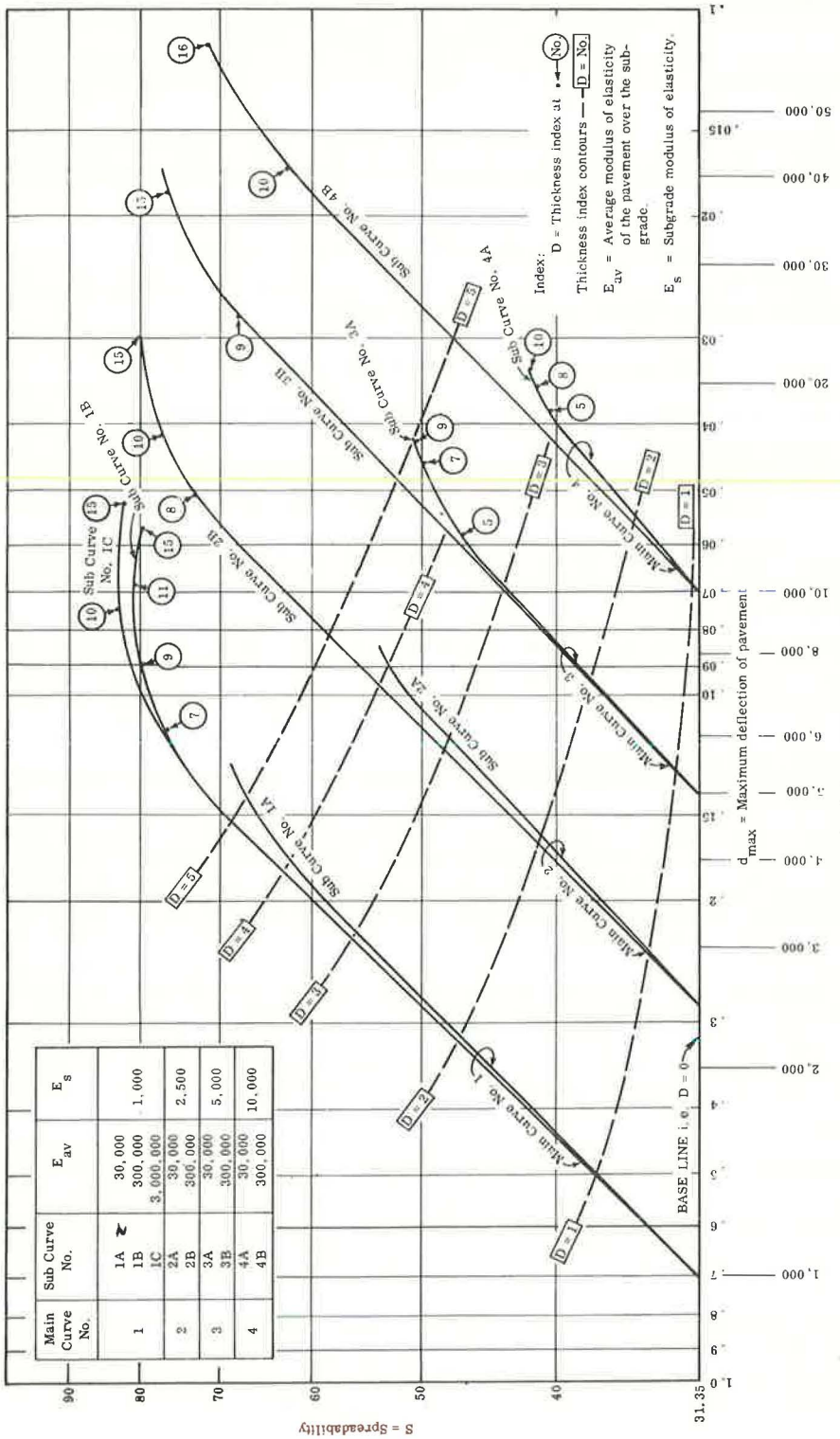

Main Curve No.	Sub Curve No.	E_{av}	E_s
1	1A	30,000	1,000
	1B	300,000	
	1C	3,000,000	
2	2A	30,000	2,500
	2B	300,000	
3	3A	30,000	5,000
	3B	300,000	
4	4A	30,000	10,000
	4B	300,000	

Figure 2. General evaluation chart for determining changes in subgrade or pavement strength of flexible pavements or both.

Pavement layers over the subgrade increase the spreadability while reducing the deflection. In some cases it may be possible to determine the amount of decrease in deflection caused by the overlying pavement layers. If this is determined, then the deflection of the subgrade could be calculated by adding this decrease in deflection to the total deflection determined on the top of the pavement. The deflection of the subgrade, along with the spreadability value of the pavement over the subgrade, will make it possible to determine the modulus of elasticity of the subgrade, the thickness index of the pavement, and the average modulus of elasticity of the pavement layers.

In Figure 2, 4 main curves have been shown. Each is for a different modulus of elasticity of the subgrade, and each is divided into subcurves. The subcurves—A, B, and sometimes C—for each of the main curves have pavement layer moduli of elasticity of 30,000, 300,000 and 3,000,000 psi respectively. Thus, if the maximum deflection and spreadability values are known, the subgrade modulus of elasticity, the thickness index of the pavement, and the average modulus of elasticity E_{av} of the pavement could be determined. For example, given d_o = 0.078 in. and S = 60, from Figure 2 it is found that E_s = 2,500 psi, D = 5.0, and E_{av} of the pavement = 300,000 psi.

The main curves shown in Figure 2 are almost parallel to each other. The spacing among them is based on the maximum subgrade deflection or on the modulus of elasticity of the subgrade. Once the subgrade deflection or modulus of elasticity of any subgrade is known, the main curve for deflection versus spreadability can be extrapolated.

The extrapolation of the subcurves is not based on a simple arithmetic relationship like that shown for the main curves. This is evident from curves 1A, 1B, and 1C for the pavements (over the subgrade) having moduli of elasticity of 30,000, 300,000, and 3,000,000 psi respectively. For the same modulus of elasticity of the subgrade, the spacing among the subcurves increases with an increase in the modulus of elasticity of the pavement over the subgrade. This change tends to zero along the tangent lengths of the curves but becomes more prominent when the curves bend. It may, therefore, be necessary to calculate and plot more curves between these bends to facilitate extrapolation.

Each of the subcurves shown in Figure 2 was determined by assuming that there is a uniform modulus of elasticity of the pavement over the subgrade. In practice the pavement consists of materials in layers with different moduli of elasticity. In that case, an average modulus of elasticity of the pavement E_{av} needs to be determined. As an example, a 3-layer system is discussed in the following, and its results are shown in Figure 3. In this example, the modulus of elasticity E_1 of the top layer is taken as 300,000 psi, and the modulus of elasticity E_2 of the second layer from the top is taken as 30,000 psi. The subgrade modulus of elasticity E_s is equal to 1,000 psi, which represents curve 1 of the general evaluation chart shown in Figure 2. The thicknesses of the top and the second layers were varied. Three cases were taken with the top layer thicknesses equal to 2, 4, and 6 in. respectively. In each case, the thickness of the second layer was varied from 0 or 2 in. up to 8 in. These 3 cases are shown in Figure 3 by curves a, b, and c. Figure 3 shows that all 3 curves a, b, and c lie within subcurves 1A and 1B, which are for the pavements having the moduli of elasticity of the pavement over the subgrade equal to 30,000 and 300,000 psi respectively. These 3 curves show that, as the average modulus of elasticity of the pavement layers over the subgrade increases, the curves move from subcurve 1A (E = 30,000 psi) toward subcurve 1B (E = 300,000 psi). The average modulus of elasticity E_{av} of the pavement over the subgrade could be calculated from the following equation:

$$E_{av} = \frac{h_1E_1 + h_2E_2 + \dots}{h_1 + h_2 + \dots} \qquad (4)$$

The preceding discussion and Figure 3 show that the curves with more than 2 layers could be extrapolated in the general evaluation chart shown in Figure 2 by evaluating the average modulus of elasticity E_{av}.

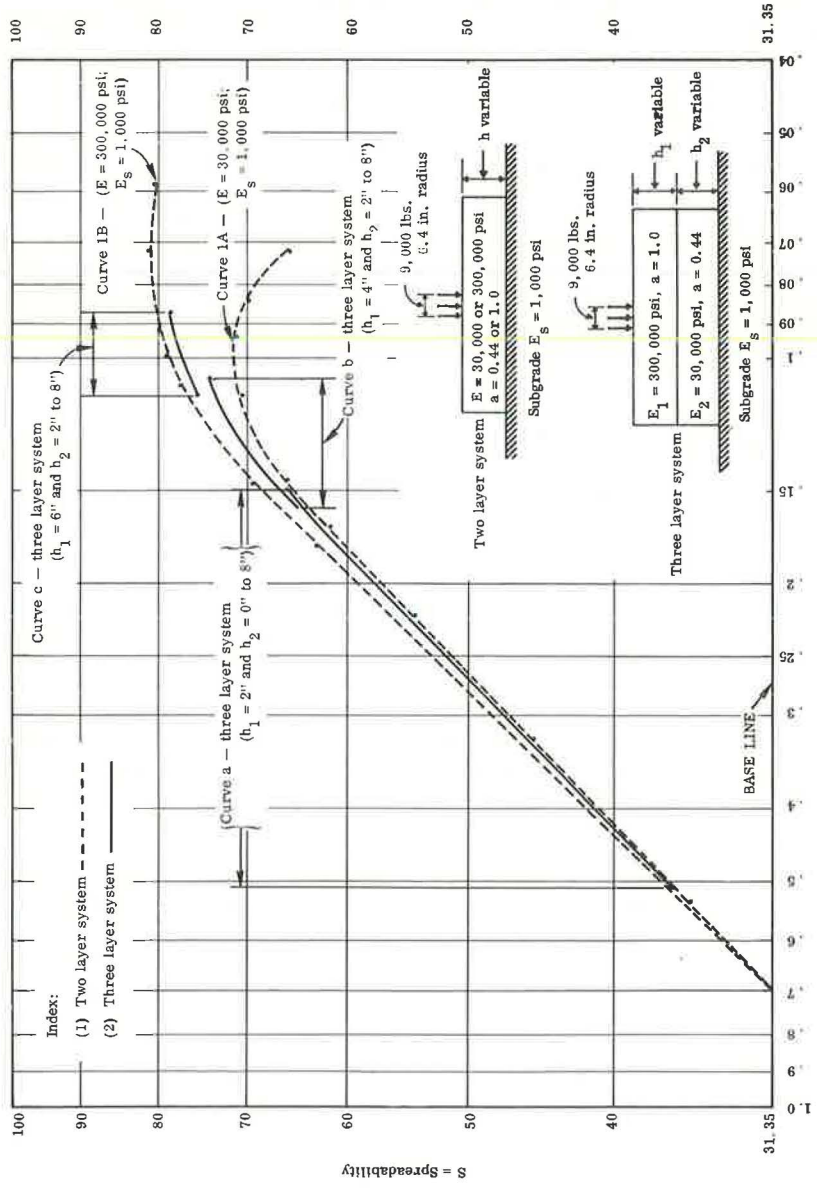

Figure 3. Fitting 3-layer system into curve 1 of general evaluation chart.

BEHAVIOR OF SUBGRADES IN PRACTICE AND THEIR EVALUATION

In the theoretical analysis, as explained previously, the spreadability of a uniform elastic subgrade was found to be constant, that is, 31.35. Measurements of the subgrade deflections of projects in Virginia have shown that the spreadability value of the subgrade varies and is usually greater than 31.35, but in extremely poor soils the value is less than 31.35. Because the projects show that the spreadability values of the subgrade are not constant as defined by a theoretical single-layer system, it is necessary that in practice the subgrade be considered a combination of 2 or more layers with their combined strengths being defined not only by the maximum deflection but also by the spreadability value. The need for specifying the spreadability value in addition to the deflection value is evident in the following discussion.

Evaluations of some of the very poor subgrades in Virginia have shown that, when the spreadability is less than 31.35, the subgrade is of a poor quality. When the value is less than 31.35, the subgrade could be considered equivalent to a layered system with a weaker layer lying over a stronger layer. Figure 4 shows 3 theoretical cases in the 2- and 3-layered systems wherein a weaker layer lies over a stronger layer. In each case the spreadability value is less than 31.35. The main curves, 1 through 5, have been calculated in the same manner as the 4 curves shown in Figure 2 and have spreadability values greater than 31.35. The 2-layer systems shown by curves b and c are for layers of E = 1,000 psi and E = 250 psi respectively, with both being over a stronger layer of E_S = 30,000 psi. Curve a is for a layer similar to that of curve b but has in addition a 2-in. layer of E = 30,000 psi. Curve a is shown as a typical example of a silty clay soil with the top 2 in. having dried to form a thick, rigid crust over the weaker moist subgrade. After the pavement is built, this top crust could regain moisture and behave like the 2-layer system defined by curve b.

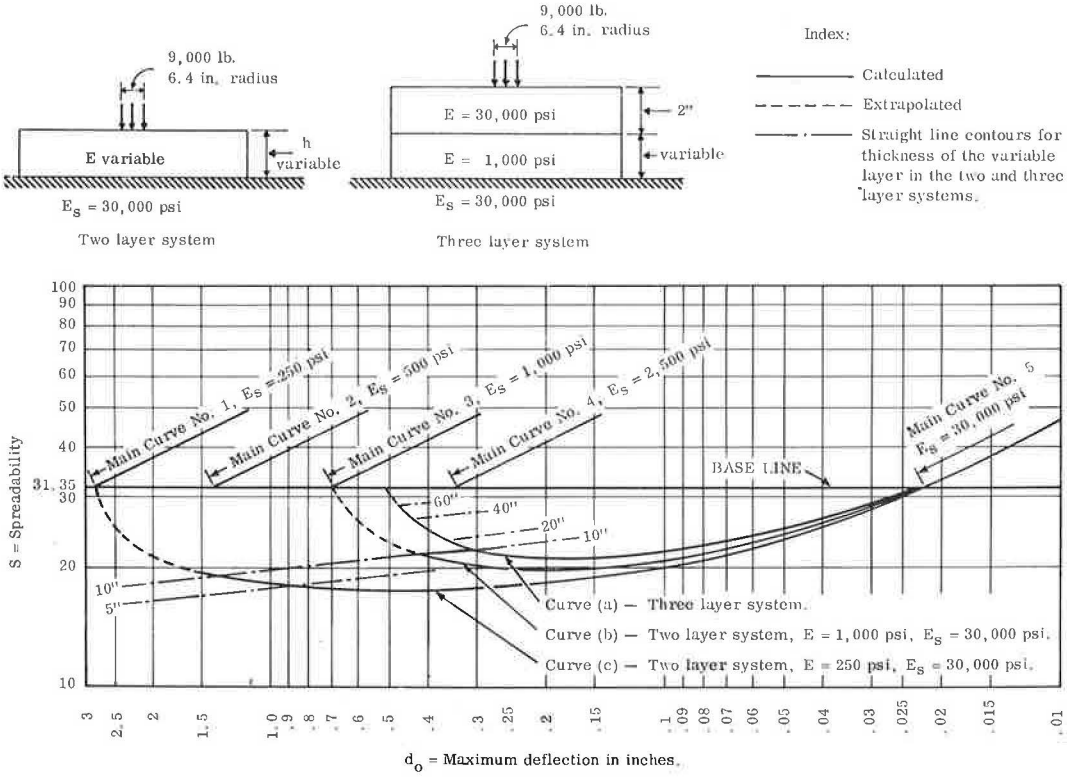

Figure 4. Examples of spreadability values lower than those given by a single-layer system.

Numerous cases were evaluated theoretically for spreadability values above and below 31.35. For cases of the former, there was no negative (upward) deflection in the deflected basin; for all cases of the latter, there was a deflection. Furthermore, as the spreadability value decreased, the location of the negative deflection in the deflection basin tended to approach the load center, which provides a higher slope in the deflected basin. Figure 5 shows 4 theoretical examples of such negative deflections. Thus, Figure 4 shows that, as the spreadability value continues to decrease below 31.35, the subgrade support should be considered poorer and poorer.

Figure 4, in combination with Figure 2, could be used to evaluate the structural strength of the subgrade from the deflection and spreadability data obtained from the

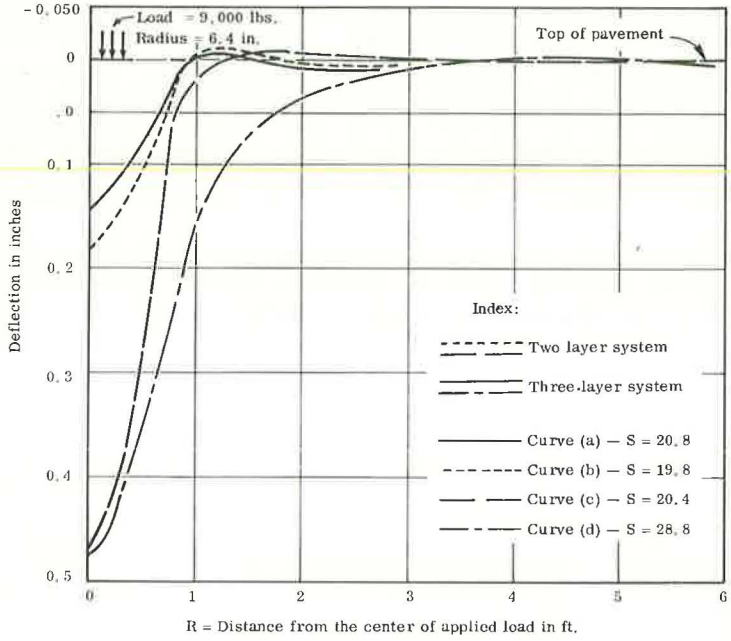

Curve Design	No. of Layers	E_s (psi)	2nd layer from top		Top layer		S	d_0
			E_2 (psi)	h_2 (in.)	E_1 (psi)	h_1 (in.)		
(a)	Three	30,000	1,000	5	30,000	2	20.8	0.147
(b)	Two	30,000	—	—	1,000	5	19.8	0.182
(c)	Two	30,000	—	—	1,000	15	20.4	0.469
(d)	Three	30,000	1,000	60	30,000	2	28.8	0.474

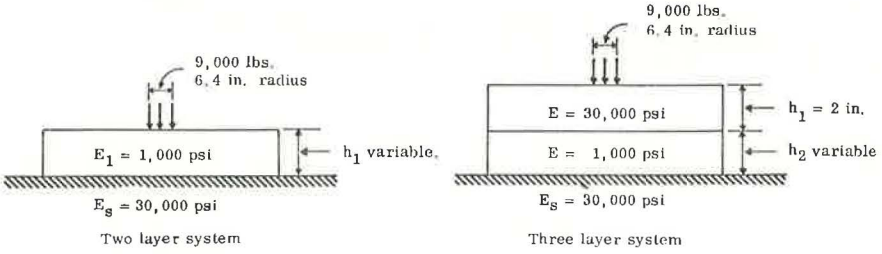

Figure 5. Deflection basin for spreadability values less than 31.35.

field. For the purpose of design, the data so obtained could be converted to the base line of spreadability equal to 31.35.

Examples of evaluating the subgrade by converting it to the base line of spreadability of 31.35 and the effect of the pavement over the subgrade are given in the following:

1. Subgrade evaluation before pavement is laid—On a project the following data were obtained for 1 basin. The Dynaflect deflection d_d of the subgrade was 0.0044 in. and the spreadability S was 40.7. Using the correlation between the maximum deflections for a 9,000-lb wheel load, with $d_{max} = 28.6\ d_d$, we have $d_{max} = 28.6 \times 0.0044 = 0.1258$ in. Plot this point in the general chart shown in Figure 2. This is shown by point a in Figure 6. Extrapolate by drawing a line parallel to the main curves. This line cuts the base line (of spreadability = 31.35) at b, where $d_{max} = 0.215$ in. Because $E_S \times d_{max} = 700$ lb per in., we have $E_S = 700/0.215 = 3{,}250$ psi. Thus, the subgrade strength is equal to a single layer of semi-infinite depth having an $E_S = 3{,}250$ psi plus a top layer of thickness index D = 2.1. This top layer consisting of the same material as the subgrade has an increase in strength, i.e., modulus of elasticity. This increase in strength could be due to drying of the top layer.

2. Subgrade evaluation after the pavement is laid—The data for pavement deflections on the same project for the same location as in the foregoing are shown by point c in Figure 6. The extrapolated line parallel to the main curves and passing through c cuts the base line at e where $d_o = 0.143$ in. This gives the value of $E_S = 700/0.132 = 5{,}300$ psi. In this case, the subgrade strength improved by a value of 5,300 - 3,250 = 2,050 psi. The increase in subgrade strength could be due to either the confining action of the pavement or the lower level of stress on the subgrade with the pavement on the subgrade.

PAVEMENT EVALUATION OF FIELD PROJECTS BASED ON GENERAL EVALUATION CHART

To develop better designs, pavement research and design engineers in Virginia and in other states regularly evaluate existing pavements. For this investigation, a number of field projects were considered to determine how the general evaluation chart shown in Figure 2 could be used as an aid to better evaluation. The details of these projects are given in Table 1. All data are the averages of the actual data recorded in the field. Most of the data were recorded in the spring. It was found that, when these data were plotted on the general evaluation chart, most of the projects had a positive downward slope, which indicates an increase in deflection and a decrease in spreadability with time. Details of 4 such projects marked A through D are given in Table 1 and are shown in Figure 6. The coordinates of these performance curves or any other curves would first be taken parallel to the main curves and then parallel to the horizontal axis as indicated by the dotted lines PQ and QR on curve C. Thus, PQ gives the decrease in the thickness index D of the pavement over the subgrade, and QR gives the reduction in the value of the modulus of elasticity of the subgrade or the subgrade support value.

In some cases, a positive upward slope indicating an increase in deflection and an increase in spreadability was noted. Four examples are given by projects E through H in Table 1 and are shown in Figure 7. The coordinate parallel to the main curves gives the increase in the thickness index of the pavement, and the coordinate parallel to the horizontal axis gives the reduction in the subgrade support value.

A few cases of very little variation in the deflection and spreadability have been noted. One example of this is given by project J in Table 1 and is shown in Figure 7. This curve shows a slight increase in the thickness index of the pavement with no change in the subgrade support.

No project with a negative upward or downward slope was found. A negative upward or downward slope would mean an increase in the subgrade support value.

Thickness equivalencies of the materials used in pavement construction in Virginia have been determined (8) and are given in Table 2. Based on these values, the thickness indexes D_V of the projects mentioned previously were calculated and are also given

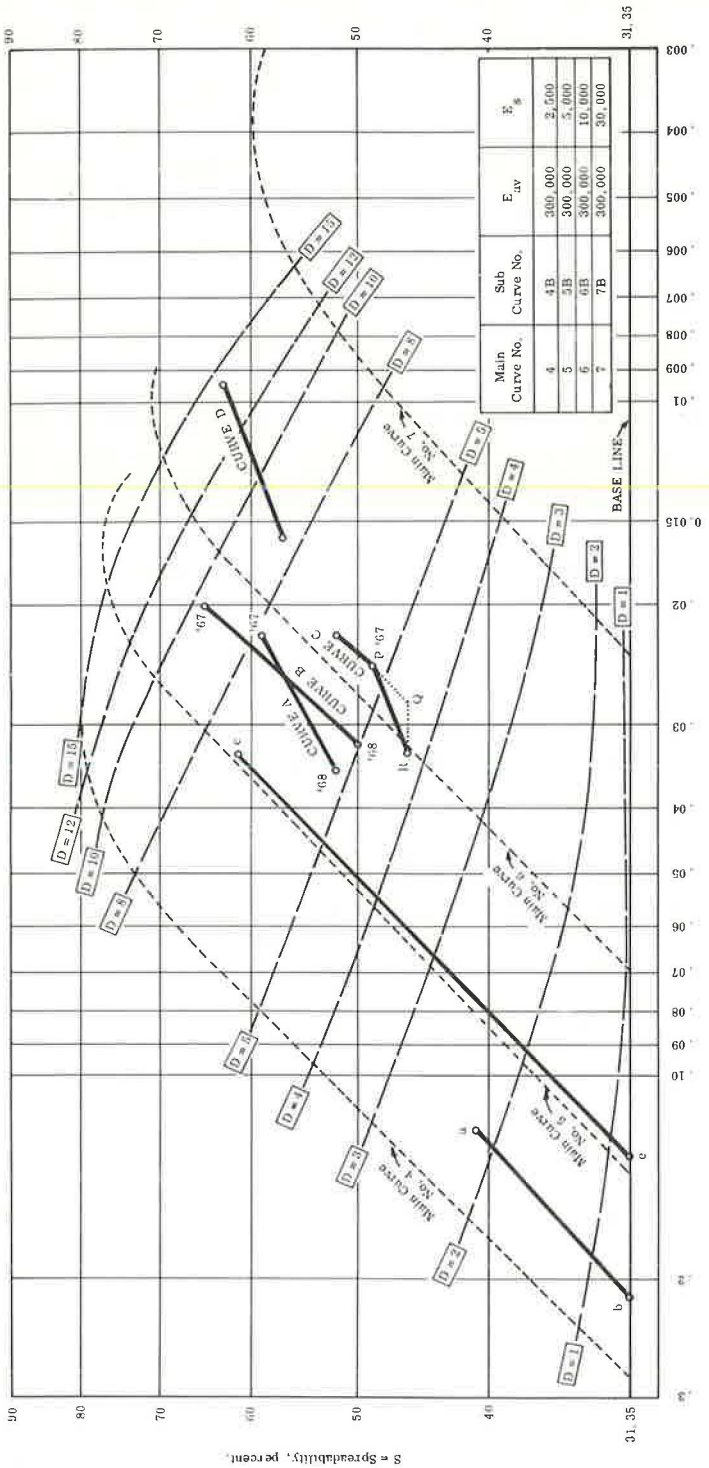

Figure 6. Examples of evaluation of field projects A, B, C, and D by means of general evaluation chart.

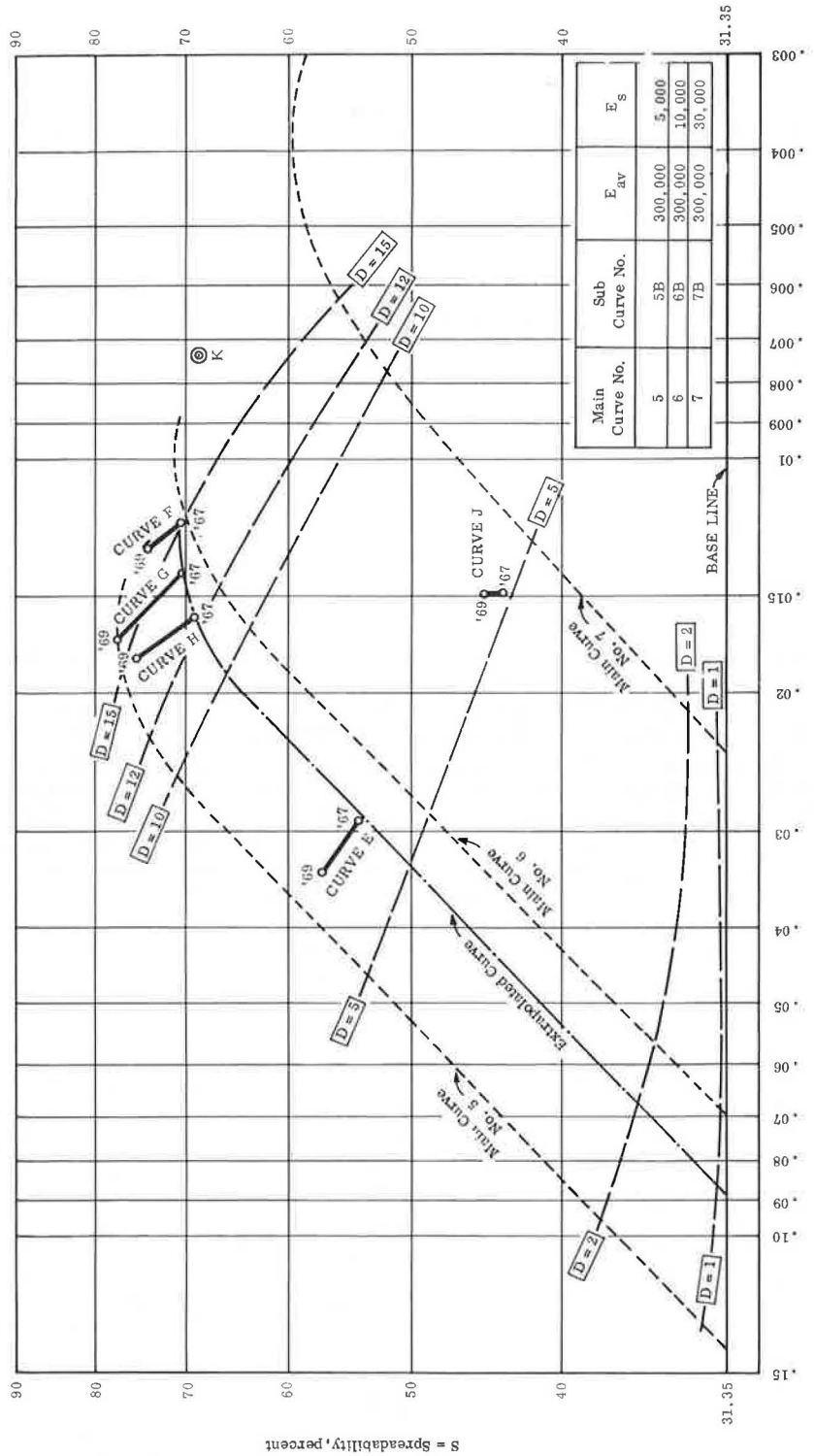

Figure 7. Examples of evaluation of field projects E, F, G, H, J, and K by means of general evaluation chart.

TABLE 1
PERFORMANCE DATA ON TYPICAL PROJECTS

Project	Pavement Section[a]	Thickness Index, D_v	Date of Construction	Deflection Data					
				Date of Collection	Average Theoretical Maximum Deflection[b]	Average Spreadability	Date of Collection	Average Theoretical Maximum Deflection	Average Spreadability
A	7 in. AC + 3 in. Agg	8.0	July 1955	10/25/66	0.022	59	4/24/67	0.037	51
B	1.5 in. AC + 6 in. CTA + 4 in. Agg	10.5	Nov. 1964	4/3/67	0.020	65	3/27/67	0.032	50
C	5 in. AC + 8 in. Agg	7.8	July 1962	11/3/66	0.022	52	4/11/67 and 4/2/68	0.024 0.033	49 47
D	9.5 in. AC + 6 in. Agg + 8 in. CTS	15.1	June 1962	10/22/66	0.0095	63	5/22/69	0.0158	57
E	7 in. AC + 6 in. Agg + 6 in. CTS	11.7	Jan. 1966	4/11/67	0.029	54	4/21/69	0.034	57
F	3 in. AC + 8 in. CTA + 6 in. CTS	13.6	Jan. 1966	4/11/67	0.021	70	4/21/69	0.013	74
G	7 in. AC + 4 in. CTA + 6 in. CTS	13.6	Jan. 1966	4/11/67	0.014	70	4/21/69	0.017	77
H	7 in. AC + 4 in. CTA + 6 in. CTS	12.8	Jan. 1966	4/11/67	0.016	69	4/21/69	0.018	75
J	7 in. AC + 10 in. Agg + 6 in. LTS (in cut)	—	Sept. 1962	5/5/67	0.0153	44	5/8/69	0.0152	45
K	8 in. CRC + 4 in. Agg + 6 in. CTS	21.2	Dec. 1969	6/15/70	0.0074	66			

[a]Full names for abbreviations of materials are given in Table 2.
[b]Maximum deflection under 9,000-lb wheel load and calculated in this table from Dynaflect deflection d_d by the equation $d_{max} = 28.6d_d$.

in Table 1. The performance of these projects based on the general evaluation chart is shown in Figures 6 and 7 and is discussed in the following.

Project A has a design thickness index $D_v = 8$ (Table 1). This value exactly corresponds with the theoretical thickness index during the year 1967 as shown in Figure 6. In 1 year, from 1967 to 1968, the thickness index of the project decreased from 8 to 5, with a little deterioration in the subgrade support value (Fig. 6). Because the subgrade deterioration is small, resurfacing—if needed—might restore the project to its original strength or the strength required for the present traffic. The Virginia design chart for the thickness index versus traffic is given in a 1969 report (8).

Project B has a design thickness index of 10.5. This value also corresponds closely with the theoretical thickness index during the year 1967 as shown in Figure 6. In 1 year (1967-68) the thickness index of the project decreased from about 9.8 to about 5. There has been no deterioration in the average modulus of elasticity of the pavement over the subgrade nor in the subgrade support (Fig. 6). The same type of improvement suggested for project A described previously would apply to this project.

Project C has a design thickness index of 7.8. The theoretical thickness index during the year 1966, as shown in Figure 6, was about 6.6. In the year 1966-67, the D-value decreased from 6.6 to about 5.4 with no change in the subgrade support. From 1967 to 1968 the D-value decreased further to 4.5, and the subgrade support value also decreased. It was found that cracking of the pavement increased considerably in the year 1967-68. The year 1967-68, therefore, indicates a period of high deterioration for this project built in 1962.

Project D has a design thickness index of 15.1, which closely corresponds with the theoretical index of about 14.5 during the year 1966 as shown in Figure 6. In the 3 years from 1966 to 1969, the value

TABLE 2
THICKNESS-EQUIVALENCY VALUES FOR PAVEMENT MATERIALS

Material	Abbreviation	Value, a_v
Asphalt concrete	AC	1.0
Cement-treated aggregate in base	CTA	1.0
Untreated aggregate	Agg	0.35
Cement-treated subgrade	CTS	0.44
Lime-treated subgrade	LTS	0.44
Continuously reinforced concrete	CRC	2.16[a]

[a]Theoretically evaluated for E = 4 million psi.

of D decreased from 14.5 to about 8.5, and the subgrade support value decreased considerably. It is, therefore, probable that the main cause of deterioration is the decrease in subgrade support. In 1966 the pavement had almost no cracks. In 1969 the pavement was mostly cracked.

Projects E through H are experimental projects built next to each other and so the subgrade modulus of elasticity of these projects ought to be the same. The curves for these projects are shown in Figure 7. The 1967 data for these projects lie on the same extrapolated curve for one subgrade support, which indicates the accuracy of this chart. These projects, completed in January 1966, have a positive upward slope with time as shown in Figure 7, which indicates a slight deterioration in the subgrade support value but an increase in the thickness index. The upward slope indicates that the pavement is performing well, unless the asphaltic concrete is becoming more and more rigid and, hence, brittle.

Project E has a design thickness index of 11.7, as given in Table 1, whereas its theoretical thickness index, as shown in Figure 7, was about 6 in 1967. Projects F, G, and H have design thickness indexes of 13.6, 13.6, and 12.8 respectively. These values are close to their theoretical index values of 15.0, 14.0, and 12.5 respectively in 1967.

Project J has a thickness index value lower than the theoretical thickness index value, but from 1967 to 1969 it showed no change in the subgrade support value and a slight increase in its theoretical index value. This project was built in 1962, and in 1969 it was still without cracks.

Project K (Table 1) is a recently built continuously reinforced concrete pavement. It is shown by the point marked K in Figure 7. The object of this point is to show the comparative relationship between flexible and rigid pavements.

The evaluation of the 9 projects on the basis of the general evaluation chart could be summarized as follows:

1. The design thickness index D_V, which is evaluated on the basis of the thickness-equivalency values a_V for paving materials used in Virginia, usually is close to the theoretical thickness index value.
2. The general evaluation chart shown in Figure 2 gives the structural performance of a pavement.

CONCLUSIONS

1. For the proper evaluation of pavements by means of deflection data, the spreadability value of the deflected basin, in addition to the maximum deflection, must be known.
2. The average modulus of elasticity of the pavement over the subgrade is an important factor in pavement evaluation.
3. The general evaluation chart based on a theoretical analysis (Fig. 2) could be applied for evaluating the changes in the subgrade and the pavement strength of flexible pavements.
4. As the spreadability value of the subgrade continues to decrease below 31.35, the subgrade support should be considered poorer and poorer.
5. The thickness index evaluated on the basis of the thickness-equivalency values for paving materials used in Virginia seems to be almost the same as the theoretical thickness-index value.

ACKNOWLEDGMENT

The support of J. H. Dillard, state highway research engineer, and the staff of the Pavement Section of the Virginia Highway Research Council is gratefully acknowledged. Special thanks are given to K. H. McGhee, C. S. Hughes, and H. T. Craft for reviewing and editing the paper. The work was financed under HPR funds made available through the Federal Highway Administration. The opinions, findings, and conclusions expressed in this report are those of the author and not necessarily those of the sponsoring agencies.

REFERENCES

1. Hughes, C. S. Regression Equation to Estimate Benkelman Beam Values From Dynaflect Results. Virginia Highway Research Council, Charlottesville, 1966.
2. Michelow, J. Analysis of Stresses and Displacements in an N-Layered Elastic System Under a Load Uniformly Distributed on a Circular Area. Chevron Research Company, Sept. 1963.
3. Size, Weight, Equipment and Other Requirements for Trucks and Trailers. Virginia Department of Highways, June 1968.
4. Vaswani, N. K. Optimum Structural Strength of Materials in Flexible Pavements. Highway Research Record 329, 1970, pp. 77-97.
5. Terzaghi, K. Theoretical Soil Mechanics. John Wiley and Sons, New York, 1943, pp. 373-376.
6. Vaswani, N. K. Design of Pavements Using Deflection Equations From AASHO Road Test Results. Highway Research Record 239, 1968, pp. 76-94.
7. Vaswani, N. K. Design of Flexible Pavements in Virginia Using AASHO Road Test Results. Highway Research Record 291, 1969, pp. 89-103.
8. Vaswani, N. K. Recommended Design Method for Flexible Pavements in Virginia. Virginia Highway Research Council, Charlottesville, March 1969.

EDICTION OF SHRINKAGE STRESSES IN
VEMENTS CONTAINING SOIL-CEMENT BASES

C. Pretorius, Bruinette, Kruger, Stoffberg and Hugo, Pretoria, South Africa; and
L. Monismith, Institute of Transportation and Traffic Engineering,
University of California, Berkeley

The occurrence of shrinkage cracks in pavements containing soil-cement bases is quite common. Whether such cracking is detrimental to the structural behavior of the pavement section depends on a number of factors, including environment and materials used in the pavement. The fact that problems have been experienced in some pavements subsequent to this cracking justifies an attempt to formulate an analytical procedure that would permit the prediction of shrinkage stresses and cracks in pavements containing soil-cement bases. This paper permits 1 such an approach using the creep characteristics of all of the materials in the pavement structure together with the shrinkage and strength characteristics of the soil cement in an incremental axisymmetric finite-element solution. Stresses are predicted at selected time intervals by increasing the shrinkage strains in the soil cement in small time increments and allowing relaxation due to creep to occur before superposition of the next shrinkage increment. Two cases are analyzed: one considers a uniform shrinkage in the soil cement; the other considers a differential shrinkage assuming that desiccation begins at the surface of the soil-cement base and migrates toward the interior. Also included is a brief discussion of the influence of asphalt concrete temperature and thermal effects on the magnitude of the shrinkage stresses.

•THOUSANDS of feet of cement-treated base can be constructed daily with modern construction equipment. Shrinkage is an inherent property of such a material and begins occurring soon after the material has hardened.

No shrinkage stresses will be developed for a cement-treated base constructed on a frictionless surface and subjected to uniform shrinkage strains throughout its depth. If shrinkage in the layer is restrained in any way, however (i.e., by continuity with other layers, by interlayer friction, or by differential shrinkage), stresses will be developed. In general, 1 factor or a combination of these factors will be present in the field, and the development of shrinkage stresses is, therefore, inevitable.

As these stresses develop, they may be relieved by relaxation because many materials that exhibit shrinkage also exhibit creep. Because the magnitude of shrinkage stresses is proportional to the length of a continuous base, stress relief by creep may initially be insufficient to keep the stresses below the tensile strength of the material, in which case cracking of the cement-bound material will occur. This cracking may be accompanied by an elastic recovery with a corresponding reduction in shrinkage stress. Shrinkage continues, however, and the process keeps repeating itself until the resulting stresses do not exceed the tensile strength of the material.

This is a difficult problem to analyze mathematically, but a method of analysis appears desirable if a better understanding of the factors that influence shrinkage cracking in cement-treated materials is to be achieved. Many authorities disagree as to whether such cracking is really a problem. Recent South African experience (1), for

Sponsored by Committee on Theory of Pavement Design and presented at the 50th Annual Meeting.

example, justifies such an investigation because the formation of wide shrinkage allowed water infiltration that weakened the subgrade and led to severe fatigue c ing in the pavement structure.

It is possible today to analyze this problem, at least to a first approximation, using the finite-element method. It is possible not only to consider different mat characteristics in each element but also to effectively treat nonlinear problems w step-by-step linear incremental procedure or with interaction (2). The developm of shrinkage stresses can be analyzed similarly by incrementing the shrinkage str in small time intervals and by allowing creep relaxation to occur after each shrink increment until the maximum shrinkage has been achieved or until cracking has oc curred. The process of elastic recovery after cracking complicates the analytical treatment of the problem considerably, and simplifications have to be introduced.

Shrinkage cracks are usually observed the first few days after construction. Th cracks are very fine, but this early crack spacing may be very close to that finally tained. Accordingly, an approach would be to assume a crack spacing and analyze pavement to predict whether further cracking will occur. By repeating this procedu a final crack spacing (and crack width) can be estimated. Stress relief at cracking i ignored by this approach, and, although it will be shown that precise values of stres are not determinable at the moment because of a number of uncertainties in the analy sis, it will be possible to show the relative importance of the factors that control the development of shrinkage stresses in a pavement.

From the discussion in the foregoing, it follows that a proper analysis requires th shrinkage, creep, and strength characteristics of the cement-treated material as wel as similar properties for the other layers present in the pavement.

For the present investigation, a 3-layer pavement was selected consisting of a 3-in asphalt concrete layer overlaying an 8-in. soil-cement base (according to the Portland Cement Association definition of soil cement) resting on a clayey subgrade. Proper- ties of the cement-treated material were determined experimentally, whereas appro- priate properties for the other materials were obtained from other test programs in which similar materials had been used.

Figure 1 shows a complete subsystem for the analysis of a pavement and one that considers shrinkage and creep as well as thermal effects and loading. In this paper, only the lower portion of the subsystem shown in Figure 1 will be described. The com

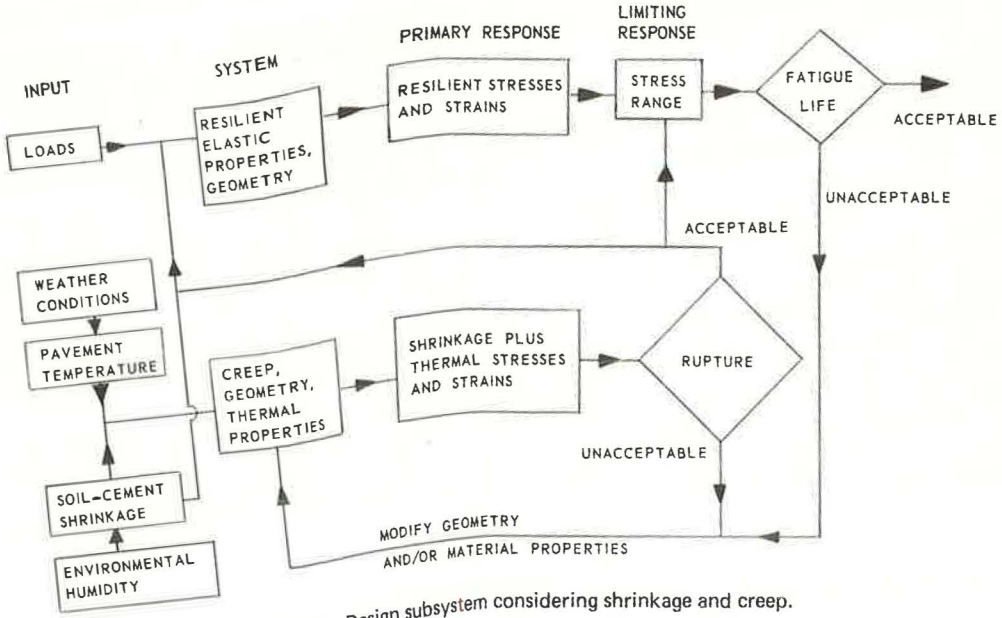

Figure 1. Design subsystem considering shrinkage and creep.

plete subsystem, including loading effects, is important for design consideration and has been treated in detail elsewhere (22).

MATERIAL PROPERTIES

Soil-Cement Base

Materials—The aggregate used in this investigation consisted of a partially crushed gravel obtained in fractions of 2 sizes (designated A and B, Fig. 2) and silty clay (C, Fig. 2) combined in the proportion 4A:1B:1C (Fig. 2) to produce a material designated A-2-4, according to the AASHO classification. The silty clay (3) exhibited the following characteristics: liquid limit, 29.2 percent; plastic limit, 19.4 percent; plastic index, 9.8 percent; organic content, 2.5 percent; clay mineral composition, illite and montmorillonite; and AASHO classification, A-4. A cement content, based on the Portland Cement Association wet-dry test, of 5.5 percent by weight was determined for the selected gradation.

Vibratory compaction at a water content of 7.5 percent by weight was used to prepare the laboratory specimens. Prior to compaction, the aggregate was oven-dried at 235 F for about 18 hours. Because such treatment would influence the properties of the silty clay, this material was air-dried until its water content was reduced to a level less than 2 percent.

Uniform mixtures were obtained by separating the aggregate into a series of sizes and then by recombining them to meet the grading shown in Figure 2. The graded aggregate and cement were thoroughly mixed in a rotating pan, after which water was added to the mixture through a nozzle under pressure. Addition of the water required 2 to 3 min. during which time mixing was continued. Immediately following mixing, the specimens were compacted as noted previously. A variation in density of less than ±2 percent about the mean (138 lb/cu ft) was obtained.

Shrinkage Properties—The magnitude and rate of shrinkage of soil cement are influenced by a variety of factors with clay content having dominant influence. Although portland cement concrete shrinks slowly and continuously and may reach a magnitude

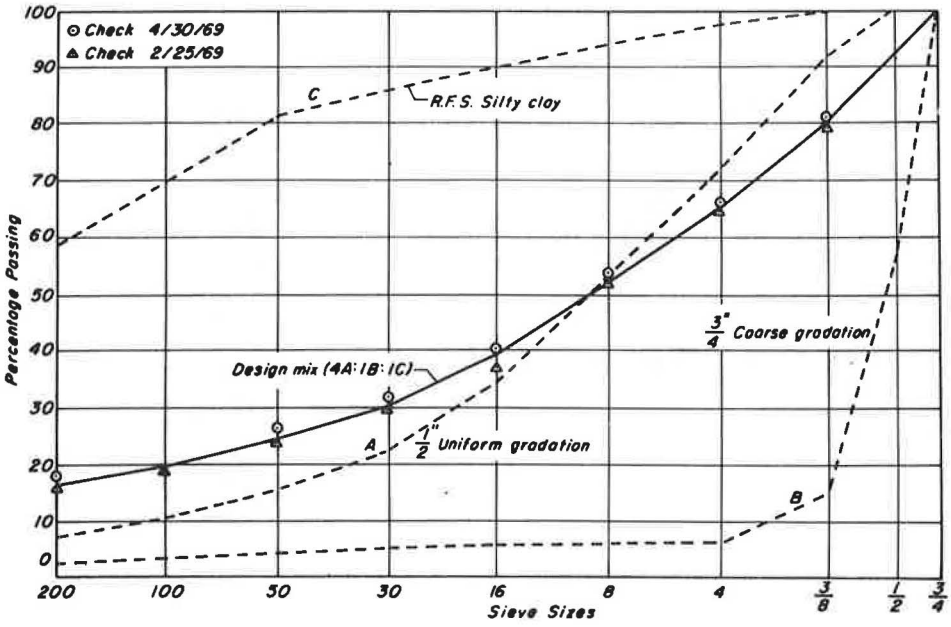

Figure 2. Distributions of grain sizes of materials used in soil-cement base.

of only 1,200 x 10^{-6} in./in. over a period of 30 years (4), soil cement can shrink as much as 2,000 x 10^{-6} in./in. in only 13 days (5).

For the soil cement under consideration, the following procedure was followed for recording shrinkage strains. Beam specimens, 3 in. square by 18 in. long, were compacted with ¼-in. diameter by 3-in. long stainless steel bolts cast 1½ in. into and perpendicular to the 3-in. square ends of the beam. The protruding points of these bolts were previously carefully rounded and served as reference points for the subsequent shrinkage measurements. Shrinkage was recorded by a vertically mounted 0.0001-in. dial gage, as is shown in Figure 3, relative to an aluminum reference beam that was insulated at handling points and stored under the same conditions as the specimens. Specimens were cured for varying periods at 100 percent relative humidity before being transferred to lower relative humidity environments. During this initial curing, little dimensional change occurred. Reductions in length on the 90, 65, and 30 percent relative humidity environments are shown in Figures 4 and 5. The data shown in Figures 4 and 5 indicate that the rate as well as the magnitude of shrinkage increases as the ambient relative humidity decreases. Also noted is the fact that prolonged moist-curing increases the shrinkage potential. This may be due to an increase in the products of hydration (and, in this respect, the behavior of the mix is similar to that of concrete).

As shown in Figures 4 and 5, most of the shrinkage occurs within the first 30 days. This high initial rate of shrinkage is probably due to the suction forces resulting from the loss of capillary water. The rate of shrinkage decreases as equilibrium is approached. In the later stages, shrinkage is more than likely caused by a loss of surface-absorbed and interlayer water (6). Figure 6 shows that a linear interpolation of shrinkage strains is possible over the range of relative humidities indicated.

For the analytical investigation, polynomials were fitted to the shrinkage data points that allowed easy interpolation for any desired time and relative humidity within the range considered.

Creep—Where the pavement layer is subjected to shrinkage under restrained conditions, creep in the layer will reduce both the rate of development and the magnitude of the resulting stresses.

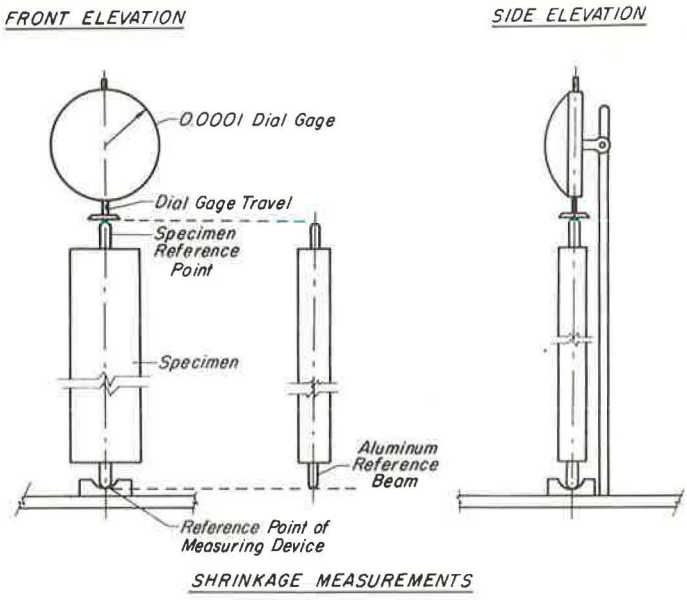

Figure 3. Equipment and specimen configuration for shrinkage measurements.

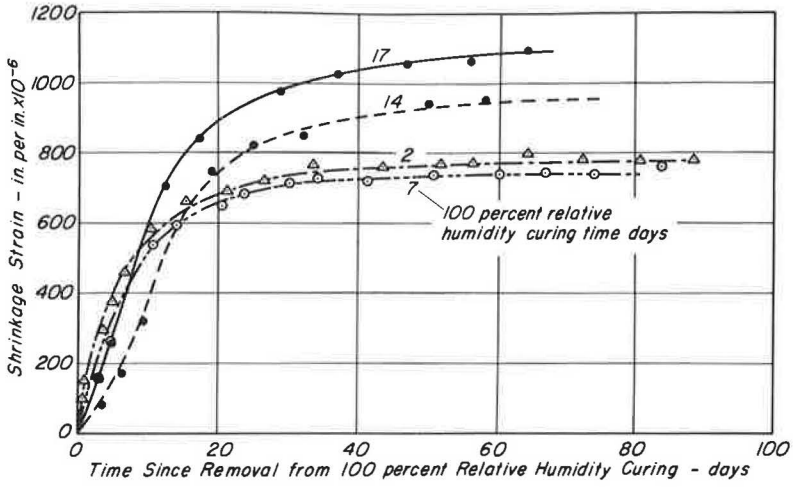

Figure 4. Shrinkage strain versus time for specimens in 30 percent relative humidity environment.

It is generally assumed that creep in tension and in compression has the same characteristics (5, 7). The usual procedure, therefore, is to determine creep in compression and apply the results to problems dealing with tension. Work by Illson (8) on concrete has indicated, however, that the rate of creep in direct tension can be much higher initially than the rate of creep in compression. If this is true for soil cement, then the stresses predicted on the basis of compression creep tests would initially be too large. Accordingly, it was decided that creep in tension would be more representative, and equipment shown in Figure 7 was developed to conduct tensile creep experiments. [Ideally, the creep experiment should be conducted in accordance with the strain gradient expected in the pavement. Because the strain gradient has a significant influence

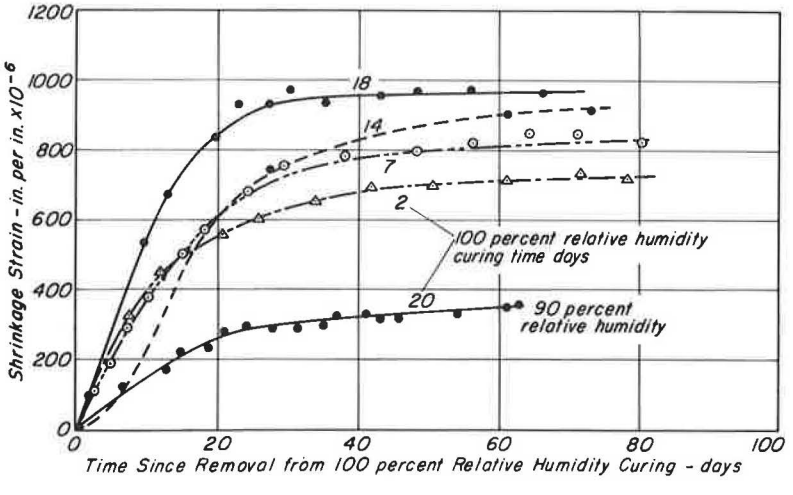

Figure 5. Shrinkage strain versus time for specimens in 65 percent and 90 percent relative humidity environments.

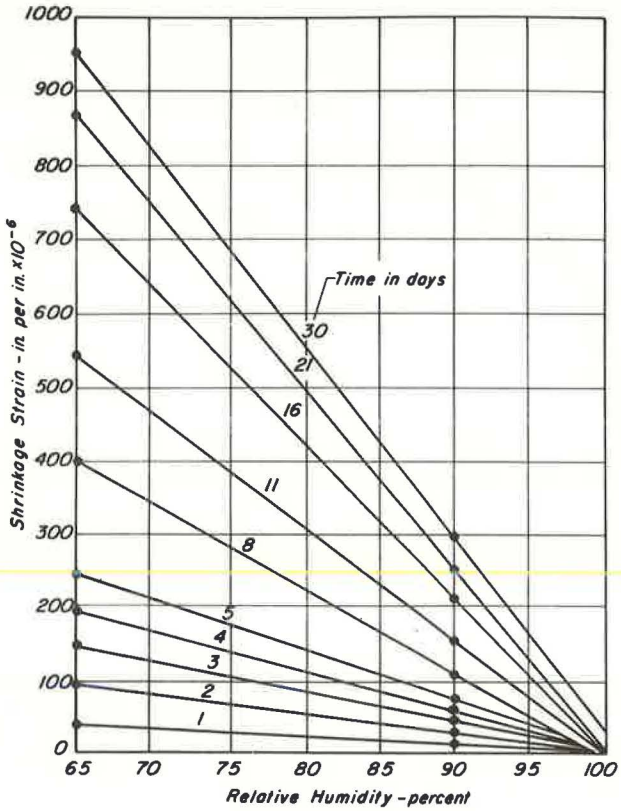

Figure 6. Influence of time on relationship of shrinkage strain and relative humidity for specimens cured initially for 17, 18, and 20 days in 100 percent relative humidity environments.

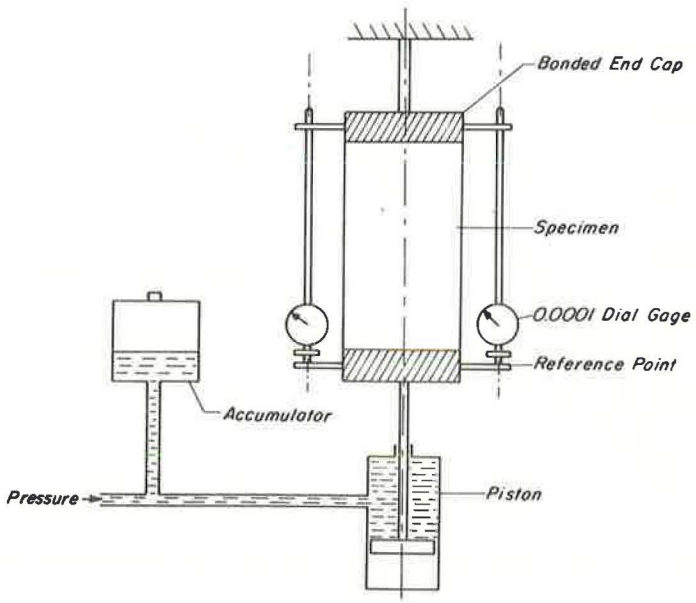

Figure 7. Creep measurement apparatus.

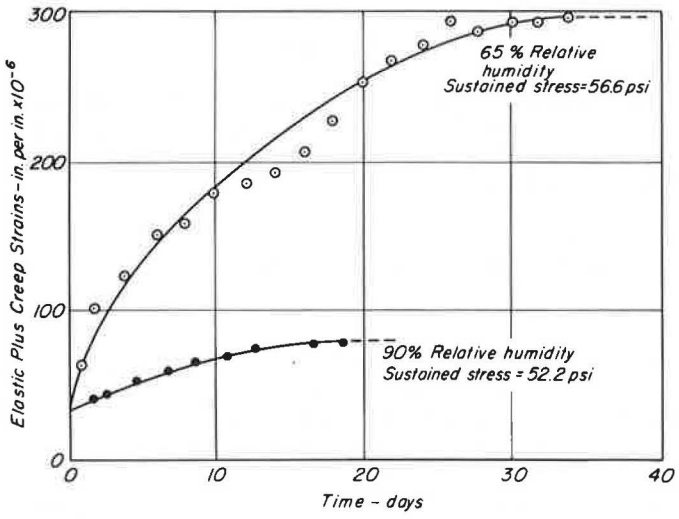

Figure 8. Creep strain versus time for specimens in 90 percent and 65 percent relative humidity environments (specimens cured initially 18 or 20 days in 100 percent relative humidity environment).

on both the strength characteristics and fatigue response of soil cement (22), it can be expected to influence creep behavior. Thus, direct tension creep tests would be applicable, strictly speaking, to uniform shrinkage problems only.]

It should be noted that there are a number of problems associated with tension creep testing of soil cement. For example, the stress level must be comparatively small to ensure that the material will not fail with time (7, 9). Because the tensile strengths of cement-treated materials are comparatively low, the stresses to be applied in creep are correspondingly smaller, with the results that small creep strains are obtained. This in turn necessitates that careful measurements be made. The procedure by which this was accomplished is shown in Figure 7. Resulting creep data are shown in Figure 8. It will be noted in Figure 8 that the creep response of the material is similar to its shrinkage behavior (Figs. 4 and 5). The rate and magnitude of creep increase as ambient humidity is reduced, and the major portion of the creep strain occurs within the first 30 days.

In the finite-element analysis used here, stiffness rather than creep characteristics are required. Ideally, the stiffness characteristics should be determined by means of a relaxation test. In this type of test, the strain ϵ_0 is kept constant while the change in stress $\sigma(t)$ with time is recorded. The relaxation modulus $E(t)$ is then defined as

$$E(t) = \frac{\sigma(t)}{\epsilon_0}$$

Such tests are extremely difficult to perform, and the usual procedure is to conduct creep tests and derive a relaxation modulus from these results. At least 2 procedures are available to make this determination. The first procedure involves the direct inversion of the creep compliance:

$$D(t) = \frac{\epsilon(t)}{\sigma_0}$$

where σ_0 = applied constant stress and $\epsilon(t)$ = strain varying with time, to yield a relaxation modulus

$$E(t) = \frac{\sigma_o}{\epsilon(t)}$$

This modulus is sometimes referred to as the reduced stiffness. Direct inversion may not necessarily produce a correct time-dependent modulus. Accordingly, a second procedure is to assume that the material is linearly viscoelastic in response and, thus, that the following superposition relation is applicable:

$$\int_0^t E(t)\, D(t - \tau)\, d\tau = \int_0^t E(t - \tau)\, D(t)\, d\tau = 1$$

This equation makes it possible to solve for 1 function (e.g., the modulus) if the other (i.e., the compliance) is defined on the time scale. Hopkins and Hamming (10) developed a technique to solve this equation by numerical means, whereas Monismith, Alexander, and Secor (11) successfully applied it to test data on asphalt concrete.

Both procedures were used to estimate the relaxation moduli from the creep data shown in Figure 8. The resulting relationships are shown in Figure 9. For use in subsequent calculations, polynomial expressions were used to represent the curves shown in Figure 9.

Because only 2 relative humidities were considered, it was necessary to develop a procedure for determining response at other humidity conditions. Based on the similarity between creep and shrinkage responses, it was assumed that linear interpolation over the relative humidity range considered was again justified. A check on reduced stiffness values determined from creep data for concrete (12) lent support to this decision.

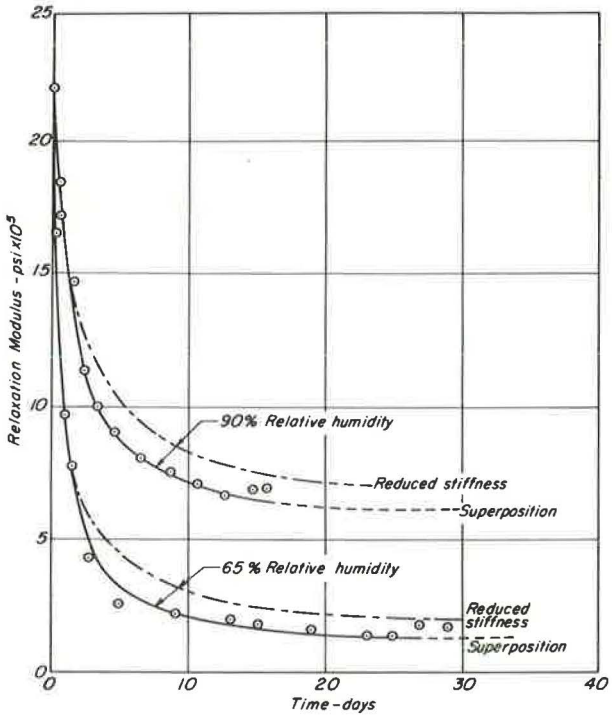

Figure 9. Relaxation moduli versus time for specimens in 90 percent and 65 percent relative humidity environments.

Strength—There are many factors that influence the strength of cement-treated materials, and a general failure criterion awaits the results of additional studies. A series of strength tests were conducted on the material used in this investigation, and the results, together with their significance, are presented in this section.

One measure of strength that is frequently used is the unconfined compressive strength. The influence of curing time on ultimate compressive strength of 4-in. diameter by 8-in. high specimens, cured under 100 percent relative humidity conditions, is shown in Figure 10.

Extensive research is being conducted on the fracture of concrete. Because many of these principles are also applicable to soil cement, they are referred to in this paper where applicable.

Shah and Winter (13) traced the nonlinear behavior of concrete to the mortar-aggregate interface that constitutes the dominant weak link in a mix. Shah and Chandra (14) related the internal microcracking and crack propagation to the external parameters of volume change and Poisson's ratio. Variation of these parameters with stress level expressed as a percentage of the unconfined compressive strength (Fig. 10) is shown in Figure 11 for the soil cement.

The initiation stress σ_i, the stress at which Poisson's ratio begins to increase, is an indication of a beginning in significant bond cracking; i.e., cracking of the mortar-aggregate interface. At the critical stress σ_{CR}, these bond cracks are bridged by mortar cracks, and the specimen begins dilating. Below σ_i, linearity in the stress-strain relationship exists.

Direct tensile strength and modulus of rupture tests were also performed. The direct tensile strength tests were conducted on specimens 4 in. in diameter by 8 in. high with load-transfer end caps bonded to each specimen with epoxy resin. Modulus of rupture tests were performed by using third-point loading on beams 15 in. in length with a 3-in. square cross section. The results are shown in Figure 12.

These results indicate that the strain gradient has a significant influence on the tensile strength of the material. Although the strain gradient is zero for a direct tensile test, it is constant in a flexural experiment. The strength in a splitting tensile test, with yet another strain distribution, is somewhere between these 2 values (15).

Materials in the pavement section are seldom subjected to only uniaxial stresses. The presence of any or both of the other principal stresses may modify the strength characteristics substantially. Figure 13 shows the influence of confining pressure on the compressive strength and stress-strain relationship of the soil cement. Confinement increases the strength significantly and also makes the material more ductile. Figure 13 also shows that curing increases the brittleness during unconfined compressive strength testing.

Of the many failure criteria for combined stresses that are available, the distortion energy theory of Van Mises would appear to hold most promise for concrete-like ma-

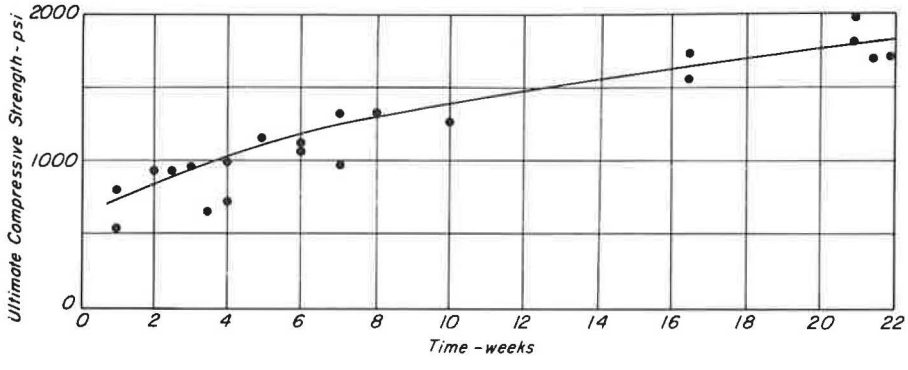

Figure 10. Relationship between unconfined compressive strength and time for soil cement.

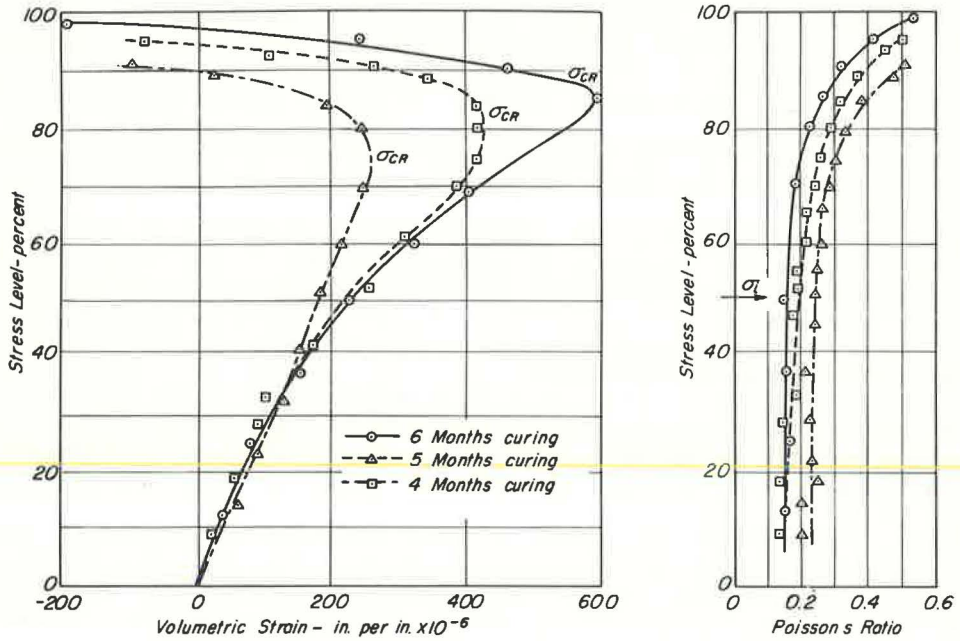

Figure 11. Influence of stress level on volumetric strain and Poisson's ratio for soil-cement specimens.

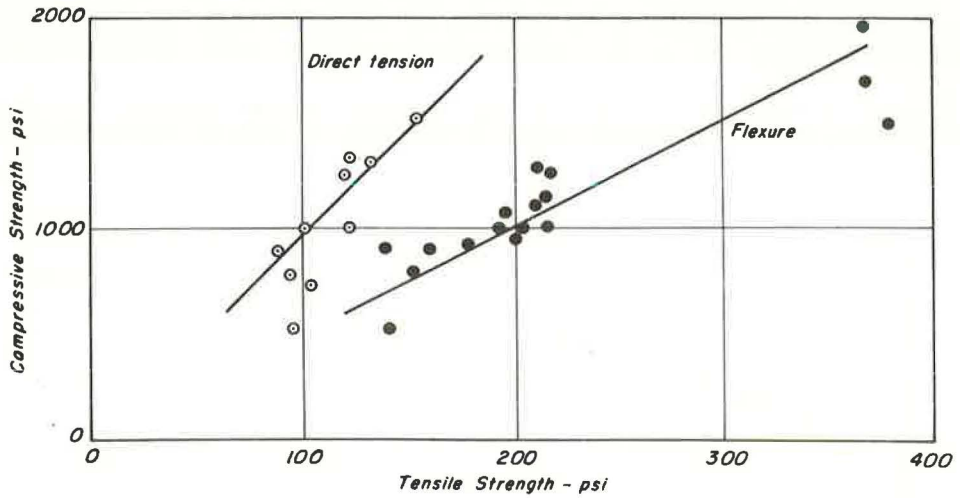

Figure 12. Relationships between tensile strength and unconfined compressive strength for soil-cement specimens.

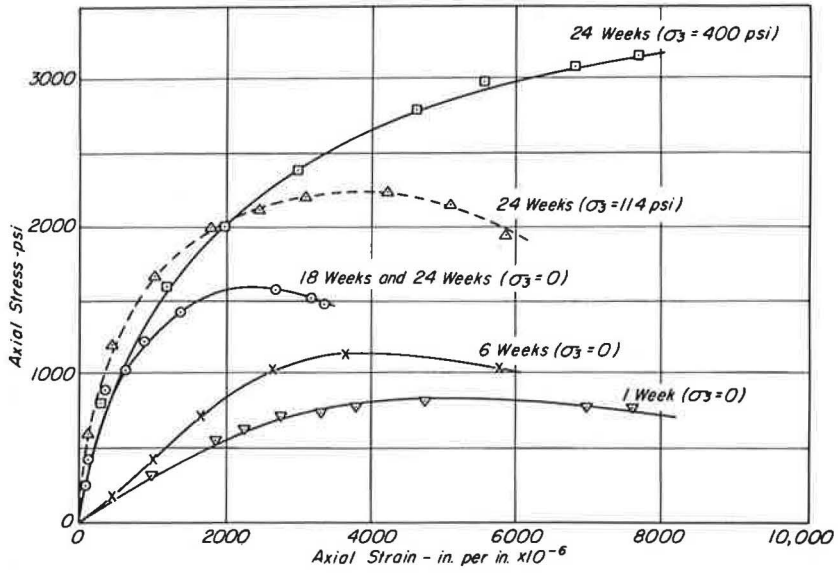

Figure 13. Typical stress versus strain relationships in triaxial compression for soil-cement specimens.

terials. According to this theory, the failure surface, in terms of octahedral stresses, is expressed by

$$\tau_o = a + b\,\sigma_o$$

where

τ_o = octahedral shearing stress = $\frac{1}{3}\,(\sigma_1 - \sigma_2)^2 + (\sigma_2 - \sigma_3)^2 + (\sigma_3 - \sigma_1)^2$,
σ_o = octahedral normal stresses = $\frac{1}{3}\,(\sigma_1 + \sigma_2 + \sigma_3)$, and
a and b = constants.

This approach has produced fair results in biaxial compression-tension tests for concrete (16, 17). Recently, Kupfer, Hilsdorf, and Rusch (18) conducted biaxial strength tests under all combinations of load for concrete. From the results presented, it was possible to plot data shown in Figure 14 in terms of octahedral stresses. It is clear that 1 linear expression is not sufficient to define the total failure envelope. It is possible, however, to define a failure criterion in the compression-tension zone, for example, by conducting only 2 tests—an unconfined compression strength test and an unconfined tensile strength test. For the soil cement, this approach yielded the following equation:

$$\tau_o/\sigma_c = 0.08571 + 1.157\,(\sigma_o/\sigma_c)$$

which is not much different from that developed by Kupfer, Hilsdorf, and Rusch (18) for concrete (Fig. 14) or the equations presented by McHenry and Karni (17) and Bresher and Pister (16). It should be noted that the confined compression test results for the soil cement showed a very distinct nonlinear deviation from the straight-line expression presented in the foregoing.

It is evident, therefore, that no simple failure criterion exists, even for the simple cases of uniaxial and biaxial stresses. For the problem of sustained shrinkage stresses in a pavement, the problem is complicated further by the presence of 2 additional factors; i.e., drying out of the specimen and sustained loading.

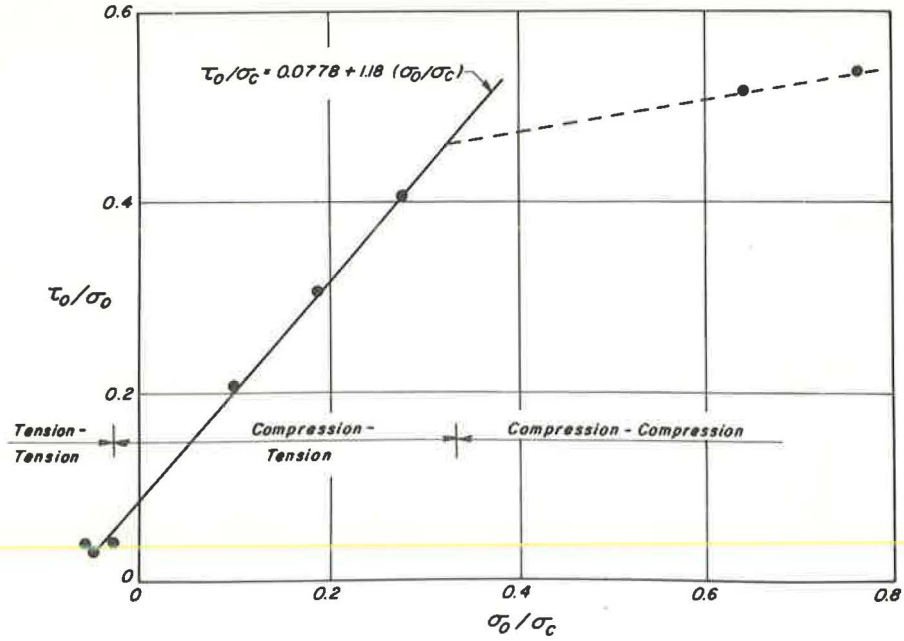

Figure 14. Results of triaxial strength tests for plain concrete (18).

A material that is shrinking is also drying, and it would be expected that drying would influence the properties of the material. In Figure 15 the influence of relative humidity on the direct tensile strength of soil cement is shown. Where a 100 percent relative humidity environment caused a steady increase in strength, lower relative

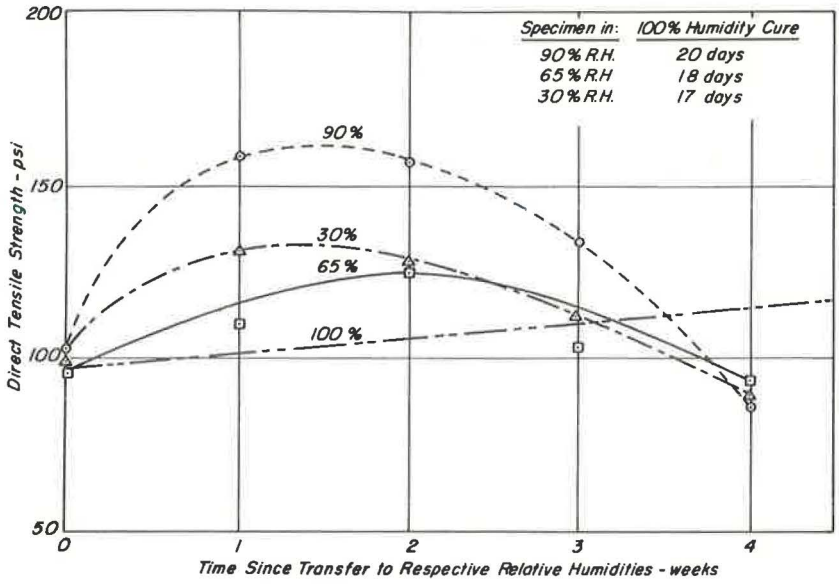

Figure 15. Influence of curing in different humidity environments on ultimate tensile strength of soil-cement specimens.

humidities had the effect of contributing initially to an increase in strength and then to a marked reduction. The same effect was noticed on the secant modulus of elasticity.

Figure 16 shows the effect of the initial curing period on the modulus of rupture after a prolonged period of drying. In Figure 16, the following is noted:

1. The strength increases with the time of initial curing;
2. Flexural strengths of specimens subjected to drying are independent of the relative humidity that caused the dried-out condition; and
3. Little difference in strength exists for specimens cured for periods longer than 20 days as compared to those cured continuously.

In general, if a material is subjected to a sustained load, failure will occur after some time if the sustained load is large relative to the short-term strength. Studies of concrete by Meyers, Slate, and Winter (9) indicate that mortar cracks should not result upon application of the sustained load if time failure is to be prevented; i.e., the stress should be below the critical stress σ_{CR}. For soil cement, this corresponds to a mean stress level as low as 75 percent (Fig. 11).

States of stress in the problem under consideration here are predominantly biaxial tension versus tension subjected to a significant strain gradient. Under such conditions, the uniaxial direct tensile strength or modulus of rupture (depending on the strain gradient) are acceptable failure criteria, and little advantage is gained, at the moment, by additional testing effort. Because of the sustained nature of the loading, failure would occur at a certain percentage of these values.

Asphalt Concrete

In the analysis presented here, the only property required for the asphalt concrete is its creep response. Rather than developing such data, we used stiffness characteristics for an asphalt concrete developed by Pagen (19). These characteristics, represented by a creep modulus, are shown for an extended time scale at 25 C (298 K). The corresponding temperature-dependent shift factor a_t is shown in Figure 17. It will be noted in Figure 18 that the modulus remains fairly constant (approximately equal to 10,000 psi) for temperatures above 40 F and relaxation times longer than about 1 day.

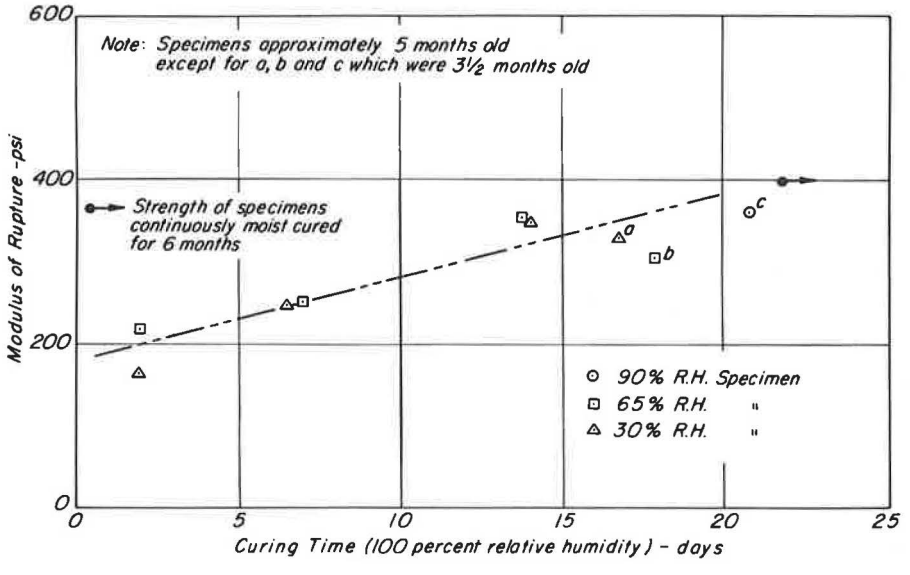

Figure 16. Influence of initial curing period on modulus of rupture of soil-cement specimens after prolonged drying period.

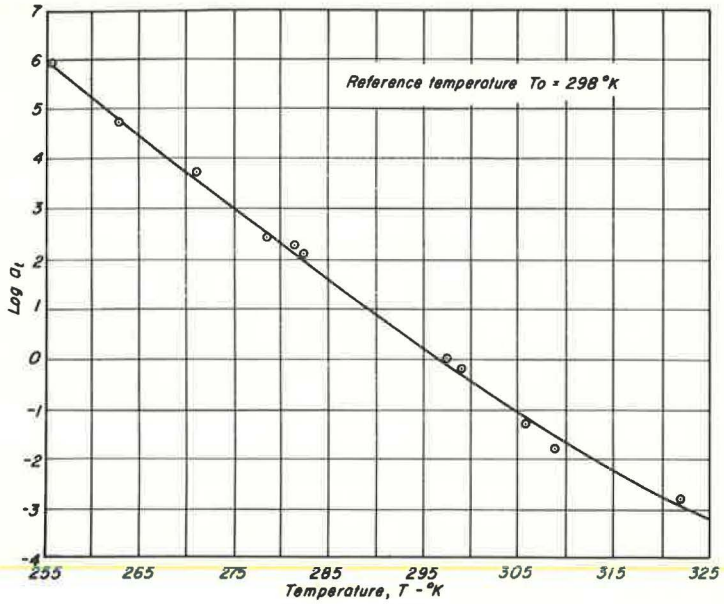

Figure 17. Influence of temperature on shift factor a_T for asphalt concrete (19).

Clayey Subgrade

Based on research conducted by Paduana (20), it was decided to use a constant modulus of 1,500 psi for the clayey subgrade because his data indicated that materials of this type reached an equilibrium value in creep fairly rapidly.

ANALYTICAL INVESTIGATION

An outline of the finite-element approach to the problem is given in the Appendix. By this approach the element nodal points are locked, and the required nodal forces

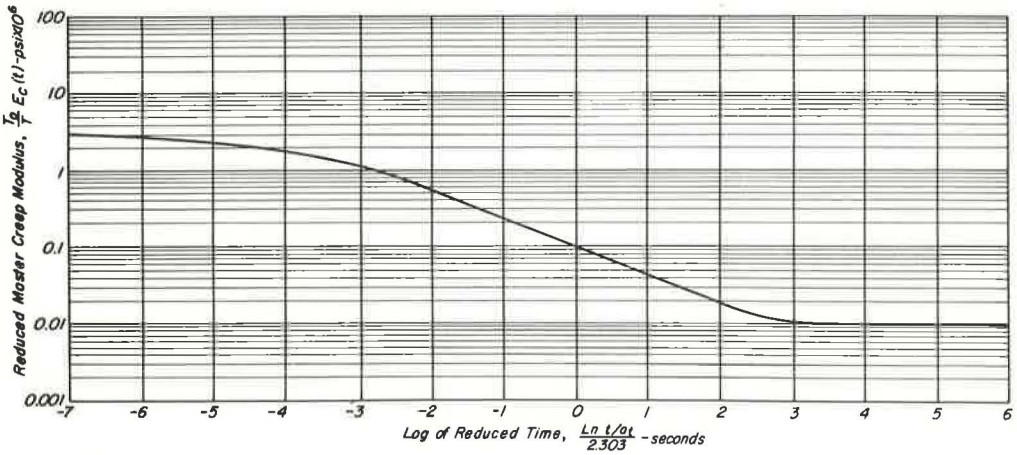

Figure 18. Composite creep curve for asphalt concrete (19).

are determined for a finite increase in shrinkage strains. These nodal forces are then reversed, applied to the system, and solved for stresses and displacements. The final stresses are obtained by a superposition of the stresses due to full restraint and the stresses due to nodal point displacements. This procedure is followed for each strain increment, and the stresses are added to those calculated in the previous increments. Relaxation due to creep is taken care of at each time increment by using the relaxation modulus corresponding to the difference in time between the final time and the time of increment.

This problem ideally should be treated with a 3-dimensional finite-element approach. Such programs currently require too much computer time to be of practical use. The other alternatives are axisymmetric, plane stress, or plane strain idealizations of the problem. Initially, before cracking occurs, a plane stress approach seems appropriate; but, after the pavement has cracked into smaller, more or less rectangular blocks, an axisymmetric idealization would appear to be the best approach. Accordingly, a constant strain axisymmetric finite-element program was used for this analysis.

In the analysis, the following assumptions were made:

1. Linear viscoelasticity is applicable to failure.
2. Continuity exists between all layers.
3. The experimental data presented here are applicable. It should be noted that laboratory creep and shrinkage results to be used in the analysis were obtained from specimens that had been cured 3 weeks prior to testing. In the field, shrinkage and creep begin almost immediately after construction, and it is not known what effect the presence of an asphalt concrete layer would have on shrinkage in the soil cement.
4. A crack penetrates the asphalt concrete to its full depth immediately and also to some depth into the subgrade. If continuity between layers did exist and a cement-treated base did crack, the layers in contact with the cement-bound material would also have to crack with it at the interface because 2 points adjacent to the crack with 0 distance between them are suddenly given a finite displacement. Even if continuity were destroyed over a certain distance, high stresses would still be developed for shrinkage after only 1 day, as shown in Figure 19. Figure 20 shows the axisymmetric finite-element mesh assumed for subsequent analysis with a crack spacing at 20 ft. The ele-

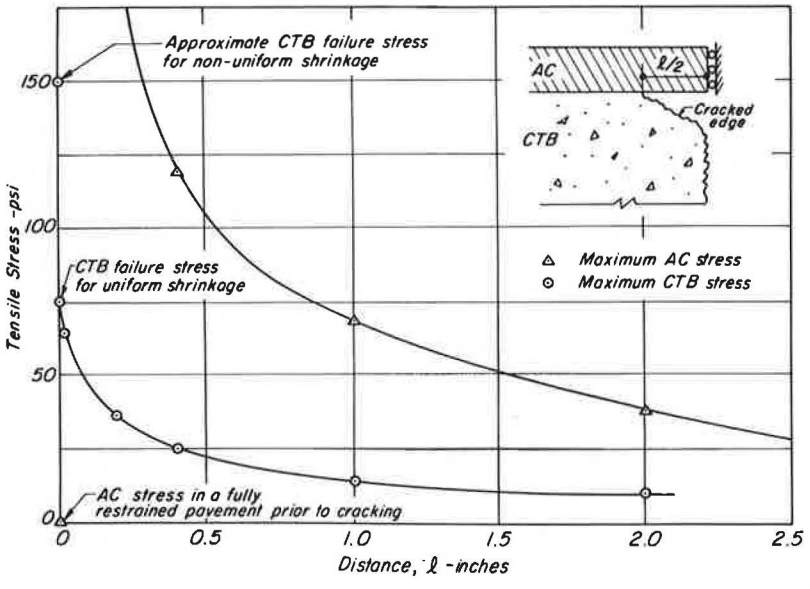

Figure 19. Influence of lack of continuity between layers on tensile stresses in asphalt-bound and soil-cement layers due to 1-day shrinkage at 65 percent relative humidity.

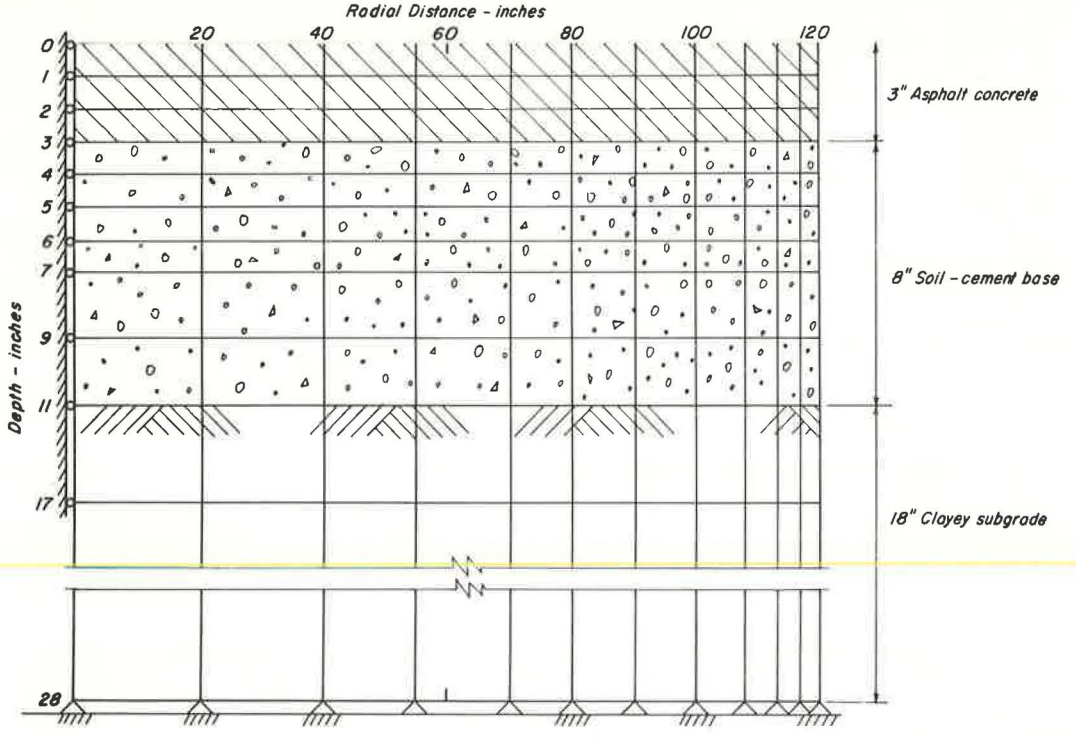

Figure 20. Finite-element representation of pavement structure for shrinkage stress determinations.

ment configuration was arrived at after some experimentation to ensure acceptable a curacy for a reasonable solution time on the computer of about 30 sec per shrinkage increment.

5. Temperatures in the asphalt concrete were varied from 87 to 50 F through its depth. Data on temperature distributions in a 2.5-in. thick asphalt layer for a pavement near Morro Bay, California, developed by Kasianchuk (21) served as a basis for this distribution.

If a pavement is subjected to a uniform shrinkage with depth, the magnitude of developed stresses depends solely on the restraint offered by the other layers. This can be regarded as a lower bound solution to the shrinkage problem.

For the pavement shown in Figure 20 subjected to uniform shrinkage, the maximum tensile stress variation with time is shown in Figure 21. These stresses are extremely small and can hardly be responsible for the final crack spacings. Factors such as thickness of asphalt concrete and its temperature have an influence on the magnitude of stresses. However, these factors are of minor importance if thermal stresses are superimposed on the uniform shrinkage stresses as seen in Figure 22. Here it is assumed that the stress-free temperature is 50 F.

It is doubtful, however, whether uniform shrinkage will ever occur in a pavement. Desiccation will probably start at the surface and migrate slowly toward the interior. One approach to this problem is to assume that the base is subjected to a parabolic distribution of relative humidity. Figure 23 shows the resulting stresses that could be developed. From the magnitude of the stresses (as compared with those shown in Figure 21), it is apparent that differential shrinkage represents a much more critical stress situation.

If the relative humidity difference between top and bottom surfaces of the cement-treated base remains fixed with time, stresses will increase at an increasing rate because the corresponding shrinkage strain difference continues to increase at an increasing rate. These stress variations are shown in Figure 24.

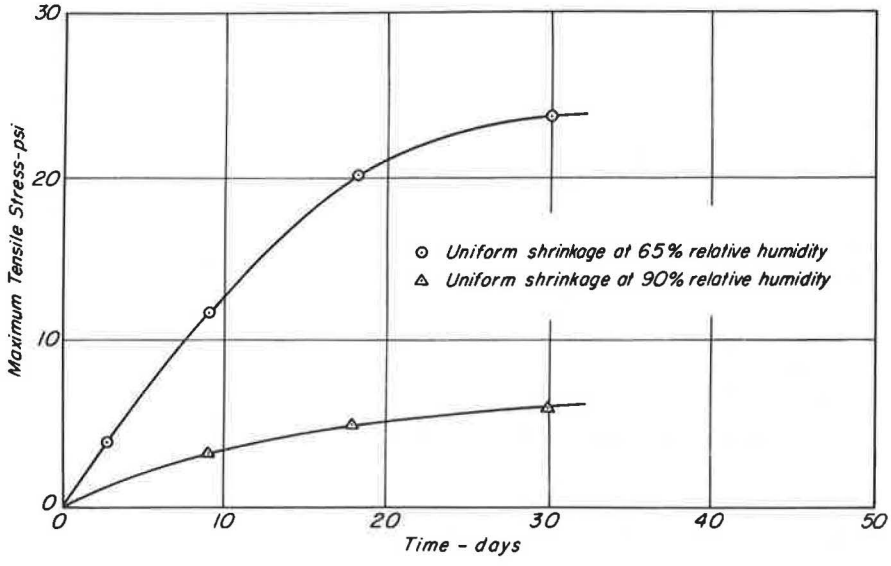

Figure 21. Development of stresses in soil-cement base resulting from uniform shrinkage (3-day strain increments).

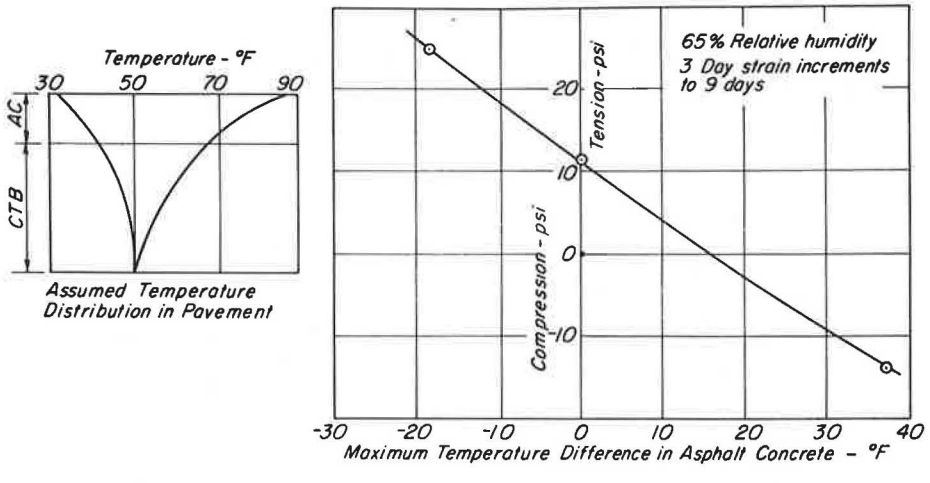

Figure 22. Superposition of shrinkage stresses for uniform shrinkage (see Fig. 21) and thermal stresses (stress-free condition at 50 F).

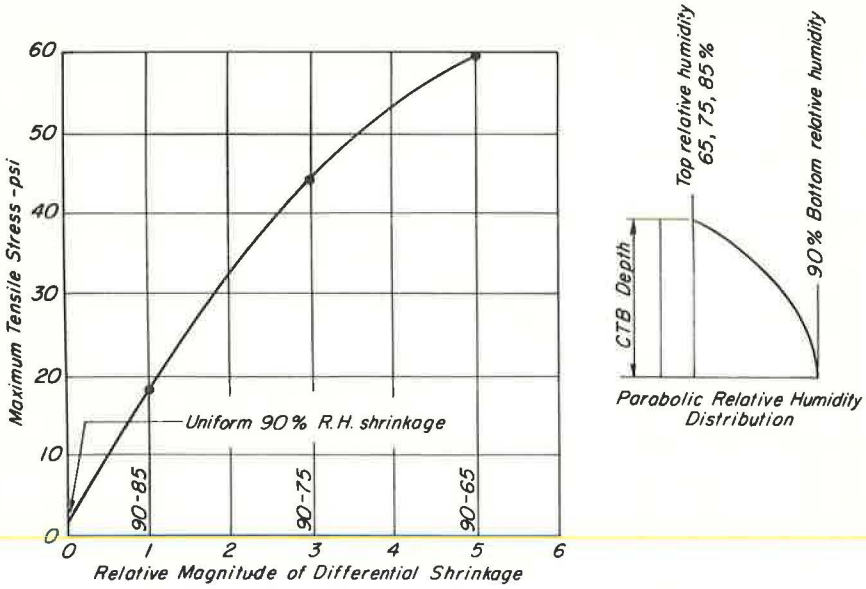

Figure 23. Influence of relative humidity distribution in soil-cement base on tensile stresses due to shrinkage.

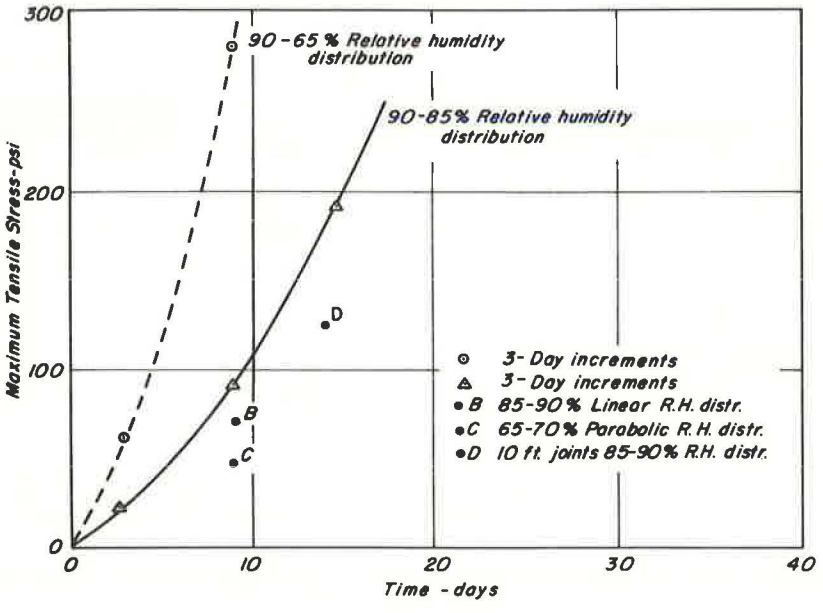

Figure 24. Influence of time on tensile stresses due to shrinkage for specific relative humidity distributions in soil-cement base.

In an actual pavement, the initial difference between the relative humidities at the top and bottom of the layer will diminish with time, until eventually the pavement will again arrive at a uniform relative humidity condition with stresses corresponding accordingly. In a finite-element analysis, this means that a redistribution of stresses is required after each strain increment to account for the diminishing differential shrinkage. Because of the uncertainties regarding the actual relative humidity distribution and rate of desiccation, as well as the extra effort and computer time required for such an analysis, this type of solution was not attempted. Instead, a rate of desiccation was assumed, and the analysis was performed without doing the stress redistribution. The resulting solution then represents an upper bound for the problem. If the lower bound solution is also known (uniform shrinkage case), an approximate solution can be obtained by simply fitting a line between the 2 extreme solutions. This approach is shown in Figures 25, 26, and 27.

Figure 25 shows the assumed humidity distributions with depth as well as with time, whereas Figures 26 and 27 indicate the results due to 2 different 5 percent humidity differentials. From the latter 2 curves, the following observations are made:

1. The band between the 2 bounds is much narrower for the 70 to 65 percent differential than for the 90 to 85 percent differential although the strains involved are exactly

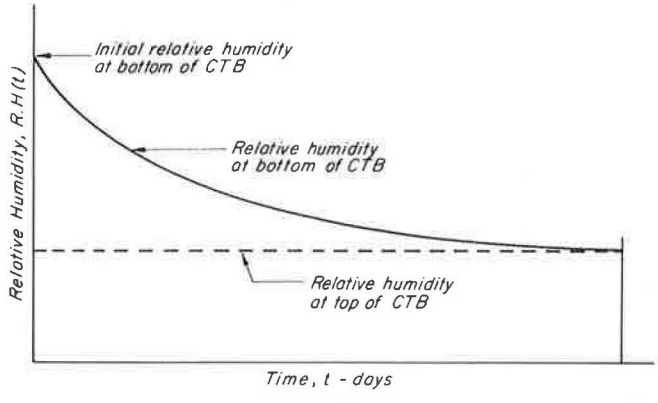

a. Relative Humidity vs. Time.

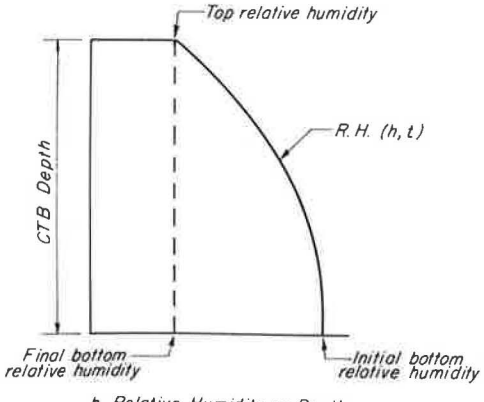

b. Relative Humidity vs. Depth.

Figure 25. Assumed time and depth variations in relative humidity for use in analyses shown in Figures 26 and 27.

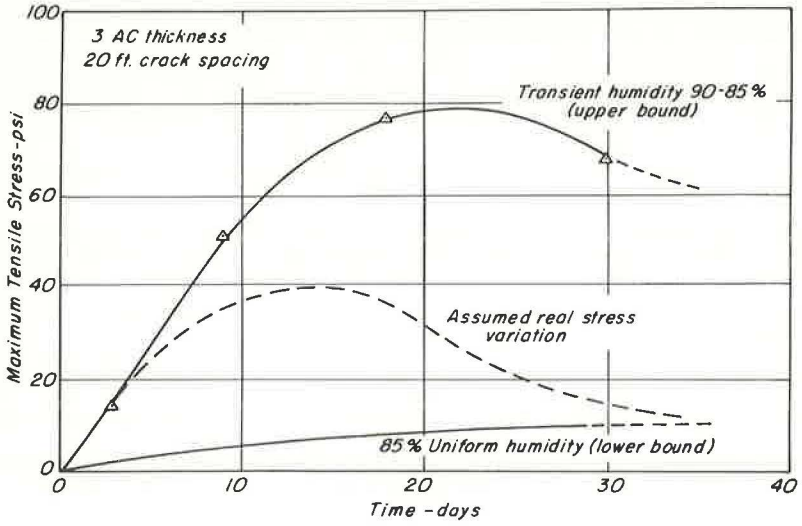

Figure 26. Variation of shrinkage stresses with time, 90 to 85 percent relative humidity differential.

the same (because of linear interpolation). This is probably due to the fact that less stress relief occurs at the higher humidities (Fig. 8), which is reflected in the higher upper bound.

2. The maximum differential shrinkage stresses are reached before the shrinkage strains reach a maximum, i.e., the shrinkage curves alone are not an indication of stress development.

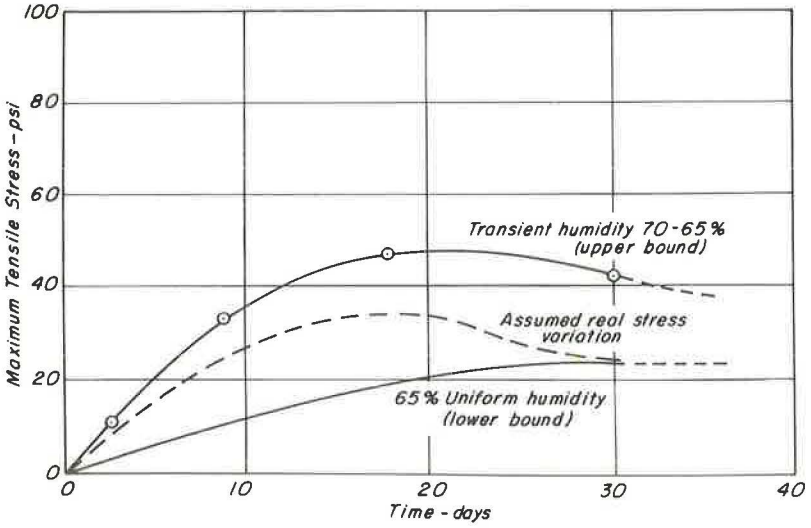

Figure 27. Variation of shrinkage stresses with time, 70 to 65 percent relative humidity differential.

SUMMARY

The results presented in this paper indicate that it is possible to approximate the crack spacing in a pavement containing a soil-cement base, provided that the actual distribution of shrinkage strains in the pavement is known. Because nodal point displacements are part of the computer output, it is also possible to predict crack widths. It is doubtful, however, that this is of significance.

Repeated loading of vehicles crossing a crack will slowly destroy any remaining friction and aggregate interlock after cracking. It is this loss of load transfer across the shrinkage crack that gives rise to fatigue cracking in the cement-bound material, and it is possible to predict the development of such distress by a 3-dimensional finite-element approach (22).

It is hoped that the approach described here or a similar approach would be applied to other types of soil-cement mixes to permit comparisons to be made. It also seems desirable that the problem of load transfer across the crack be thoroughly studied to assist in developing improved utilization of cement-stabilized soils in pavement construction.

ACKNOWLEDGMENT

This study was made possible through grants by the Portland Cement Association and the South African Council for Scientific and Industrial Research. Computer time was provided by the Computer Center, University of California, Berkeley. C. K. Chan provided valuable guidance in the design of equipment that was constructed by the shop staff of the Institute of Transportation and Traffic Engineering, University of California, Berkeley.

REFERENCES

1. Williams, A. A. B., and Dehlen, G. L. The Performance of Full-Scale Base and Surfacing Experiments on National Route 3-1, at Key Ridge, After the First Six Years. First Conf. on Asphalt Pavements for Southern Africa, Durban, Aug. 1969.
2. Duncan, J. M., Monismith, C. L., and Wilson, E. L. Finite Element Analysis of Pavements. Highway Research Record 228, 1968, pp. 18-33.
3. Wang, M. C. Stresses and Deflections in Cement-Stabilized Soil Pavements. Univ. of California, Berkeley, PhD dissertation, 1968.
4. Troxell, G. E., Raphael, J. M., and Davis, R. E. Long-Time Creep and Shrinkage Tests of Plain and Reinforced Concrete. ASTM Proc., Vol. 58, 1958, pp. 1101-1120.
5. George, K. P. Shrinkage Characteristics of Soil-Cement Mixtures. Highway Research Record 255, 1968, pp. 42-58.
6. Aroni, S., and Mehta, P. K. Fundamentals Underlying Shrinkage in Concrete—A Review. The Indian Concrete Journal, Dec. 1965.
7. Neville, A. M. Properties of Concrete. John Wiley and Sons, New York, 1963.
8. Illson, J. M. The Creep of Concrete Under Uniaxial Tension. Magazine of Concrete Research, Vol. 17, No. 51, June 1965.
9. Meyers, B. L., Slate, F. O., and Winter, G. Relationship Between Time-Dependent Deformation and Microcracking of Plain Concrete. ACI Jour., Vol. 66, No. 1, Jan. 1969, pp. 60-68.
10. Hopkins, I. L., and Hamming, R. W. On Creep and Relaxation. Jour. of Applied Physics, Vol. 28, No. 8, 1957.
11. Monismith, C. L., Alexander, R. L., and Secor, K. E. Rheologic Behavior of Asphalt Concrete. ASTM Proc., Vol. 35, Feb. 1966.
12. Davis, R. E., and Davis, H. E. Flow of Concrete Under Sustained Compressive Stress. ASTM Proc., Part 2, Vol. 30, 1930.
13. Shah, S. P., and Winter, G. Inelastic Behavior and Fracture of Concrete. ACI Jour., Vol. 63, No. 9, Sept. 1966, pp. 925-930.
14. Shah, S. P., and Chandra, S. Critical Stress, Volume Change, and Microcracking of Concrete. ACI Jour., Vol. 65, No. 9, Sept. 1968, pp. 770-781.

15. Davies, J. D., and Bose, D. K. Stress Distribution in Splitting Tests. ACI Jour., Vol. 65, No. 8, Aug. 1968, pp. 662-669.
16. Bresler, B., and Pister, K. S. Failure of Plain Concrete Under Combined Stresses. ASTM Proc., Vol. 81, Sep. No. 674, April 1955.
17. McHenry, D., and Karni, J. Strength of Concrete Under Combined Tensile and Compressive Stresses. ACI Jour., Vol. 54, No. 10, April 1958.
18. Kupfer, H., Hilsdorf, H. K., and Rusch, H. Behavior of Concrete Under Biaxial Stresses. ACI Jour., Vol. 66, No. 8, Aug. 1969, pp. 656-666.
19. Pagen, C. A. An Analysis of the Thermorheological Response of Bituminous Concrete. Eng. Exp. Station, Ohio State Univ., Columbus, PhD dissertation, 1963.
20. Paduana, J. A. The Effect and Amount of Clay on the Strength and Creep Characteristics of Clay-Sand Mixtures. Univ. of California, Berkeley, PhD dissertation, 1966.
21. Kasianchuk, D. A. Fatigue Considerations in the Design of Asphalt Concrete Pavements. Univ. of California, Berkeley, PhD dissertation, 1968.
22. Pretorius, P. C. Design Considerations for Pavements Containing Soil-Cement Bases. Univ. of California, Berkeley, PhD dissertation, 1970.
23. Wilson, E. L. A Digital Computer Program for the Finite Element Analysis of Solids With Non-Linear Material Properties. Dept. of Civil Engineering, Univ. of California, Berkeley.

APPENDIX

AXISYMMETRIC FINITE-ELEMENT ANALYSIS OF SHRINKAGE STRESSES IN PAVEMENTS

The finite-element approach to the determination of shrinkage stresses in a pavement, for 1 increment of time, is briefly summarized in the following.

The potential energy of an elastic solid is given by

$$\phi = \int_{\text{volume}} \tfrac{1}{2}\epsilon_i\sigma_i dV - \int_{\text{volume}} w_i F_i dV - \int_{\text{area}} w_i P_i dA \qquad (1)$$

where

w = displacement of point i in an elastic solid,
F = body force, and
P = surface traction.

Written in matrix form, Eq. 1 becomes

$$\phi = \int_{\text{volume}} \tfrac{1}{2}[\epsilon]^T[\sigma]dV - \int_{\text{volume}} [w]^T[F]dV - \int_{\text{area}} [w]^T[P]dA \qquad (2)$$

For a finite-element system composed of M arbitrary elements, Eq. 2 is written as a sum of integrals (23):

$$\phi = \sum_{m=1}^{M} \left\{ \int_{\text{volume}} \tfrac{1}{2}[\epsilon]^T[\sigma]dV - \int_{\text{volume}} [w]^T[F]dV - \int_{\text{area}} [w]^T[P]dA \right\} \qquad (3)$$

The potential energy is expressed in terms of unknown nodal point displacements by assuming a displacement field within each element, satisfying compatibility between elements of the system

$$[w] = [d]\,[u] \tag{4}$$

where $[u]$ = unknown nodal point displacements. Element strains are expressed as

$$[\epsilon] = [a]\,[u] \tag{5}$$

For an elastic material the stresses are expressed in terms of corresponding strains and environmental effects by the elastic stress-strain relationship

$$[\sigma] = [C]\,[\epsilon] - [\tau] \tag{6}$$

Equations 4, 5, and 6 are substituted into Eq. 3 to result in the following expression for the potential energy:

$$\phi = \sum_{m=1}^{M} \left\{ \tfrac{1}{2} \int_{\text{volume}} [u]^T [a]^T [C] [a] [u]\, dV - \int_{\text{volume}} [u]^T \left([d]^T [F] + [a]^T [\tau] \right) dA - \int_{\text{area}} [u]^T [d]^T [P]\, dA \right\} \tag{7}$$

The potential energy is minimized by the requirement

$$\frac{\delta \phi}{\delta u_i} = 0 \text{ for } i = 1, \ldots, N$$

where N is the number of unknown nodal point displacements.

After matrix differentiation, the equilibrium of the finite-element system is given by

$$\sum_{m=1}^{M} \int_{\text{volume}} [a]^T [C] [a] [u]\, dV = \Sigma \int_{\text{volume}} [d]^T [F] + [a]^T [\tau]\, dV + \Sigma \int_{\text{area}} [d]^T [P]\, dA$$

or

$$[K]\,[u] = [Q] \tag{8}$$

where $[K]$ is the stiffness matrix given by

$$[K] = \sum_{m=1}^{M} [k^m]$$

The individual-element stiffnesses are given by

$$[k^m] = \int_{\text{volume}} [a]^T [C] [a]\, dA$$

The load vector $[Q]$ is defined as

$$[Q] = \sum_{m=1}^{M} \left\{ \int_{\text{volume}} ([d]^T [F] + [a]^T [\tau])\, dV + \int_{\text{area}} [d]^T [P]\, dA \right\} \tag{9}$$

Equation 8 can now be solved for the unknown nodal point displacements $[u]$.

Shrinkage and thermal effects are included in Eq. 6 for the axisymmetric solid as

$$\begin{Bmatrix}\sigma_{rr}\\ \sigma_{zz}\\ \sigma_{\theta\theta}\\ \sigma_{rz}\end{Bmatrix} = \begin{bmatrix}C_{11} & C_{12} & C_{13} & 0\\ C_{21} & C_{22} & C_{23} & 0\\ C_{31} & C_{32} & C_{33} & 0\\ 0 & 0 & 0 & C_{44}\end{bmatrix} \begin{Bmatrix}\epsilon_{rr}\\ \epsilon_{zz}\\ \epsilon_{\theta\theta}\\ \epsilon_{rz}\end{Bmatrix} - \begin{bmatrix}C_{11} & C_{12} & C_{13} & 0\\ C_{21} & C_{22} & C_{23} & 0\\ C_{31} & C_{32} & C_{33} & 0\\ 0 & 0 & 0 & 0\end{bmatrix} \begin{Bmatrix}T\alpha_{tt} + S_{rr}\\ T\alpha_{zz} + S_{xx}\\ T\alpha_{\theta\theta} + S_{\theta\theta}\\ 0\end{Bmatrix} \tag{10}$$

where

T = temperature,
α = coefficient of thermal expansion, and
S = shrinkage strain.

These thermal and shrinkage stresses for the restraint conditions are transformed to nodal point forces by Eq. 9.

The step-by-step time incremental procedure is handled as follows. For a 1-dimensional viscoelastic material subjected to a strain rate, the stress after an elapsed time t is given by

$$\sigma(t) = \int_0^t E(t-\tau)\frac{d\epsilon(\tau)}{d\tau}\,d\tau$$

$$\sigma(t) = \sum_{i=0}^{n-1} \int_{t_i}^{t_{i+1}} E(t-\tau)\frac{d\epsilon(\tau)}{d\tau}\,d\tau$$

If the time increments are made small enough, the trapezoidal rule can be used.

$$\sigma(t_n) = \sum_{i=0}^{n-1} \tfrac{1}{2}\left[E(t_n - t_{i+1}) - E(t_n - t_i)\right]\left[\epsilon(t_{i+1}) - \epsilon(t_i)\right]$$

$$= \sum_{i=0}^{n-1} \left[E(t_n - t_{i+\frac{1}{2}})\right]\left[\epsilon(t_{i+1}) - \epsilon(t_i)\right]$$

For an axisymmetric solid, this equation becomes

$$\begin{Bmatrix}\sigma_{rr}\\ \sigma_{zz}\\ \sigma_{\theta\theta}\\ \sigma_{rz}\end{Bmatrix} = \sum_{i=0}^{n-1} \frac{E(t_n - t_{i+\frac{1}{2}})}{(1+\nu)(1-2\nu)} \begin{bmatrix}1-\nu & \nu & \nu & 0\\ \nu & 1-\nu & \nu & 0\\ \nu & \nu & 1-\nu & 0\\ 0 & 0 & 0 & \frac{1-2\nu}{2}\end{bmatrix} \begin{Bmatrix}\Delta\epsilon_{rr}(t_{i+1})\\ \Delta\epsilon_{zz}(t_{i+1})\\ \Delta\epsilon_{\theta\theta}(t_{i+1})\\ \Delta\epsilon_{rz}(t_{i+1})\end{Bmatrix}$$

where $\Delta\epsilon(t_{i+1}) = \epsilon(t_{i+1}) - \epsilon(t_i)$.

METHOD FOR CALCULATING EQUIVALENT 18-KIP LOAD APPLICATIONS

J. F. Shook and T. Y. Lepp, The Asphalt Institute, College Park, Maryland

Several thickness design methods make use of traffic analysis procedures based on equivalent 18-kip single-axle load applications (EWL_{18}). The basic method for determining EWL_{18} uses load equivalency factors with axle weight distribution data from truck weight study reports for calculating equivalent applications, but this method is somewhat tedious to follow, and sufficient data often are not readily available. To produce a more usable method, an investigation into factors affecting EWL_{18} was made by using results of truck weight and loadometer data from 47 states. It was found that EWL_{18} correlated well with the number of heavy trucks, but the correlation coefficients varied considerably among states. A similar study using only ADT also showed considerable variation among both states and highway class within a given state. Both of these were not as good as relationships using some measure of average axle weight or average truck gross weight. The most useful relationship and highest correlation of all those investigated was found among EWL_{18}, legal axle load limit, average heavy truck weight, and number of heavy trucks.

•A NUMBER of thickness design methods use traffic analysis procedures that are based on equivalent 18-kip single-axle load applications (EWL_{18}). Among them is the AASHO method (1), those derived from it by various state agencies, and The Asphalt Institute method (2). The basic method for determining EWL_{18} uses load equivalency factors with axle weight distribution data from truck weight study reports for calculating equivalent applications. The calculations are given in Table 1 and elsewhere (4).

Several states having access to computers use truck weight study data routinely to calculate, for design purposes, equivalent applications such as that given in Table 1. However, for states not having access to computers, the traffic analysis method shown in Figure 1 is quite tedious and time-consuming. Many other organizations, not having ready access to truck weight study data or to computers for calculating equivalent applications, may use short-cut methods, and these are often very helpful. Sometimes, traffic situations are categorized without any real resort to computations. A proper accounting of traffic, however, is necessary for accurate design of both new and overlay pavements. Therefore, the most useful method for determining EWL_{18} is one that is intermediate in complexity between those that use full truck weight study data and those that make essentially no use of the data.

One example of a very simple method for calculating EWL_{18}, expressed as DTN and shown in Figure 2, was published in an early edition of the Thickness Design Manual (3). This method was derived from studies of truck weight study data from 47 states for the years 1959 through 1963. It is primarily based on a correlation between EWL_{18} and traffic volume for different classes of highways and streets. The procedure was simple to use but inexact. For example, for an interurban freeway with a vehicle-per-day count of 10,000, the EWL_{18} could vary from 400 to 3,000 equivalent applications per day. This represents a difference of 2 in. of asphalt base or surface in a new pavement design, or perhaps the difference between none and 2 in. of overlay, a substantial difference in some situations.

Sponsored by Committee on Flexible Pavement Design and presented at the 50th Annual Meeting.

TABLE 1

COMPUTATION OF EQUIVALENT APPLICATIONS

Axle Load (lb)	Mean Axle Load (lb)	Load Equivalency Factor[a]	Number of Axles	Percent Axles	Equivalent Applications, EWL_{18}
Single axle					
Under 3,000	2,000	0.01165	0	0	0
3,000 to 6,999	5,000	0.02672	332	16.4	8.87
7,000 to 7,999	7,500	0.0538	278	13.7	14.96
8,000 to 11,999	10,000	0.108	762	37.6	82.30
12,000 to 15,999	14,000	0.3285	121	6.0	39.75
16,000 to 17,999	17,000	0.757	101	5.0	76.50
18,000 to 19,999	19,000	1.321	181	8.9	239.10
20,000 to 21,999	21,000	2.305	173	8.5	398.76
22,000 to 22,399 22,400 to 23,400 23,401 to 23,999	23,000	4.019	64	3.2	257.22
24,000 to 25,999	25,000	7.017	11	0.5	77.19
26,000 to 29,999	28,000	16.17	5	0.2	80.85
Total					1,275.50
Total weighed			2,028		
Total counted			8,020		
Tandem axle					
Under 6,000	3,000	0.0108	1	0.10	0.0108
6,000 to 11,999	9,000	0.0278	203	20.02	5.64
12,000 to 17,999	15,000	0.0719	181	17.85	13.01
18,000 to 23,999	21,000	0.186	93	9.17	17.30
24,000 to 29,999	27,000	0.484	133	13.12	64.37
30,000 to 31,999	31,000	0.912	85	8.38	77.52
32,000 to 33,999	33,000	1.253	106	10.46	132.82
34,000 to 35,999	35,000	1.721	93	9.17	160.05
36,000 to 37,999	37,000	2.363	57	5.62	134.69
38,000 to 39,999	39,000	3.246	35	3.45	113.61
40,000 to 41,000	40,500	4.113	12	1.18	49.36
41,000 to 42,000	41,500	4.827	5	0.49	24.14
42,000 to 43,999	43,000	6.125	6	0.59	36.75
44,000 to 45,999	45,000	8.412	3	0.30	25.24
46,000 to 49,999	48,000	13.45	1	0.10	13.45
Total					867.96
Total weighed			1,014		
Total counted			4,010		
Total single and tandem					2,143.46
Avg per axle					0.705
Avg per vehicle					2.114

Note: Computations apply for 4-axle tractor-semitrailer combinations according to 1961 Maryland FAPR.

[a]Asphalt Institute load factors.

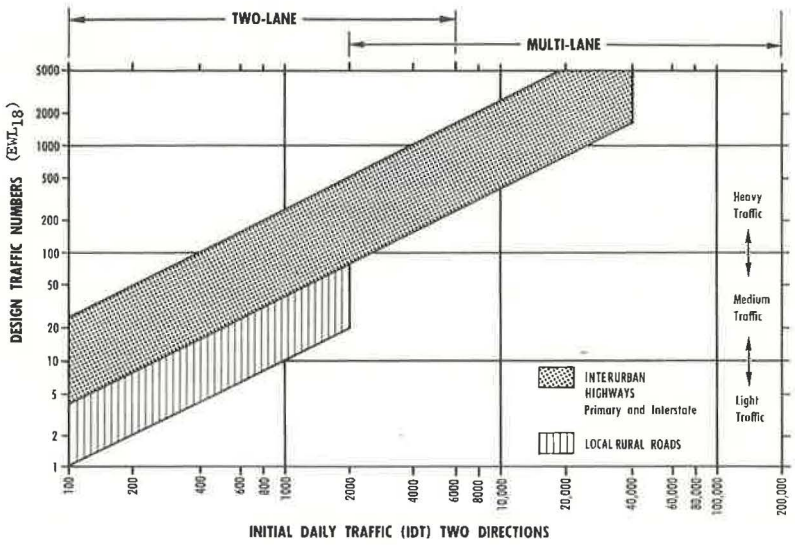

Figure 1. Simple traffic analysis method of The Asphalt Institute, 1969 Manual (2).

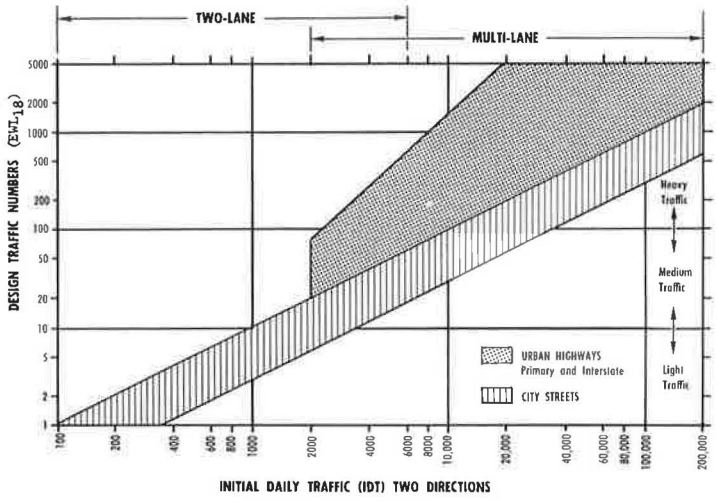

Figure 2. Simple traffic analysis method of The Asphalt Institute, 1963 Manual (3).

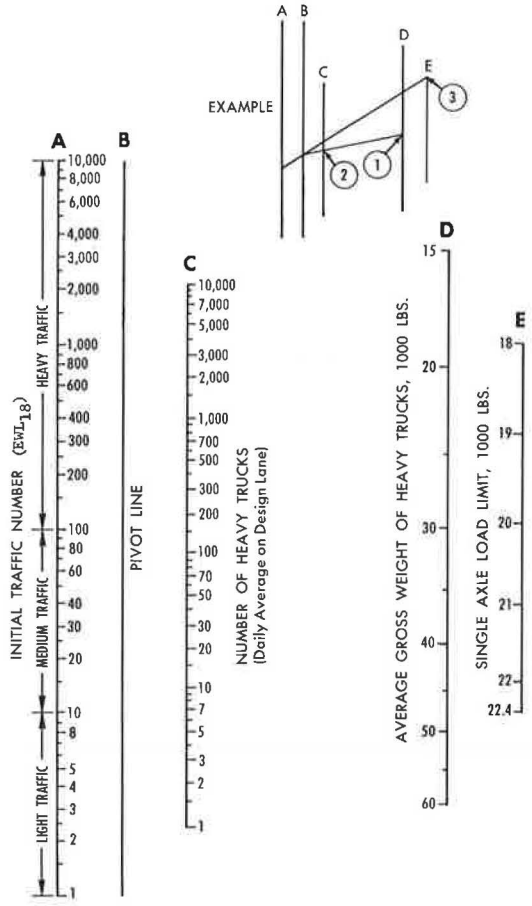

Figure 3. New traffic analysis method of The Asphalt Institute.

A method is presented in this paper that attempts to overcome some of the deficiencies of the design traffic analysis procedures discussed briefly in the preceding. It is based on studies of truck weight study data from the same 47 states mentioned previously for the years 1959 through 1963 and additional data from 11 states for the years 1964 through 1967. The method is shown in Figure 3.

The new method is based on a correlation among EWL_{18}, single-axle load limit, average gross weight of heavy trucks, and number of heavy trucks. All of the inputs are readily obtained except, perhaps, average truck weight. Unfortunately, as explained in the following, there are too many differences among states to permit the developing of any across-the-board correlation without using some measure of average truck weight or average axle weight. The authors felt that gross weight of trucks was more easily obtained than average axle weight, and so they chose this for use with the method. In several cases, particularly those involving truck-loading facilities and parking lots, this has proved to be the case. The method also has been checked against axle weight distribution data from several countries outside the United States and has been found to work. We feel, therefore, that the method does have merit and should prove useful to persons making traffic analyses for asphalt pavement structural design.

DISCUSSION OF ANALYSIS METHOD

Correlations Between EWL_{18} and Number of Heavy Trucks

The traffic analysis procedure shown in Figure 3 has the following mathematical expression:

$$\text{Log } EWL_{18} = -10.68 + 3.40 \log S + 1.33 \log W + 1.05 \log N$$

where

S = legal single-axle load limit, 1,000 lb;
W = average heavy truck gross weight, lb, for 2-axle, 6-tire trucks or larger; and
N = number of heavy trucks.

This relationship was developed from a study of factors that affect EWL_{18}. This study indicated that increasing axle load trends seemed to correlate well with increasing truck volumes, although there were important differences among various states. Average truck weights and volumes vary from state to state and can vary considerably from highway to highway in the same state. Also, it has been found through calculations of EWL_{18}, using truck weight study data, that automobiles and light trucks contribute little to EWL_{18} in most cases. With this in mind, it was felt that heavy truck traffic alone might serve as the basis for developing a simplified traffic analysis procedure. This, of course, depended on whether there was a reasonable correlation between the number of heavy trucks and EWL_{18} calculated by using axle weight distribution data. A least squares regression of each state's loadometer data indicated that this was so.

Regressions were made on truck weight data from 47 states with the log of the number of heavy trucks and the log of the calculated EWL_{18} as the variables. The following model was used:

$$\text{Log } EWL_{18} = A_0 + A_1 \log (\text{number of heavy trucks})$$

Data for the study were obtained from Tables W-1 and W-4 of reports on loadometers and truck weights submitted by most states to the Federal Highway Administration each year. In this study, calculations were made for each loadometer station for each highway classification reported by the states.

The mean EWL_{18}, number of heavy trucks, and number of loadometer stations for each of the states used in the study are given in Table 2. Asphalt Institute load equivalency factors were used to calculate EWL_{18} (4). Average equivalent applications per vehicle were calculated from the data in the $\bar{W}$-4 tables as given in Table 1. The vehicle factors were then used with truck count data in the W-1 tables to calculate EWL_{18} for each loadometer station.

It was noted that the majority of the A_1 values were close to 1.1. This indicated that a 1.1 slope could be used in developing a traffic analysis chart. This was supported by the high values obtained for the correlation coefficients. Typical data obtained in the regression analyses are given in Table 2 and shown in Figure 4. As expected, the regression analyses resulted in a spread in A_0 values because of the variation in average axle load from state to state.

Because most regression lines had slopes of about 1.1, the possibility of using the results for making a simplified design procedure was considered. A traffic analysis chart (Fig. 5) was constructed. The chart consisted of a series of arbitrarily selected lines (design lines) that could be identified with numbers determined for each state. These are given by highway classification in Table 3. The procedure was not adopted for use in The Asphalt Institute manual, however, because it was felt that it would require too much updating as traffic patterns and weight restrictions were changed in each state.

It is also significant to note that, because the majority of A_1 values given in Table 2 are greater than 1.0, the EWL_{18} contributed per truck is not a constant, but it increases as the volume of heavy truck traffic increases. Thus, choosing a rate of growth for volume alone could result in underestimates of the total EWL_{18} expected during the de-

TABLE 2

RURAL HIGHWAY REGRESSION VALUES

State	Year	A_0	A_1	R^2	RMSE	Mean EWL_{18}	Mean Number Heavy Trucks	Counting Period (hours)	Number of Load-ometer Stations
Alabama	1962	-0.2970	1.02	0.987	0.0287	383	667	24	10
	1963	—	—	—	—	—	—	—	—
Alaska	1962	0.0823	0.84	0.866	0.1403	43	71	16	7
	1963	—	—	—	—	—	—	—	—
Arizona	1962	-0.8678	1.24	0.797	0.1402	106	212	8	10
	1963	-1.1738	1.34	0.942	0.0699	330	578	24	10
Arkansas	1962	-1.1675	1.33	0.850	0.0791	423	716	24	11
	1963	—	—	—	—	—	—	—	—
California	1962	0.5153	0.77	0.683	0.1091	415	548	8	14
	1963	-0.7311	1.20	0.990	0.0385	1,974	2,321	24	13
Colorado	1962	—	—	—	—	—	—	—	—
	1963	—	—	—	—	—	—	—	—
Connecticut	1962	-0.1923	1.10	0.981	0.0955	784	654	8	8
	1964		1.05	0.990	0.0521	1,906	1,073	24	8
Delaware	1962	-0.1897	1.14	0.997	0.0349	513	357	8	8
	1963	0.0390	1.09	0.997	0.0380	1,947	977	24	7
Florida	1962	-0.4231	1.14	0.953	0.0891	316	363	16	32
	1963	-0.3024	1.08	0.948	0.0979	282	352	16	32
Georgia	1962	-0.3644	1.12	0.978	0.0668	271	316	13-8, 2-24	15
	1963	—	—	—	—	—	—	—	—
Hawaii	1962	-0.1325	1.06	0.903	0.1098	406	377	12	7
	1963	-4.0760	2.72	0.423	0.3661	192	220	12	6
Idaho	1962	-0.0412	0.94	0.987	0.0012	230	353	24	5
	1963	—	—	—	—	—	—	—	—
Illinois	1962	-0.5446	1.10	0.975	0.0510	172	328	8	17
	1963	—	—	—	—	—	—	—	—
Indiana	1962	-0.7429	1.17	0.902	0.0825	281	527	8	20
	1963	-0.7269	1.18	0.910	0.0659	282	498	8	20
Iowa	1962	-1.1949	1.40	0.966	0.0961	343	456	24	11
	1963	-0.6799	1.25	0.974	0.0762	457	466	24	11
Kansas	1962	-0.6996	1.19	0.941	0.0519	117	213	8	12
	1963	-0.3933	1.06	0.981	0.0351	265	453	24	12
Kentucky	1962	0.0518	0.97	0.963	0.0420	636	692	24	8
	1963	-0.1143	1.00	0.934	0.0600	640	854	24	10
Louisiana	1962	-0.3836	1.12	0.859	0.1287	186	231	8	10
	1963	-0.7490	1.26	0.951	0.0697	375	434	24	10
Maine	1962	-0.4728	1.17	0.965	0.0870	527	540	24	10
	1963	—	—	—	—	—	—	—	—
Maryland	1962	-0.2596	1.12	0.976	0.0853	1,299	1,019	24	12
	1963	-0.0578	1.06	0.993	0.0444	1,471	1,076	24	12
Massachusetts	1962	—	—	—	—	—	—	—	—
	1963	—	—	—	—	—	—	—	—
Michigan	1962	-0.6821	1.15	0.988	0.0752	443	762	24	9
	1963	—	—	—	—				
Minnesota	1962	-0.4751	1.08	0.970	0.0719	178	332	7-16, 14-24	21
	1963	—	—	—	—	—	—	—	—
Mississippi	1962	-0.0206	0.93	0.760	0.0705	226	350	8	14
	1963	—	—	—	—	—	—	—	—
Missouri	1962	-0.6762	1.12	0.914	0.0594	390	832	24	19
	1963	-0.3740	1.01	0.943	0.0454	410	876	24	19
Montana	1962	-0.0115	0.92	0.800	0.1157	178	267	8-16, 1-24	9
	1963	—	—	—	—	—	—	—	—
Nebraska	1962	-0.5650	1.14	0.915	0.0823	86	153	8	25
	1963	-0.2222	0.98	0.628	0.1847	246	451	24	25
Nevada	1962	-0.4108	1.17	0.973	0.0944	87	103	8-8, 2-24	10
	1963	—	—	—	—	—	—	—	—
New Hampshire	1962	—	—	—	—	—	—	—	—
	1963	—	—	—	—	—	—	—	—
New Jersey	1962	—	—	—	—	—	—	—	—
	1963	—	—	—	—	—	—	—	—
New Mexico	1962	0.1047	1.01	0.791	0.1331	222	166	8	12
	1963	-0.2903	1.20	0.894	0.1082	617	378	24	12
New York	1962	-0.0960	1.01	0.858	0.097	624	731	24	22
	1963	—	—	—	—	—	—	—	—
North Carolina	1962	-0.4592	0.92	0.830	0.0802	72	339	8	21
	1963	—	—	—	—	—	—	—	—
North Dakota	1962	-0.5026	1.06	0.969	0.0501	130	288	24	16
	1963	—	—	—	—	—	—	—	—
Ohio	1962	-0.9373	1.28	0.956	0.0719	946	1,139	24	12
	1963	—	—	—	—	—	—	—	—
Oklahoma	1962	-0.1663	1.16	0.943	0.0616	859	472	8-16, 2-24	10
	1963	—	—	—	—	—	—	—	—
Oregon	1962	-0.3297	1.11	0.969	0.0410	277	307	8	6
	1963	—	—	—	—	—	—	—	—

Table 2 (continued)

State	Year	A_0	A_1	R^2	RMSE	Mean EWL_{18}	Mean Number Heavy Trucks	Counting Period (hours)	Number of Load-ometer Stations
Pennsylvania	1962	-0.7456	1.16	0.982	0.0466	443	854	16	14
	1963	-0.5147	1.08	0.980	0.0616	599	1,121	24	14
Rhode Island	1962	-1.2990	1.51	0.95	0.1388	761	589	25	5
	1963	—			Rural and Urban Stations Combined for 1962				
South Carolina	1962	-0.1752	1.02	0.911	0.0909	324	429	8	11
	1963	-0.0983	1.03	0.957	0.0536	883	904	24	10
South Dakota	1962	-0.3149	0.96	0.913	0.0739	82	213	16	18
	1963	—	—	—	—	—	—	—	—
Tennessee	1962	-0.1091	1.07	0.741	0.0783	433	370	8	8
	1963	—	—	—	—	—	—	—	—
Texas	1962	-0.0117	0.99	0.878	0.0923	553	597	1-16, 18-24	19
	1963	—	—	—	—	—	—	—	—
Utah	1962	-0.1928	0.95	0.955	0.0684	79	154	8	9
	1963	-0.4354	1.07	0.946	0.0823	114	218	8	9
Vermont	1962	-0.8089	1.24	0.786	0.1292	100	186	8	5
	1963	—	—	—	—	—	—	—	—
Virginia	1962	-0.3004	1.03	0.845	0.0953	298	499	8	12
	1963	-0.3406	1.05	0.974	0.0612	651	972	24	11
Washington	1962	-0.0165	0.92	0.869	0.0855	211	318	8	8
	1963	-0.1725	0.89	0.704	0.1144	624	892	24	8
West Virginia	1962	-0.8492	1.39	0.931	0.1401	236	206	8-8, 2-16	10
	1963	-0.6869	1.21	0.906	0.1291	124	202	9-8, 2-16	11
Wisconsin	1962	-1.7203	1.55	0.958	0.1358	119	286	16	28
	1963	—	—	—	—	—	—	—	—
Wyoming	1962	-0.5712	1.14	0.966	0.0697	63	119	8	8
	1963	—	—	—	—	—	—	—	—

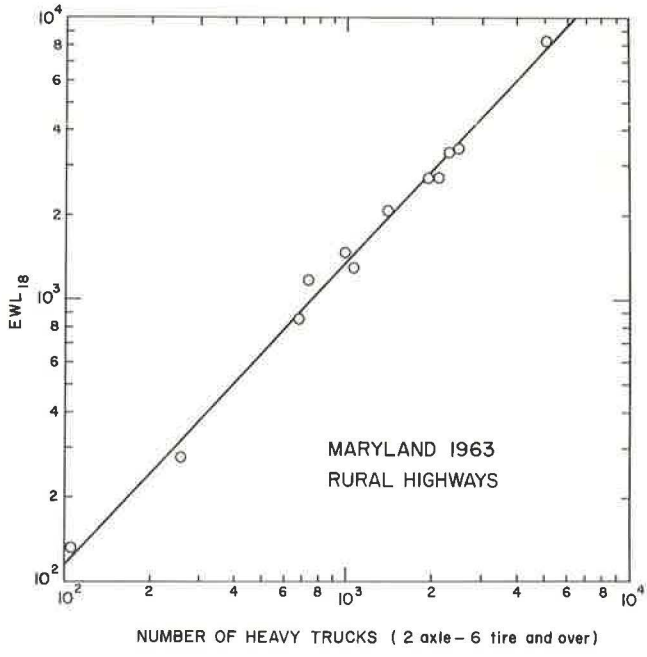

Figure 4. Typical regression curve.

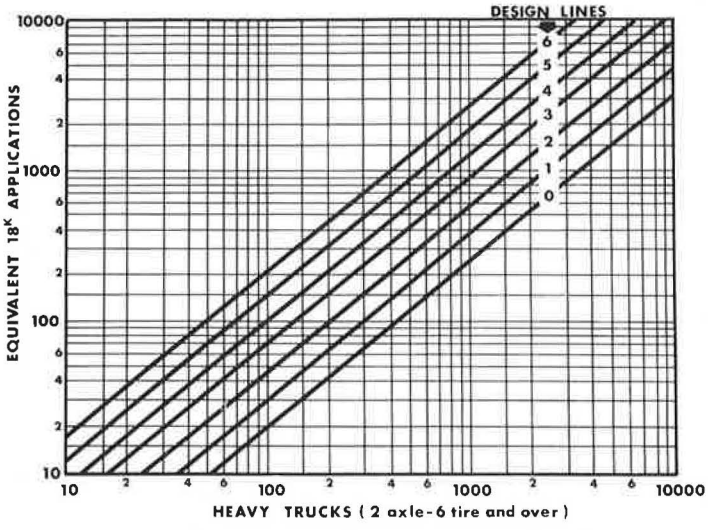

Figure 5. Possible traffic analysis chart.

TABLE 3

DESIGN LINES FOR HEAVY TRUCK CORRELATION CHART

State	Interstate and Primary Rural	Primary Urban and Local Roads	State	Interstate and Primary Rural	Primary Urban and Local Roads
Alabama	2		Montana	3	
Alaska	3		Nebraska	2.5	0
Arizona	2.5		Nevada	3.5	
Arkansas	2.5	1	New Hampshire		
California	3.0	1.5	New Jersey		
Colorado			New Mexico	5	No urban
Connecticut	5.0	3	New York	3	1.5
Delaware	5	2.5	North Carolina	0	
Florida	3.5	2.5	North Dakota	2	
Georgia	3.5		Ohio	3	3
Hawaii			Oklahoma	5.5	1.5
Idaho	2.5	1.5	Oregon	3.5	
Illinois	2		Pennsylvania	2	1.5
Indiana	2		Rhode Island	5	3
Iowa	4	3	South Carolina	3	2.5
Kansas	2.5	0.5	South Dakota	1.5	
Kentucky	2.5	0.5	Tennessee	4.5	
Louisiana	3.5	2.5	Texas	3.5	1.5
Maine	4	2	Utah	2	
Maryland	4	3.5	Vermont	2.5	
Massachusetts			Virginia	2.5	1.5
Michigan	2	1.5	Washington	2.5	1
Minnesota	2	2	West Virginia	3	
Mississippi	2.5		Wisconsin	2.5	1.5
Missouri	1.5	0	Wyoming	2	

Note: Refer to chart shown in Figure 5.

sign period. On the other hand, a traffic analysis procedure based on the reported regression slopes allows for an increase in average axle weight with increases in truck traffic volume.

TABLE 4
EFFECT OF TIME OF COUNT

Duration of Count (hours)	Number of Regressions	Range in R^2		
		Low	High	Mean
24	28	0.70	0.997	0.95
16	16	0.87	0.98	0.94
8	22	0.68	0.997	0.88

Note: Data taken from 1962 and 1963 rural highway information.

Effect of Time of Count

It will be noted from the data given in Table 2 that states report loadometer and traffic survey data based on differing count periods, which vary from 8 to 24 hours. Table 4 gives the correlation coefficient information for 64 least squares regressions of main rural highway data for different times used in collecting the data. Generally, it was found that 24-hour count data gave the highest correlation values, whereas 8-hour count data yielded the lowest. However, this may not be true for highways with uniformly distributed daily truck traffic. For example, Delaware had a 0.997 value for both the 8-hour counts in 1962 and the 24-hour counts in 1963. This indicates that the heavy truck distribution for Delaware's main rural highways is approximately the same for either an 8- or 24-hour count. On the other hand, the regressions for California data gave correlation values of 0.683 for the 8-hour count and 0.99 for the 24-hour count. In view of these differences, it would be better to use 24-hour count data when present and future equivalent applications are estimated. However, in these studies we had to use the data available and believe that there are no serious consequences to the method presented.

Correlations Among EWL_{18}, Legal Load Limit, Average Heavy Truck Weight, and Number of Heavy Trucks

Variations among states, as given in Table 2, result from variations in both the axle-weight and the truck-type distributions. However, these differences are not consistent for all states or highways. Legal weight-limit variations, character of vehicle, load prevailing in a given area, and many other factors account for these differences. Regardless of the differences, a study of the 2-year data indicated that regression values for a given state are similar from year to year if changes such as increased legal axle limit do not occur.

Nevertheless, changes can be expected from time to time in factors that affect the relationship between EWL_{18} and the number of heavy trucks. For this reason, the correlation study was expanded to include a search for a method that would not require identification of analysis factors (e.g., design lines shown in Figure 5) with individual states.

It was shown in the foregoing that EWL_{18} correlates well with the number of heavy trucks but that differences among states have significant effects on design. After considerable study of many possible factors, including average axle weight, we found the most useful relationship and highest correlation to be among EWL_{18}, legal axle load limit, average heavy truck weight, and number of heavy trucks for all data available from 1962 through 1967. The final form of the relationship is given in the nomograph shown in Figure 3.

Data used were collected at 10 to 23 weighing stations on all classes of highways in 11 states during the years 1962 through 1967. There were 383 data points altogether. The resulting correlation was $R^2 = 0.91$. The equation was

$$\text{Log } EWL_{18} = -10.683 + 3.401 \log S + 1.334 \log W + 1.051 \log N$$

where

S = legal single-axle load limit, 1,000 lb;
W = average heavy truck gross weight, lb; and
N = number of heavy trucks.

The nomograph shown in Figure 3 was developed from this equation and is included in the latest edition of The Asphalt Institute manual (2). Although designed specifically for the Asphalt Institute method, it can be used with reasonable accuracy with other methods derived from AASHO Road Test data. Preferably, however, a similar nomograph should be developed by using AASHO load equivalency factors instead of Asphalt Institute factors to calculate EWL_{18}. Also, the inclusion of more data than those used in this study might result in a slightly different set of coefficients for the equations.

Modifications now under study include relationships among average truck weight, truck count data, and percentage of loaded trucks. The intent is to make as much use as possible of data that can be collected by counting instead of by weighing. The use of 1963 interstate rural data from 31 states in trial models have given correlations of $R^2 = 0.82$ for average heavy truck weight expressed as a function of the log of count data. The percentage of heavy trucks loaded contributed at least 63 percent of the correlation. It seems possible that further modifications of the model will yield a more accurate equation that could be applied throughout the United States and elsewhere.

CONCLUSION

Simple methods for calculating equivalent 18-kip single-axle load applications for traffic analysis for pavement structural design are useful to designers not able to use full truck weight study data. Three methods are presented in this paper utilizing relationships correlating EWL_{18} and other factors, including number and average weight of heavy trucks, based on studies of truck weight study data collected from state highway departments. One method is currently used by The Asphalt Institute in its design manual. Even simpler methods are possible for use in states or smaller jurisdictions.

REFERENCES

1. Interim Guide for the Design of Flexible Pavement Structures. American Assn. of State Highway Officials, Washington, D. C., Oct. 1961.
2. Thickness Design—Full-Depth Asphalt Pavement Structures for Highways and Streets. The Asphalt Institute, College Park, Md., Manual Series 1 (MS-1), 8th Ed., Dec. 1969.
3. Thickness Design—Asphalt Pavement Structures for Highways and Streets. The Asphalt Institute, College Park, Md., Manual Series 1 (MS-1), 7th Ed., Sept. 1963.
4. Shook, J. F., Painter, L. J., and Lepp, T. Y. Use of Loadometer Data in Designing Pavements for Mixed Traffic. Highway Research Record 42, 1963, pp. 41-56.

STRUCTURAL DESIGN OF UNSURFACED ROADWAYS AND AIRFIELDS

George M. Hammitt, II, U.S. Army Engineer Waterways Experiment Station, Vicksburg, Mississippi

ABRIDGMENT

•AN INVESTIGATION was conducted concerning the development of a structural design procedure using soil as a surfacing layer for roadway and airfield pavements. A review of the literature revealed limited pertinent testing that consisted of a total of 78 full-scale controlled tests conducted by the U.S. Army Engineer Waterways Experiment Station. The test items were generally 2-layer systems composed of a higher strength soil material overlying a weaker soil layer. These soils were of various types, thicknesses, and strengths (subgrade and cover). They were tested under various conditions of load, tire pressure, and tire size. Only failed items used in single-wheel load tests were considered in an analysis to develop equations for design of cover layers.

A multiple linear regression analysis was performed, and prediction equations were developed for thickness, coverage (service life), subgrade strength, load, and tire pressure in terms of the independent variables most affecting these values. These prediction equations are a method of presenting design criteria for unsurfaced roads and unsurfaced airfields based on the results of the full-scale testing.

The 5 independent variables of tire pressure, load, coverage, subgrade soil CBR, and cover soil CBR were tentatively selected as best defining thickness, the dependent variable. The 1 dependent variable and the 5 independent variables were put in a common logarithm form, and a linear correlation was developed in an equation form. The addition of more variables did not significantly increase the degree of correlation. Deleting any of the 5 variables decreased the degree of correlation and the increased standard error of estimate. An attempt to analyze the performance of different test items on the basis of material components revealed that there was no appreciable difference in the performance. Also, the correlation values were better when the type-of-material variable was deleted. The following equation is presented as best predicting thickness requirements:

$$\begin{aligned}\text{Log thickness} = &-1.02165 + 0.63624 \log \text{tire pressure} \\ &+ 0.21484 \log \text{load} + 0.23937 \log \text{coverage} \\ &- 0.402813 \log \text{subgrade CBR} \\ &- 0.31404 \log \text{cover CBR}\end{aligned} \quad (1)$$

This correlation has a standard error of estimate of 2.5 in. and an R-value of 0.815; R^2 equals 0.665. A shape number relating tire dimensions and deflections, $b \cdot d(\delta)^{1/2}$, was used as an additional variable. In this form b is equal to width, d is equal to diameter, and δ is equal to deflection of tires. However, the addition of this variable did not improve the degree of correlation; therefore, it was not included. Also, deletion of the cover CBR variable weakened the correlation and increased the standard error of estimate; therefore, this variable was retained.

Sponsored by Committee on Theory of Pavement Design.

A similar type of analysis was used for each of the other 4 variables with the following results:

$$\begin{aligned}\text{Log coverage} = {} & 5.90386 - 1.73226 \log \text{tire pressure} \\ & - 1.75002 \log \text{load} + 1.21599 \log \text{subgrade CBR} \\ & + 1.10497 \log \text{cover CBR} + 0.851912 \log \text{shape number} \\ & + 2.64158 \log \text{thickness} \end{aligned} \tag{2}$$

$$\begin{aligned}\text{Log subgrade CBR} = {} & - 1.57455 + 0.49026 \log \text{tire pressure} \\ & + 0.58114 \log \text{load} + 0.17190 \log \text{coverage} \\ & - 0.00123 \log \text{cover CBR} - 0.38251 \log \text{shape number} \\ & - 0.65471 \log \text{thickness} \end{aligned} \tag{3}$$

$$\begin{aligned}\text{Log load} = {} & 1.74026 + 0.20493 \log \text{tire pressure} \\ & - 0.07135 \log \text{coverage} + 0.16762 \log \text{subgrade CBR} \\ & + 0.07199 \log \text{cover CBR} + 0.74112 \log \text{shape number} \\ & + 0.20042 \log \text{thickness} \end{aligned} \tag{4}$$

$$\begin{aligned}\text{Log tire pressure} = {} & 1.47676 + 0.28537 \log \text{load} - 0.09836 \log \text{coverage} \\ & + 0.19691 \log \text{subgrade CBR} + 0.20471 \log \text{cover CBR} \\ & - 0.44815 \log \text{tire shape number} \\ & + 0.31440 \log \text{thickness} \end{aligned} \tag{5}$$

The assumptions of a linear relationship are generally sound for the ranges of variables described from actual tests, but the true relationship may be far from linear for wider ranges. Specific reverification tests are needed in the lower and higher ranges of extrapolation where test data did not exist. Six additional tests in these ranges would confirm the findings and substantiate the assumption of linear relationship for the entire range of prediction.

Additional study is needed to better define the load-carrying capability of soils of large values of modulus of elasticity E in a 2-layer system. For identical subgrade conditions, this study revealed only very small actual reduction of thicknesses when increases of cover soil strength occurred. A series of tests is needed in which identical sections, with the exception of cover soil type and strength, are constructed, tested, and compared.

The 5 prediction equations for thickness, coverage, subgrade CBR, load, and tire pressure represent a method that previously was not available for the design of road shoulders and unsurfaced roads and airfields. The equations are the results of analysis of 78 full-scale test items.

HIGH-SPEED PROFILOMETRY

J. R. Darlington, Testing and Research Division,
Michigan Department of State Highways, Lansing

The General Motors rapid travel profilometer has been evaluated by the Michigan Department of State Highways. It meets or exceeds all specifications for accuracy and reliability. It does not return a survey type of elevation map because long-wave features must be filtered out. For this reason, its profiles must be viewed as correct in the frequency domain but incorrect in the spatial domain. An inertial guidance system capable of recording long-wave features would solve the problem. Profile analysis in the frequency domain is confined to the 4 basic measures: mean squares, amplitude distributions, autocorrelation, and power spectral density. It is possible to extract some single number indexes based on the 4 standard measures. Power spectral density appears to be most interesting for highway work.

•THE RAPID TRAVEL PROFILOMETER (RTP) developed by General Motors (1) has ushered in a new era of road profile measurement. At the same time significant advances in data acquisition and signal analysis methods have provided powerful tools for profile study. Opportunities to use these new techniques became apparent during an evaluation of the RTP. This paper discusses the theory of the RTP, the outcome of the evaluation study, and the use of modern data acquisition and signal analysis on RTP profiles.

Profiles may be viewed as an elevation map for a narrow strip of roadway (width of wheel) or as a random signal with certain properties in common with all other random signals. Implications of this dual viewpoint are discussed.

THE GENERAL MOTORS RAPID TRAVEL PROFILOMETER (RTP)

The RTP is based on 2 systems. The first is hardware consisting of acceleration and displacement transducers. The second is software consisting of a signal-processing concept that can be implemented in various ways. The first system is relatively straightforward and consists of 2 transducers mounted in a vehicle. These are a linear potentiometer connected between a small road-following wheel and the vehicle body, and an accelerometer mounted in the vehicle body. Each transducer senses 2 components of vertical motion. The road-following wheel senses body bounce and changes in surface elevation that occur too rapidly to move the vehicle as a unit. The accelerometer picks up body bounce and elevation changes that occur slowly enough to move the entire vehicle as a unit. Acceleration data are then integrated twice to produce a displacement signal. When road-following wheel and accelerometer displacement signals are algebraically summed, the result is a road surface profile. Body bounce is canceled because it appears with equal magnitude but opposite polarity in each signal.

It is evident that long-wave features, such as hills or grade changes, are picked up by the accelerometer, and short-wave features are picked up by the road-following wheel. At this point, signals from the transducers, if processed as described, would

Sponsored by Committee on Surface Properties—Vehicle Interaction and presented at the 50th Annual Meeting.

yield a true elevation profile measured with respect to a reference established by the accelerometer when it was first turned on. Accuracy in recording long-wave, high-amplitude features such as hills would depend only on the quality of the accelerometer. If it responded to very low accelerations, even curvature of the earth would appear in long profile runs.

Explanation of the second system embodied in the RTP concept requires a digression into the nature of road profiles. Road profiles possess 1 characteristic that makes them difficult to measure. In terms of signal theory, profiles are said to exhibit a very high dynamic range of perhaps 80 dB (decibel) or more. In other words, it means that there is a great difference in amplitude between large features such as hills and surface details. For this reason, the attempt to measure surface detail, when it is accompanied by high-amplitude features, is similar to hearing a whisper next to Niagara Falls. Profile surface details will be invisible if the recording instruments are scaled to accommodate hills. If the instruments are scaled to make surface details visible, recorder overload will occur on the hills. This problem is avoided in surveying methods because instruments are continually moved to keep within range of the rod and the results are recorded numerically; this provides infinite dynamic recording capacity.

It is evident that some way had to be found to eliminate high-amplitude signals when profile is recorded on a medium of limited dynamic range. Fortunately, the nature of road profiles ensures that high-amplitude data will consist of long-wave features such as hills or grade changes. For this reason, a high-speed profilometer need only filter out the low-frequency signals induced in its sensors by high-amplitude hills and grade changes.

This filtering is accomplished by the second system associated with the RTP. It is actually a signal-processing concept that can be implemented in different ways depending on desired results. Basically, the fundamental operations of integrating acceleration twice and summing the result with road-following wheel displacement are combined with filtration. This is accomplished by forming the product of transfer functions for the operations desired and programming the result on an analog or digital computer. The computer then acts as a processor for the acceleration and road-following wheel signals. An illustration of this concept is as follows:

$$\left(\begin{array}{l}\text{transfer}\\ \text{function}\\ \text{for double}\\ \text{integration}\end{array} + \begin{array}{l}\text{road-following}\\ \text{wheel}\\ \text{displacement}\\ \text{signal}\end{array}\right) \times \left(\begin{array}{l}\text{transfer}\\ \text{function}\\ \text{for}\\ \text{filtration}\end{array}\right) = \text{profile}$$

The function labeled "filter" can be a transfer function for any third or higher order high-pass filter. Developers of the RTP chose the Butterworth design but could have used the Chebeyshev, Paynter, elliptical, or other type of design depending on needs. In practice the RTP operator chooses a filter cutoff frequency, feeds the transducer signals into the computer, and records a final profile that has all frequencies below the cutoff point attenuated. The filter not only removes the high-amplitude long-wave features but also permits use of a less-than-perfect accelerometer and eliminates concern over low-frequency noise contamination of the accelerometer signal. This contamination arises from drifts in the electronics and tilts of the accelerometer from a true vertical during the profile run.

It is valuable to note an important fact at this point. The transducer signals themselves do not span a great dynamic range. It is only after processing the accelerometer signal through double integration that high-amplitude hills and grade changes emerge. This is made clear by noting that double integration of a very small positive or negative acceleration over a long period of time results in a very large output. In other words, the second derivative of road profiles does not have a high dynamic range. Consequently, one could obtain long-wave, high-amplitude features by installing a near-perfect accelerometer on a nontilting mount and digitally processing the resulting signal. Digital processing provides a very high dynamic recording range, as was seen

in the case of surveying. Filtration to remove the very lowest frequencies would probably still be needed, even with digital processing, because some low-frequency contamination is unavoidable.

The major effects of filtration depend on the intended use of the profile. If the profile is viewed as a random signal, the filter merely specifies the lower cutoff frequency of the data. The profile can then be analyzed by modern signal-analysis techniques without further difficulty. If the profile is viewed as an elevation map for a narrow strip of roadway, the filter introduces some problems. The main difficulty is lack of a fixed reference such as that used in surveying. This results in a final profile that does not look at all like the actual terrain. The filter introduces what might be called a piecewise linear reference for wavelengths up to one-tenth as long as the longest wave passed by the filter without attenuation. Thus, if the filter is passing 1,000-ft waves with no attenuation, waves up to 100 ft will be measured with respect to a linear reference. This reference is located at some arbitrary height and angle over the roadway. The next 100-ft segment, even if overlapping most of the first segment, will be measured with respect to a slightly different reference. Waves longer than one-tenth of maximum get shifted in phase and appear in the RTP profile ahead of their actual location on the roadway.

At present, the only way to produce a survey type of terrain map is by restoring long-wave features through a process called tipping. This requires transit shots at some predetermined interval, such as every 100 ft. When transit data and RTP profiles are processed by the tipping program, a true elevation map results with far less work than would be required by transit alone. With improved accelerometers, mounts, and digital processing, the required known elevation points could be thousands of feet apart.

EVALUATION OF RTP

We have seen how the RTP works and what it can do in theory. Evaluation of the device by the Research Laboratory Section of the Michigan Department of State Highways has shown close agreement between theory and practice. Accuracy under static conditions was easy to check and was found to be within specifications. Accuracy under dynamic conditions was considerably more difficult to determine.

Dynamic accuracy of any system is usually checked by feeding in a sine wave of fixed amplitude and noting the ratio of output to input for all frequencies of interest. Another method has recently been used that consists of feeding in broad-band random noise and measuring the power spectral density of the output. Random noise presents the system with all frequencies at once, thus providing a more realistic test. It was not feasible to apply either test to the RTP because very costly and complex drivers, generators, and delay networks would be needed.

Dynamic accuracy was determined by a technique developed in the early 1960's as part of a general attack on problems in signal theory. It is a statistical process defined by the expression

$$\gamma_{xy}^{2}(f) = \frac{\left| G_{xy}(f) \right|^{2}}{G_{x}(f)\, G_{y}(f)}$$

in which $G_x(f)$ and $G_y(f)$ are power spectral estimates for each of 2 signals, and $G_{xy}(f)$ is the cross spectrum at frequency (f). This coherence function statistic reveals the extent of agreement between 2 signals in a narrow frequency band centered at frequency (f). The result, after the function is evaluated for various (f), is a graph or table showing amplitude correlation (0:1) for all wavelengths in question. The analysis requires uniform and closely spaced, precise level readings from a test section containing equal intensity of roughness at all wavelengths. The RTP profile for the same test section was digitized, and the analysis was performed by computer. Analysis was complicated by the necessity to get RTP and precise level profiles in phase and by the arbitrary RTP reference that required tipping of the precise level profile to match the RTP reference. Analysis spanned wavelengths from 100 to 1 ft, and all coherence

values were significantly high indicating high dynamic accuracy. Table 1 gives the wavelength, frequency in cycles per foot, and coherence value for each estimate.

TABLE 1

COHERENCE VALUES BETWEEN AN RTP PROFILE AND A PRECISE LEVEL PROFILE

Wavelength (ft)	Frequency (cycles per foot)	Coherence Value (correlation)
100.0	0.01	0.997
50.0	0.02	0.984
25.0	0.04	0.979
16.7	0.06	0.959
12.5	0.08	0.947
10.0	0.10	0.951
8.4	0.12	0.956
7.2	0.14	0.909
6.3	0.16	0.963
5.5	0.18	0.843
5.0	0.20	0.872
4.2	0.24	0.944
3.1	0.32	0.918
2.5	0.40	0.954
2.1	0.48	0.991
1.8	0.56	0.979
1.4	0.72	0.858
1.3	0.87	0.816
1.1	0.91	0.891
1.0	1.00	0.916

With accuracy established, the RTP was evaluated as a tool for highway work. The RTP itself has been found to be very reliable, easy to maintain, and straightforward to operate. Beyond this, its high speed is essential in view of ever-increasing traffic loads that make older devices too slow and hazardous to operate. Several small improvements were made in the underbody photocell that was originally intended to sense cracks and joints, but that is now used as a test section marker to sense reflective strips placed on the roadway. The road-following wheel was fitted with a distance-sensing pulse marker to aid in horizontally scaling the computer profile.

The most important aspect of evaluation concerns the question already mentioned. How is the profile to be used? If only signal analysis is desired, there are no difficulties with the RTP. If the elevation map view is held, there is strong impetus to develop a system that can handle very long waves, conceivably as long as 5,000 ft. This became an issue when more uses were found for the elevation map. One use, for example, was airport runway profiles requiring the recording of 2,000-ft waves. Another case involved estimates of bituminous material needed in resurfacing jobs. This problem has been studied at the Research Laboratory, and the general solution is evident. Recording of very long waves requires a very high-quality accelerometer on a stable platform and digital processing of the output. Experimentation along these lines using gyro stabilization has yielded encouraging results. Because the RTP is actually a small-scale inertial guidance system, it would be possible to install a true inertial guidance system, such as those used in missiles, if the proper security environment could be achieved. This would allow pickup of very long waves similar to true surveying.

PROFILE ANALYSIS

Research Laboratory findings indicate that the major impact of the RTP concept lies in the field of profile analysis. Again, the signal versus elevation map view of road profiles has a strong bearing on analysis considerations. If the profile is viewed as a random signal with properties common to all random signals, the analysis possibilities are limited to modern signal analysis techniques.

These methods of signal analysis that make it possible to rationally analyze random signals began to develop about 1958. To quote from Bendat and Piersol (2), "Four main types of statistical functions are used to describe the basic properties of random data: (a) mean square values, (b) probability density functions, (c) autocorrelation functions and (d) power spectral density functions." These 4 categories allow classification of the 2 traditional roughness measures: inches per mile and slope variance. Inches per mile is found to fit no standard classification and is, in fact, an undefined measure. It is not supported by signal measurement theory even though it may correlate with subjective ride quality or other objective measures. Slope variance is classifiable under mean square values and is a rudimentary measure of average intensity for the profile's first derivative. Neither measure provides any information about average intensity in a given wavelength band. This is vital information because it relates roughness to specific profile features. In addition, of course, current instruments used to produce the traditional roughness measures "see" a distorted version of the actual profile.

Power spectral density (PSD) alone, of the 4 available measures, supplies average intensity of the profile in given wavelength bands. For this reason, PSD is said to completely characterize the random process.

The RTP lends itself perfectly to a PSD analysis because an undistorted profile is recorded on magnetic tape and because vital filtering functions are performed. Long-wave, high-amplitude data would bias the PSD function if it were not removed by the profile process filter.

Research Laboratory work with PSD analysis led to the 4 following points:

1. A study of the available literature indicates that no measure is available that is more comprehensive or that is supported by a body of statistical and engineering expertise;
2. The investigator using PSD analysis must specify his statistical decisions so others may compare their work;
3. Data for which PSD analysis would be unreliable will not yield a statistically valid measure of any other type; and
4. PSD analysis must be done with great care because any contamination of the profile by even weak periodic or nonperiodic noise will seriously bias the analysis.

Even though PSD is the analysis of choice, there are at least 2 other possibilities for a single-number index that can then be used for correlation with other measures—contractor evaluations or the like. These 2 measures are statistically valid because they are derived from the 4 basic signal analysis measures. The first is merely mean squares but is computed for a narrow band of wavelengths important to the study at hand. The second is an amplitude distribution for a narrow wavelength band. This measure will usually form a Poisson distribution and is, therefore, fully specified by a single number. This is due to the fact that any Poisson distribution can be specified by its mean or variance, and, although this measure is not physically meaningful at this time, it is statistically valid.

If the profile is viewed as an elevation map for a narrow strip of roadway, another analysis viewpoint prevails. In this case the profile is used directly for a growing variety of purposes. In order to reproduce long-wave features or orient a profile segment to the true elevation, it is necessary to tip the profile as discussed previously. True elevation profiles have been used for a variety of maintenance purposes including joint blowups, potholed areas, and heaved slabs. They have been used in pavement studies involving comparison of profiles recorded at different times. A current use of elevation map profiles is in determining amounts of bituminous material needed in resurfacing jobs. In this case a computer simulation of the paving machine is passed over the elevation profile, and bituminous quantities are computed.

SUMMARY

The General Motors rapid travel profilometer embodies principles of inertial guidance that will undoubtedly underlie all high-speed profilometers to come. The device is best understood in terms of filter theory because the important feature of the RTP concept is its filter. Evaluation of the device by the Research Laboratory Section of the Michigan Department of State Highways has shown it to be accurate and reliable. It will, however, need improvement if very long waves are to be recorded. The RTP permits use of modern signal-analysis techniques. Of these, power spectral density analysis seems to be most important.

REFERENCES

1. Spangler, E. B., and Kelly, W. J. GMR Road Profilometer, a Method for Measuring Road Profile. General Motors Research Laboratories, Warren, Mich., Pub. GMR-452, Dec. 1964.
2. Bendat and Piersol. Measurement and Analysis of Random Data. Wiley and Sons, 1966.
3. Marshall, J. L. Introduction to Signal Theory. International Textbook Co., 1965.

4. Carey, W. N., Jr., Huckins, H. C., and Leathers, R. C. Slope Variance as a Measure of Roughness and the CHLOE Profilometer. HRB Spec. Rept. 73, 1962, pp. 126-135.
5. Hutchinson, B. G. Analysis of Road Roughness Records. Department of Highways, Ontario, Rept. 101, 1965.
6. Quinn, B. E., and VanWyck, R. A Method for Introducing Dynamic Vehicle Loads Into Design of Highways. HRB Proc. Vol. 40, 1961, pp. 111-124.
7. Quinn, B. E., and Zable, J. L. Evaluating Highway Elevation Power Spectra From Vehicle Performance. Highway Research Record 121, 1966, pp. 15-26.
8. Blackman, R. B. Data Smoothing and Prediction. Addison Wesley, 1965.

PRACTICAL USES OF SPECTRAL ANALYSIS WITH SURFACE DYNAMICS ROAD PROFILOMETER

Roger S. Walker and W. Ronald Hudson, Center for Highway Research, University of Texas at Austin

This paper presents some practical uses of power spectral analysis and coherence analysis of data obtained from the surface dynamics road profilometer. A brief description of spectral and coherence analyses is provided, along with some practical examples of their use. The first application is an investigation of differences between an inexpensive replacement road-following wheel and the standard wheel that comes with the profilometer. The second example involves construction control and identification of differences between 2 methods for laying asphaltic base materials. Both of these investigations involved statistically designed experiments so that more reliable conclusions could be obtained and confidence limits defined. Slope variance and roughness index statistics were also examined for the work and are compared with the spectral and coherence analyses results. These methods appear to be a practical use of spectral techniques. Extension of these methods may provide the best approach yet available for development of adequate road profile specifications and construction control.

•DEVELOPMENT of the General Motors surface dynamics (SD) profilometer has made it possible to rapidly obtain road profile data. In addition, the data provided by the SD profilometer are better than those provided by other profilometers in that long wavelength information is included (1, 2). This new device, however, brought many problems of how to process and use the large quantities of data obtained. Initially, research efforts at the Center for Highway Research at The University of Texas at Austin were primarily directed toward computing various summary statistics, such as slope variance and roughness index values from the digitized road profile data. These values were then used for correlations with ratings made by a panel in order to develop equations to predict pavement serviceability index (PSI) (3). Recent work has been expanded to include the use of spectral analysis for analyzing these data.

Spectral analysis, which separates road profile data into the various frequencies contained in the data, has been discussed by Quinn and Hagen, who used rod and level measurements for obtaining profile data (4), and briefly by Whittemore and others, who used the SD profilometer as the measuring device (5). In the studies by Quinn and Hagen, problems in obtaining a standardized method for computing power spectra were discussed. Some of these problems still exist although the profile data obtained by Quinn and Hagen for these studies were not obtained with the profilometer, and the fast Fourier transform (FFT) was not used to compute the power spectral estimates. (The fast Fourier transform is an algorithm that provides Fourier coefficients directly. Use of this method is much faster for computing power spectral estimates than the mean-lagged product method that was most commonly used up until the past 10 years.)

The General Motors report (5) includes several power spectral plots of road profile data obtained with the profilometer. In this study, however, the investigators towed

Sponsored by Committee on Pavement Condition Evaluation.

the profilometer behind a test truck at 3 mph so that usable data could be obtained for their investigations. Wheel bounce at higher speeds of the road-following wheel was said to be detrimental to their studies. (The profilometer was towed so that approximately the same wheelpath used by the towing or test truck would be measured as required by the experiment.)

Consideration of this brief background would seem to suggest rejection of the use of power spectrum or spectral analysis as an analysis tool for examining road profile data obtained with the SD profilometer. In this paper, however, a way to avoid many of the problems in the reports mentioned previously is discussed, and some practical methods of using spectral analysis on data obtained with the SD profilometer are given. The Appendix briefly discusses spectral analysis and some problems that should be avoided when computing power spectral and coherence estimates. Accurate power spectral estimates require certain statistical assumptions about the data to be analyzed. This paper discusses the conditions imposed on road profile data to satisfy these assumptions.

STATISTICAL ASSUMPTIONS FOR SPECTRAL ANALYSIS METHODS OF ROAD PROFILE DATA

Accurate power spectral estimates of road profile data require data from a stationary Gaussian random process. An ensemble of random time functions (or a random process) is stationary if any translation of the time (or distance) origin leaves its statistical properties unchanged. Because a power spectrum may be thought of as a second-moment spectrum (see spectral analysis discussion in Appendix), its first and second moments fall under this category. The profilometer filters out all low-frequency and direct current components. Data characteristics of the first moment or mean approximately meet this definition (see also trend removal discussions in Appendix). The second moment or variance requirement is not generally satisfied. Darlington, however, has found that road profile variance is reasonably constant on newer concrete and bituminous pavements (6). The total problem of nonstationarity can be somewhat ignored by a change in viewpoint from a local to an overall or averaging effect. That is, from the overall viewpoint, an averaging of several regions of rough and smooth pavements is of primary concern. For this viewpoint, if stationarity is not met, the variance values would be too high for the smooth regions and too low for the rough regions. It should be noted that the stationarity problems are not confined to spectral analysis. They also affect slope variance or other summary statistics and must always be watched for in any such statistical analysis. In most analyses of this type, the overall viewpoint is usually assumed.

Darlington (6) provides a good discussion concerning the random characteristics of road profile data. These discussions lead to the assumption that typical highway profile data, as obtained with the SD profilometer, are usually Gaussian or near-Gaussian because they are an ensemble of random time functions and have a mean approximately equal to zero.

These statistical restrictions are not so serious as they might first appear because it has been shown (7) that the power spectral estimates are fairly robust with respect to non-Gaussian signals. Furthermore, using the combination of data from the profilometer, spectral analysis from an overall viewpoint, and trend removal techniques (7) alleviates the problems of stationarity.

Coherence analysis (Appendix) has been found to be quite useful for current road profile analysis because of its capacity to detect differences between 2 different road profiles on a frequency basis. In addition, it also has several other advantageous features that should be noted. First, Foster and Guinzy (8) found that coherence is also fairly insensitive to non-Gaussian signals. Second, a comparison was made of run-to run profiles, or right wheelpath versus left wheelpath, for the same road section, and profiles are stationary or nonstationary in the same manner. Because each coherence value is a statistic, confidence limits can be applied; and statistical tests on these coherence values can be made. It is in the use of coherence analysis that recent progress has been made at the Center for Highway Research.

Some of the problems that one must avoid in using spectral analysis are discussed in the Appendix. The next 2 sections describe how a combination of coherence and statistics has been used in detecting road-following wheel characteristics of the profilometer and differences in construction methods for laying an asphalt base material.

SD PROFILOMETER—REPLACEMENT WHEEL STUDIES

The SD profilometer (1, 2) was developed so that road profile data could be obtained at high speeds without causing undue traffic interference. A potentiometer mounted to a road-following or sensor wheel is used to detect sensor-wheel and vehicle-body displacements (high-frequency roughness). The weakest link in the overall system has been this sensor or road-following wheel for the following reasons:

1. The mechanical equipment causes most of the system troubles, at least more than the electronic equipment;
2. The usable life of these wheels is too short in relation to their high cost; and
3. Wheel bounce is not uncommon, and has been noted at speeds as low as 10 mph on relatively good roads with a PSI > 4.0.

Many of the mechanical problems mentioned can probably be solved only by use of a noncontact probe, which should also greatly enhance operation of the SD profilometer.

The limited usable life of the sensor wheel, its susceptibility to cutting, and its high cost (about $500) prompted investigations for a substitute. K. J. Law Engineers, Inc., is now selling a less expensive wheel for about $300, and recent but incomplete investigations have proved it to be acceptable, thus far, in terms of its measurement capabilities. Indications of its usable life have yet to be obtained.

Several inexpensive wheels were carefully examined and tested (e.g., in terms of balancing, construction, and visual measuring quality), and all but one were eliminated as a potential replacement wheel candidate. A test was then conducted (9) to determine whether any differences could be discerned between the standard $500 wheel delivered with the system (from now on referred to as the control wheel) and the replacement wheel candidate.

At the beginning of this experiment, the various measurement characteristics that could be used to discern possible differences were defined. Because a set of PSI prediction equations was developed (3), it was decided to use the independent variables in this set of equations as 1 group of characteristics, i.e., log slope variance and roughness index. Significant differences in these statistics would then indicate significant differences in PSI measurements. As indicated previously, these 2 variables, however, provide only 1 index for the total profile wave form. Thus, it was also decided to use coherence values between repeat runs for each frequency range as a further check on possible wheel differences. The following experiment was then designed (Fig. 1):

1. Wheel type—2 levels (control wheel and replacement wheel);
2. Roughness—3 levels (PSI values of 4.0, 2.5, and 1.7);
3. Speed—2 levels (50 mph and 20 mph); and
4. Replications—6 replications.

The analysis of variance for the log slope variance and roughness index statistics is given in Table 1. There is a significant difference only in roughness type, as expected.

From these findings, it can be concluded that the inexpensive wheel could replace the control wheel for computing PSI. Examination of the marginal means (Table 2) seems to provide further evidence to support using the relacement wheel because the marginal mean of the replacement wheel is less than that of the control wheel in the log slope variance analysis. However, just the reverse is true in the roughness index analysis. Thus, it might be suspected, particularly with the large number of degrees of freedom, that there are no significant differences between the replacement wheel and the control wheel. However, an examination using spectral analysis revealed that the characteristics of the 2 wheels had certain significant differences.

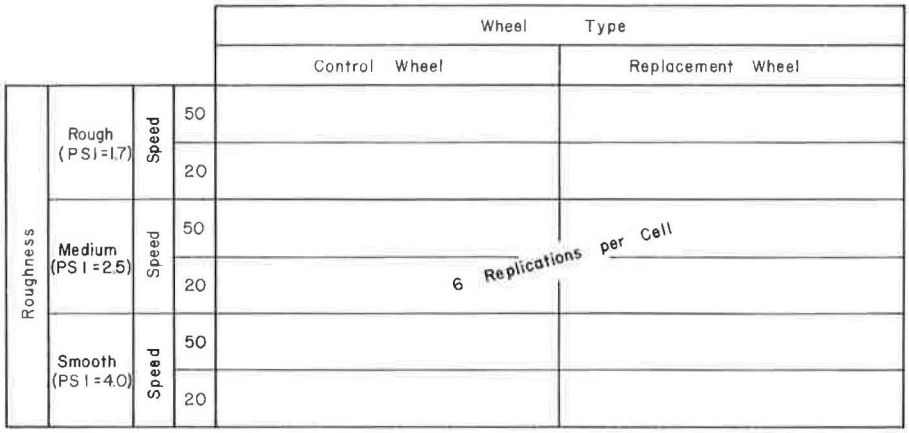

Figure 1. Experiment design for replacement wheel experiment.

For the spectral analysis, coherences between repeat runs were used as the dependent variable. Table 3 gives the general analysis of variance that was then run on all spectral frequencies. For this experiment, the frequency spectrum was divided into 128 frequency bands; hence, there were 128 analysis-of-variance runs. As noted from this table, the third-order interaction term is used as the experimental error with only 2 degrees of freedom. To get a better test, the other interaction terms were tested and pooled if not found significant at the 75 percent confidence level. This yields a possible maximum of 7 degrees of freedom as noted. In all cases, at least some terms were pooled.

A few comments should be made in regard to the assumptions of normality necessary for the analysis of variance tests. The coherence samples do not come from a normal distribution, as may be noted elsewhere (10). However, for coherence about 0.25 or more and 1.0 or less and for 10 or more degrees of freedom, these curves are near normal or at least fairly symmetrical. In addition, the F-test in the analysis of variance has been found to be fairly robust for some symmetrical distributions. The restriction of normality, however, is a stringent restriction in many cases and should be considered when conclusions are drawn about the analysis of variance results.

From the results of the coherence analysis of variance test, roughness was found significant as expected in the range from the 99 percent confidence level, in most cases, down to wavelengths of about 4.5 ft. Speed was found significant at the 97.5 percent level at the 83- and 43-ft wavelengths. This is logical because these frequencies are affected by the filtering action of the analog computer because of the 20- and 50-mph

TABLE 1

ANALYSIS OF VARIANCE FOR LOG SLOPE VARIANCE AND FOR ROUGHNESS INDEX

Source	Degrees of Freedom	Log Slope Variance		Roughness Index	
		Sums of Squares	Mean Squares	Sums of Squares	Mean Squares
Wheel type, 1	1	0.04289	0.04289	3,870.11278	3,870.11278
Roughness, 2	2	20.74885	10.37443[a]	2,997,657.24426	1,498,828.62213[a]
Speed, 3	1	0.04714	0.04714	11,002.62726	11,002.62726
12	2	0.87306	0.43653	43,553.67089	21,776.83545
13	1	0.11598	0.11598	359.85474	359.85474
23	2	0.61547	0.30773	9,182.44606	4,591.22303
123	2	0.00036	0.00018	745.69207	372.84603
Experimental error	60	8.55918	0.14265	114,013.74619	1,900.22910
Total	71	31.00293		3,180,385.39424	

[a]Significant at 99 percent confidence level.

TABLE 2

MARGINAL MEANS FOR LOG SLOPE VARIANCE AND FOR ROUGHNESS INDEX

Factor	Category	Log Slope Variance Mean	Roughness Index Mean
1	1, replacement wheel	1.96151	417.04149
	2, control wheel	2.01032	402.37841
2	1, smooth	1.22690	136.82475
	2, medium	2.35175	464.90328
	3, rough	2.37909	627.40182
3	1, 50 mph	2.01150	422.07176
	2, 20 mph	1.96033	397.34814

TABLE 3

ANALYSIS OF VARIANCE FOR COHERENCE

Source	Degrees of Freedom	
Wheel type, 1	1	
Roughness, 2	2	
Speed, 3	1	
12	2	Pool when possible
13	1	
23	2	
Error, 123	2	

speed differences. Most important, the wheel type was found significant at the 99 percent confidence level at wavelength bands corresponding to ½, 2, and 3 times the sensor wheel circumference. There was a small mean square error term corresponding to the sensor wheel circumference, but it was not found to be significant at the 90 percent confidence level. Finally, speed, roughness, and wheel type were all significant at the 99 percent confidence level at the third harmonic of the wheel circumference. From these results, it can be concluded that both wheels bounce (as was noted from the power spectral plots) but that the bounce of the replacement wheel significantly affects the variance amplitudes at harmonics of the wheel circumference and that, furthermore, this bounce is a function of roughness, type, and speed. These conclusions appear to be quite reasonable and yield more confidence to the analysis of variance assumptions.

The results of this experiment make the use of the replacement wheel tempting when PSI is computed, particularly where many runs are required over rough sections and might result in more rapid wear of the sensor wheel. On the other hand, the experiment may indicate the robustness of the log slope variance and roughness index statistics and recommend that the control wheel be used for accurate profile measurements.

Repeat runs on many different road sections reveal that, at 20-mph and greater speeds, wavelengths less than 4.5 ft (which correspond to the third harmonic of the wheel circumference) are difficult to measure twice unless perhaps the exact same wheelpath is rerun. That is, these coherence values (including their respective confidence limits) tend to drop below 0.5. This result can be accounted for by considering, first, the wheel bounce problems at these speeds and, second, the failure to drive the vehicle over the exact same wheelpath. On roads, the longer wavelengths are usually more uniform, whereas the short wavelengths tend to be more localized. In addition, the ability of the vehicle to measure the very small amplitude roughness, particularly on smooth roads, becomes a problem and in most roads cannot be detected.

An example of wheel bounce with the control wheels on a smooth section run at 10 mph is shown in Figures 2 and 3 for both left and right sensor wheels. The PSI computed for the section was 3.7. The section is located on I-45 near Buffalo, Texas. As may be noted, the spectral peaks at 0.645 cycles per foot, which is in the same frequency band as the wheel circumference. A more pronounced effect of this bounce exists for the left wheel; however, further plots indicate that this is simply a function of the road traveled.

Coherence between repeat runs seldom yields high coherence values less than about 4.5-ft wavelengths that are much greater than 9 in. or 0.75 ft (the base length is used in computing slope variance). Because wheel bounce occurs at 0.645 ft, slope variance is clearly biased by both wheel bounce and the inability of the vehicle to travel over the same wheelpath (i.e., without the special concerted effort of driving over the exact same wheelpath). Furthermore, it should be noted that much of the right portion of the spectrum is near horizontal, or that the energy in these frequencies is all about equal. This characteristic can be considered system noise (coherence is 1 measure of its randomness) and is similar to white noise, i.e., an ensemble whose spectral density is sensibly constant through the frequencies of interest. (System noise will include not only electronic noise but also the failure of the system to obtain the exact same profile

twice. This may be due to the electronic noise, the measuring limits of the profilometer, or simply the exact wheelpath not being repeated.) Slope variance is, thus, lower bounded by the system or random noise and probably measures roughness indirectly through wheel bounce in many cases of smooth sections at high speeds.

These general observations seem to further support the use of the cheaper wheel, particularly when PSI is measured and when high speeds and longer wavelength results are desired. For precise road profile measurements and short wavelengths, it would seem though that the control wheel should be used and then at a very low speed. This is consistent with the earlier comments on use of a profilometer (5).

With spectral analysis, measuring characteristics of the system for particular road types can be investigated by studying the coherence of repeat runs. Additional use of spectral analysis for determining differences between construction methods is discussed in the next section.

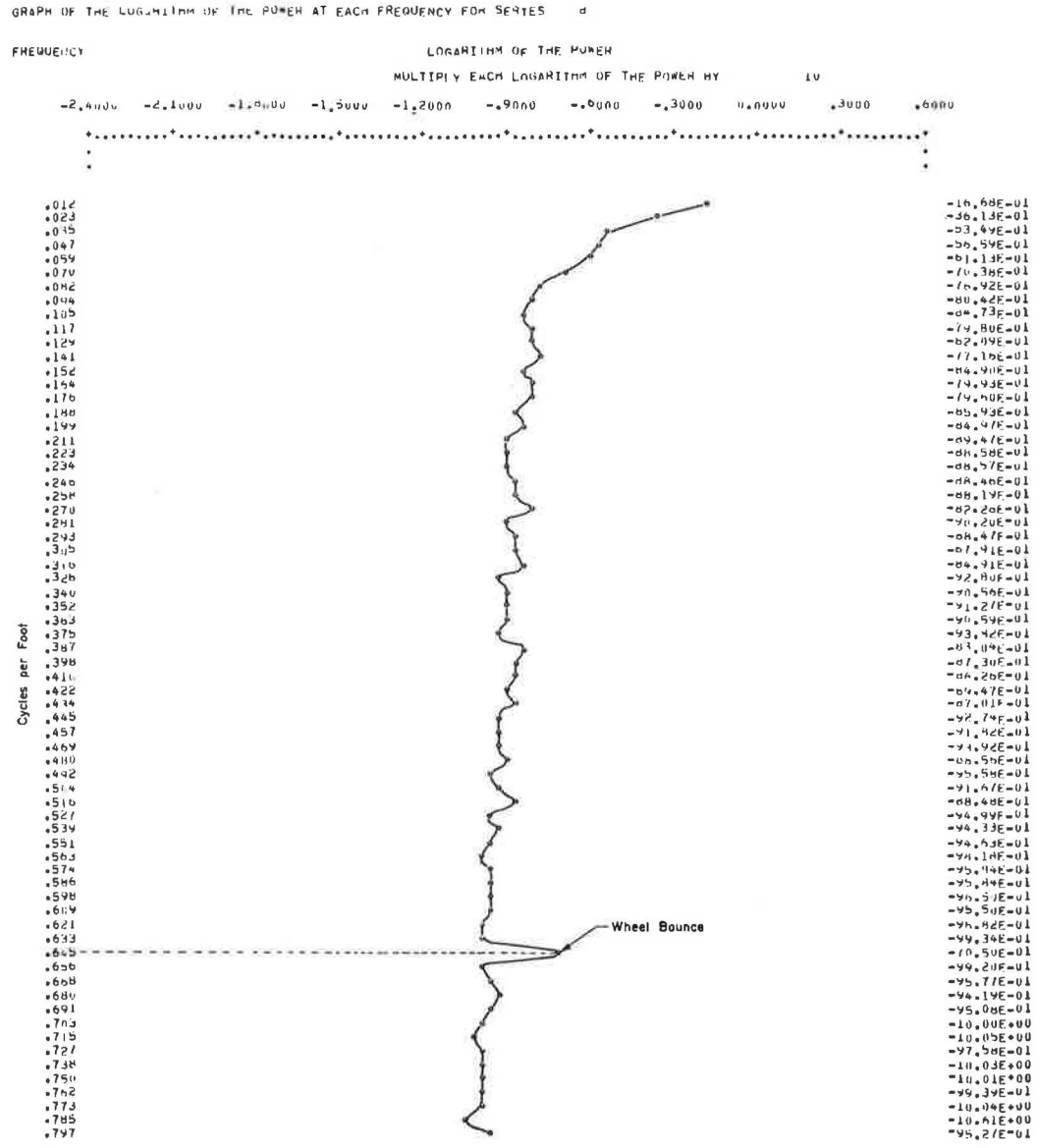

Figure 2. Power spectral plot for left wheelpath.

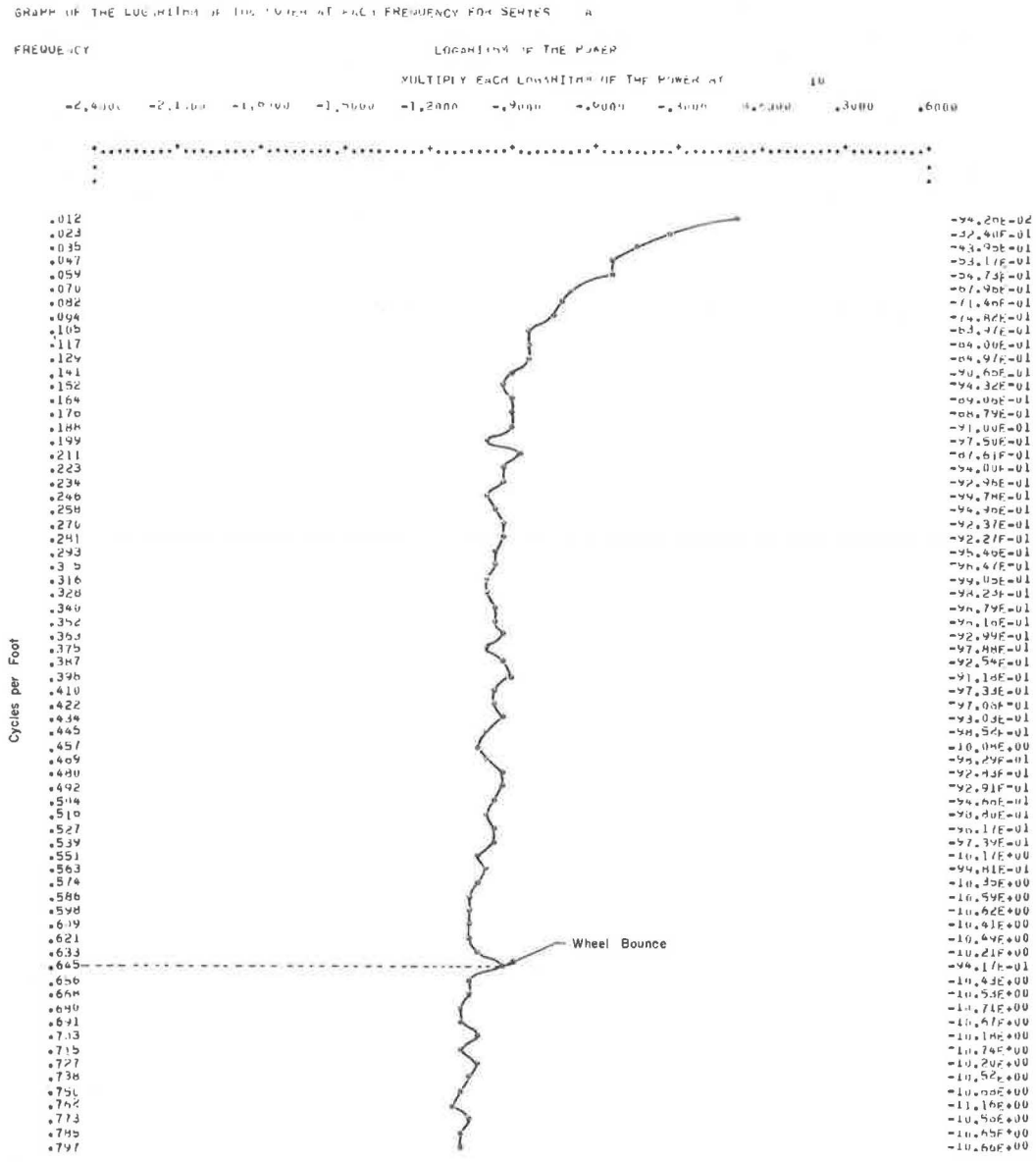

Figure 3. Power spectral plot for right wheelpath.

USE OF SPECTRAL ANALYSIS IN CONSTRUCTION CONTROL

In the preceding section, the use of spectral analysis for investigating system characteristics of the SD profilometer was discussed. This section describes some recent results in investigating differences between 2 methods of laying an asphalt base material on an Interstate highway (I-45) in Texas. The 2 methods are the traveling straightedge and the stretched-wire methods. The stretched-wire method had been used in this particular area, but, because it costs more than the traveling straightedge method, there was interest in determining whether any differences between the methods could be found and what conclusions could be drawn from these differences, if any. In the following discussions, it will be shown that differences between these methods were found (10). However, what effects these differences may yield are yet to be determined.

For the experiment, the SD profilometer was driven over 2 sample sets: 1 set was driven in July and 1 set in August for each construction method; the sample set or sections in July were geographically different from the set run in August. For each method, each sample set consisted of 4 randomly selected 1,200-ft sections of about 2 miles of road in the July runs and of about 1 mile of road in the August runs. The 2 methods were used side by side on the northbound and southbound lanes respectively.

TABLE 4

AVERAGE PSI VALUES (BASE MATERIALS)

Run Set	Traveling Straightedge	Stretched Wire
July, sets 1 and 2	3.7	3.4
August, sets 3 and 4	3.6	3.4

Note: PSI values were computed from 20-mph equation.

From the road profiles measured with the SD profilometer, slope variance, cross-slope variance, roughness index, PSI, and spectral analysis were all computed. The slope variance, cross-slope, roughness index, and PSI values all revealed that the traveling straightedge method yielded a less rough road, and, in many of the cases, this statistic was found significant at the 95 percent level. These findings would all seem to indicate that the traveling straightedge should be used not only because it costs less but also because it actually yields a less rough road. A few facts, however, should be noted. The material being laid, over which the runs were made, was only the base material; portland cement concrete is used on top of this base, and it changes the short wavelength roughness. Also, the base length used for computing slope variance (9 in.) is very sensitive to the small-amplitude, short wavelengths.

Because these small-amplitude bumps are probably taken out, or at least changed, by the concrete top layer, the use of slope variance and roughness index is not too useful as a basis for deciding that the first method is better than the second for laying an asphaltic base material. However, as far as indicating the small roughness differences, they do provide some measurements that might be useful for other problems. Table 4 gives the average PSI values for the 4 sets of runs. For smooth roads such as these, the PSI is almost completely determined from the log slope variance.

Possible uniform wavelength differences, which 1 method might consistently introduce over the other, were discerned by computing coherence between right and left wheelpaths or profiles. t-tests were then made on these values for each frequency range to see whether 1 method had higher coherence for a particular frequency. These tests indicated that there were differences at the 99 percent confidence level for wavelengths in the 24- to 34-ft range and at the 95 percent confidence level for wavelengths in the 55- to 100-ft range. Tests to ensure that the frequencies on the 2 common sets were not significantly different were made to provide further validation. These yielded the proper indications. Furthermore, the 10-mph runs yielded the same set of results for the 24- to 34-ft results. The 55- to 100-ft band could not be called significantly different at the 95 percent confidence level; however, this band has begun to be affected by analog computer filtering in the profilometer. The coherence means were higher for the 10-mph runs, as was expected. Table 5 gives the results of these runs.

These findings, of course, are dependent on how well the 2 sets of runs represent all the sections in which these 2 construction methods were used. The consistency in the 2 run sets as well as in the 10- and 20-mph runs, however, lends strong support to the measurement accuracies.

TABLE 5

WAVELENGTH ANALYSIS

Wavelength Bands (ft)	Mean Coherence at 20 mph		Notes
	Traveling Straightedge	Stretched Wire	
24 to 34, 20 mph	0.751 (0.851 at 10 mph)	0.524 (0.610 at 10 mph)	Significant at 99 percent
55 to 100, 20 mph	0.960 (0.877 at 10 mph)	0.815 (0.806 at 10 mph)	Significant at 95 percent

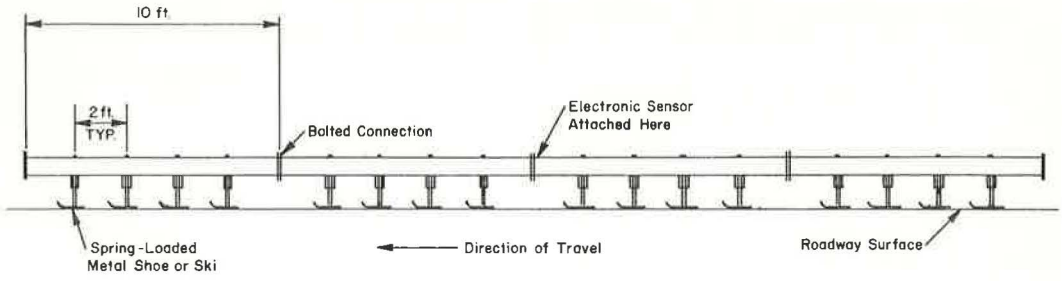

Figure 4. Longitudinal grade-reference ski.

With regard to the statistical characteristics of coherence, the coherence values were obtained at about 30 degrees of freedom from a population that is fairly symmetrical. The normality assumption of this population, however, is not now as important because of the central limit theorem, particularly with the peaks in these distributions and the number of degrees of freedom used (14 for the 20-mph runs) in the t-tests.

Further investigation of the physical characteristics of the longitudinal grade reference ski, which was used in the northbound lane where the frequency band, 24 to 34 ft, was found to be significant, revealed a definite relationship between the ski dimensions and this band. Figure 4, a schematic of the ski dimensions, shows that, although the

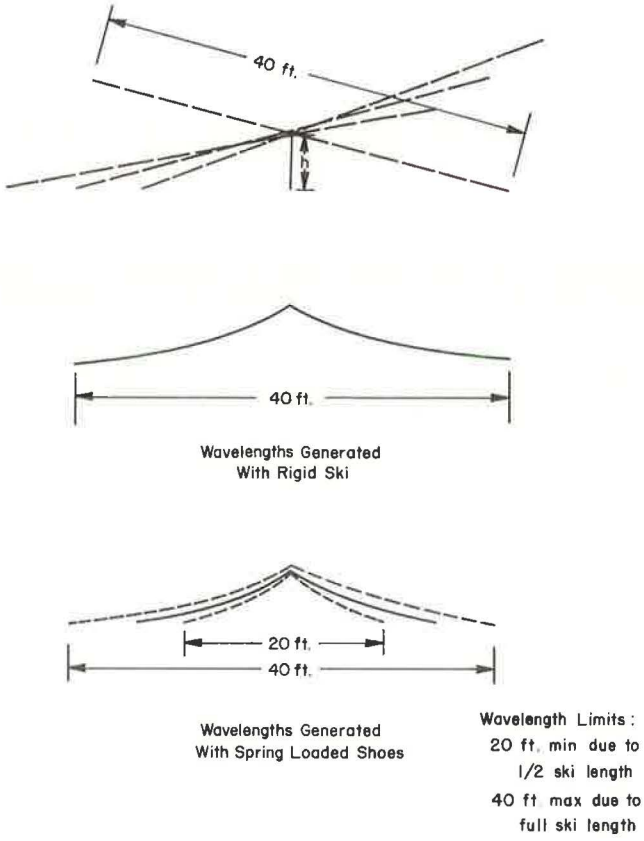

Figure 5. Wavelengths generated by longitudinal grade-reference ski transversing abrupt bump.

40-ft frame is rigid, spring-loaded metal shoes are used for roadway contact. Without these shoes, the ski would tend to generate 40-ft wavelengths, as shown in Figure 5. With the shoes, however, the ski frame deflects only when the spring for the contacting shoe reaches its maximum contraction. This tends to reduce the width of these bumps to values between 20 to 40 ft, and these most likely tend to be distributed around 30 ft or in the 24- to 34-ft wavelength bands. The other band found significant is in the vicinity of the second harmonic.

Spectral analysis was used to discern differences between roads constructed by the 2 methods. Determining such differences is 1 problem; relating these differences to pavement ridability or deterioration is another. For example, even though the traveling straightedge method might have introduced these wavelength differences, their effect on PSI might be negligible. The next section discusses a method of relating PSI to wavelengths in a road with the use of coherence.

USE OF SPECTRAL ANALYSIS FOR COMPUTING PSI

As mentioned in the previous section, identifying wavelength differences in construction methods is 1 area of concern. Determining how these differences affect pavement ridability and wear is an additional area of concern. Investigations are currently in progress to obtain a PSI prediction equation with wavelength coherences as the independent variables. The procedure being used to find such an equation involves computing coherence values for the right versus left and for repeat runs from profile data obtained during 2 large-scale rating sessions held in Texas in 1968 (3). Regression analysis will be run on the results, and PSI values will be determined from the rating panel that is used as the dependent variable. If the procedure is successful, the results of the regression analysis not only will yield a new method for computing PSI as a function of wavelengths in a road but also will provide a measure of wavelengths that are most undesirable to a rider. This information could be used as a scale for specifications in construction control. It would be much more meaningful than slope variance because wavelength bands are physically more easily taken into account than a single statistic, such as slope variance or roughness index measurement.

SUMMARY AND CONCLUSIONS

This paper discusses some uses of spectral analysis as a tool for analyzing road profile data obtained with the SD profilometer. Assumptions necessary for using spectral analyses are summarized briefly; the uses of spectral analysis in the identification of system characteristics of the SD profilometer and in the control of construction are described, and some general comments on current investigations of its use in obtaining a new PSI prediction equation are given. The Appendix briefly defines power spectrum and coherence and discusses some of the more common computational problems that must be avoided in using the FFT for spectral analysis.

Some of the more important conclusions drawn from this paper are as follows:

1. Spectral analysis is a useful tool for analyzing road profile data obtained with the SD profilometer;
2. The combined use of spectral analysis and slope variance provides conditions in which an inexpensive sensor wheel can be used in place of the much more expensive wheel delivered with the system;
3. Spectral analysis is useful for establishing measurement accuracies of the SD profilometer for the various operating speeds; and
4. Spectral analysis can be successfully used for discerning differences in various construction techniques not discernible with other common statistics such as slope variance.

It may be possible to use spectral analysis to obtain a measurement of the wavelengths that are most bothersome to the rider. Work is currently proceeding in this area.

ACKNOWLEDGMENTS

The findings discussed in this paper are those obtained from research on the feasibility of high-speed road profilometer equipment. Support is gratefully acknowledged from the Texas Highway Department and the Federal Highway Administration. The opinions, findings, and conclusions expressed in this publication are those of the authors and not necessarily those of the Federal Highway Administration.

REFERENCES

1. Spangler, E. B., and Kelly, W. J. GMR Road Profilometer, a Method for Measuring Road Profile. General Motors Research Laboratories, Warren, Mich., Publ. GMR-452, Dec. 1964.
2. Walker, R. S., Roberts, F. L., and Hudson, W. R. A Profile Measuring, Recording and Processing System. Center for Highway Research, Univ. of Texas at Austin, Res. Rept. 73-2, April 1970.
3. Roberts, F. L., and Hudson, W. R. Pavement Serviceability Equations Using the Surface Dynamics Profilometer. HRB Spec. Rept. 116, 1970, pp. 68-91.
4. Quinn, B. E., and Hagen, K. Problems Encountered in Using Elevation Power Spectra as Criteria of Pavement Condition. Highway Research Record 189, 1967, pp. 166-181.
5. Whittemore, A. P., et al. Dynamic Pavement Loads of Heavy Highway Vehicles. General Motors Corp., Research Project 15-5, GM Rept. PG-26744, Feb. 1969.
6. Darlington, J. R. Evaluation and Application Study of the General Motors Coporation Rapid Travel Profilometer. Michigan Department of State Highways, Res. Rept. R-731, April 1970.
7. Blackman, R. B., and Tukey, J. W. The Measurement of Power Spectra. Dover Publ., Inc., N.Y. 1958.
8. Foster, M. R., and Guinzy, N. J. The Coefficient of Coherence: Its Estimation and Use in Geophysical Data Processing. Geophysics, Vol. 32, No. 4, Aug. 1967, pp. 602-616.
9. Walker, R. S., Hudson, W. R., and Roberts, F. L. Development of a System for High-Speed Measurement of Pavement Roughness, Final Report. Center for Highway Research, Univ. of Texas at Austin, Res. Rept. 73-5F, Nov. 1970.
10. Walker, R. S., Center for Highway Research, Univ. of Texas at Austin, unpublished research notes, 1970.
11. Goodman, N. R. On the Joint Estimation of the Spectra, Cospectrum, and Quadrature Spectrum of a Two-Dimensional Stationary Gaussian Process. Princeton Univ., New Jersey, thesis, 1957.
12. Gossard, E. G. A Review of Power Spectrum and Cross Analysis by Digital Methods. Naval Electronics Laboratory Center, San Diego, Calif., Tech. Memo. 600.
13. Bergland, G. D. A Guided Tour of the Fast Fourier Transform. IEEE Spectrum, July 1969, pp. 41-51.
14. Roth, P. R. Digital Fourier Analysis. Hewlett-Packard Jour., June 1970, pp. 2-9.
15. Arsac, J. Fourier Transforms. Prentice-Hall, Englewood Cliffs, N.J., 1966.
16. Bracewell, R. The Fourier Transform and Its Applications. McGraw-Hill, N.Y., 1965.
17. Paponles, A. The Fourier Integral and Its Applications. McGraw-Hill, N.Y., 1962.
18. Cooley, J. W., Lewis, P. A. W., and Welch, P. D. Historical Notes on the Fast Fourier Transform. IEEE Trans., Audio and Electroacoustics, Vol. AU-15, June 1967, pp. 76-79.
19. Brigham, E. O., and Morrow, R. I. The Fast Fourier Transform. IEEE Spectrum, Vol. 4, Dec. 1967, pp. 63-70.
20. Cochran, W. T., et al. What Is the Fast Fourier Transform? IEEE Trans., Audio and Electroacoustics, Vol. AU-15, June 1967, pp. 45-55.
21. Cooley, J. W., Lewis, P. A. W., and Welch, P. D. The Fast Fourier Transform Algorithm and Its Application. IBM Corp., Res. Paper RC-1743, Feb. 1967.

22. Cooley, J. W., and Tukey, J. W. An Algorithm for the Machine Calculation of Complex Fourier Series. Mathematics of Computation, Vol. 19, April 1967, pp. 297-301.
23. Gentleman, W. M., and Sande, G. Fast Fourier Transforms—for Fun and Profit. AFIPS Proc., 1966 Fall Joint Computer Conference, Vol. 29, Washington, D.C.
24. Alexander, M. J., and Vok, C. A. Tables of the Cumulative Distribution of Sample Multiple Coherence. Rocketdyne Division of North American Aviation, Canoga Park, Calif., Res. Rept. 63-37, 9 Vols., 1963.
25. Edmonds, F. N., Jr. A Coherence Analysis of Fraunhofer-Line Fine Structure and Continuum Brightness Fluctuations Near the Center of the Solar Disk, II. Publications of the Department of Astronomy, Univ. of Texas at Austin, Vol. 1, No. 14, May 1966; reprint from Astrophysical Jour., Vol. 144, No. 2, 1966.
26. Amos, D. E., and Koopmans, L. H. Tables of the Distribution at the Coefficient of Coherence for Stationary Bivariate Gaussian Processes. Sandia Corporation, Mono. SCR-483, March 1963.

APPENDIX

BRIEF DISCUSSION OF SPECTRAL ANALYSIS

The term spectral analysis, as it is used in this paper, includes all techniques for summarizing time series functions by separating these functions into their frequency components. A detailed discussion of spectral analysis techniques such as Fourier transformations, power spectrum, and coherence is not provided here, but information on these analysis tools can be found in the listed references. A brief description of these terms is given to supplement the paper.

In 1807, Fourier discovered that an "arbitrary" function could be expressed as a linear combination of sine and cosine terms. The mathematical transformation, which performs this operation on a function to transform data from the time domain to the frequency domain, was appropriately named a Fourier transformation.

The following equation provides the formula for this transformation for a smooth function:

$$G(t) = \frac{a_0}{2} + \sum_{n=1}^{\infty} (a_n \cos nt + b_n \sin nt) \qquad (1)$$

where

$$a_n = \frac{1}{\pi} \int_{-\pi}^{\pi} f(t) \cos nt \, dt, \text{ and}$$

$$b_n = \frac{1}{\pi} \int_{-\pi}^{\pi} f(t) \sin nt \, dt \; - \pi \leq t \leq \pi.$$

Figure 6, which consists of a very simple wave form composed of only 2 sine waves, shows a simple example of this transformation. The more complicated wave forms can, of course, consist of an infinite number of these terms.

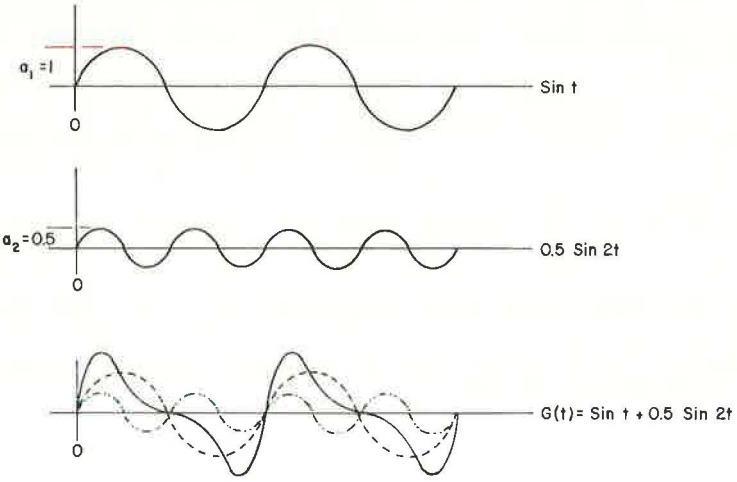

Figure 6. Wave consisting of first and second sine terms of its Fourier coefficients.

Equation 1 is one of several formulations of the Fourier transformation. Another formulation, which at first appears less meaningful, is given by

$$S(f) = \int_{-\infty}^{\infty} G(t) \times e^{-i2\pi ft} dt \tag{2}$$

$$G(t) = \int_{-\infty}^{\infty} S(f) \times e^{i2\pi ft} df \tag{3}$$

The exponential terms can be easily derived by using trigonometric identities. For road profile analysis, the function G(t) is the road profile as measured with the SD profilometer, where t is the time or distance variable.

Transforming profile data from the time or distance domain to the frequency domain is 1 form of spectral analysis. However, although this form may have certain uses, it is of limited value because of its dependence on time or distance. That is, a profile wave form of constant shape will have the same energy or variance at any 1 frequency, but the distribution of this energy or variance between the sine and cosine terms depends on the phase shift or time position of the profile wave form. The energy or variance of the profile wave form at each frequency is obtained by squaring the amplitude of each sine and cosine term for each frequency with the phase angle being obtained from the arc tan of the ratio of the amplitudes. This spectrum, consisting only of amplitude and phase angles, is referred to as the power spectrum.

The autocovariance of a function x(t) at lag λ may be given as

$$C(\lambda) = \lim_{T \to \infty} \frac{1}{T} \int_{-\frac{T}{2}}^{\frac{T}{2}} x(t) \times x(t + \lambda) dt \tag{4}$$

It can be shown that the power spectrum is also the Fourier transform of the autocovariance function, or

$$P(f) = \int_{-\infty}^{\infty} C(\lambda) \times e^{-i2\pi f\lambda} d\lambda \tag{5}$$

These equations have been discussed because use of a power spectrum as a means of analyzing road profile data may be relatively unfamiliar to some readers. From the foregoing interpretation, it can be seen that a power spectrum, so commonly used in communications engineering, geophysics, and other sciences, can also be referred to as a covariance spectrum (7). Thus, P(f)df represents the contribution to the variance of the road profile wave form from frequencies f and (f + df). A power spectrum, therefore, is another statistic, like slope variance, except that it provides a set of spectral values or variance densities for a road profile section, whereas slope variance or simple variance yields only 1 such value. It is this fact that prompted an interest in the investigation of spectral analysis as a means of providing some measure of roadway roughness.

Information on energy differences between 2 or more time series can be obtained with cross-spectral analysis. Whereas the power spectrum is the Fourier transform of the autocovariance, the cross-power spectrum is the Fourier transform of the cross-covariance function between 2 separate time signals. Coherence can be thought of as a kind of normalized cross-power spectrum where the values range from zero to one. The coherence function is defined by the following equation:

$$\partial xy = \begin{cases} \dfrac{|P_{xy}(w)|}{\sqrt{P_{xx}(w)P_{yy}(w)}} & \text{when } P_{xx}(w) \text{ and } P_{yy}(w) > 0 \\ 0 & \text{when } P_{xx}(w) \text{ and } P_{yy}(w) = 0 \end{cases} \tag{6}$$

where

$P_{xy}(w)$ = cross-power spectrum between x(t) and y(t),
$P_{xx}(w)$ = power spectrum of x(t), and
$P_{yy}(w)$ = power spectrum of y(t).

Also associated with coherence is a phase lage between x(t) and y(t).

Multiple coherence is analogous to the multiple-correlation matrix in statistics, and, just as significance levels are used in correlation analysis, confidence levels may be used in cross-spectral analysis. Goodman (11) discusses the theory and practices of cross-spectral analysis. Foster and Guinzy (8) and Gossard (12) provide good discussions of some of the relationships and uses of cross-spectral analysis.

COMPUTATIONAL PROBLEMS IN USING SPECTRAL ANALYSIS FOR ANALYZING ROAD PROFILE DATA

Some of the common problems that must be avoided if accurate measurements in spectral analysis are to be obtained are discussed here. Greater details of these problems may be found elsewhere (4, 7-23).

Aliasing

The problem of aliasing is probably the best known of the pitfalls that will be discussed. It results from the fact that high-frequency components of a time function, such as a profile signal, can imitate low frequencies if the sampling rate is too low. In Figure 7, which shows this effect, high-frequency and low-frequency signals are sharing identical sample points. Once sampled, there is no way of filtering this high-frequency imitation out of the data. The solution to the problem is to ensure that the sampling rate is at least twice as high as the highest frequency present.

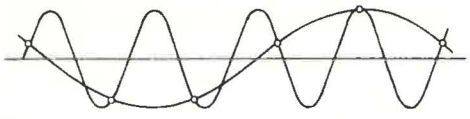

Figure 7. Aliasing effect of high-frequency wave.

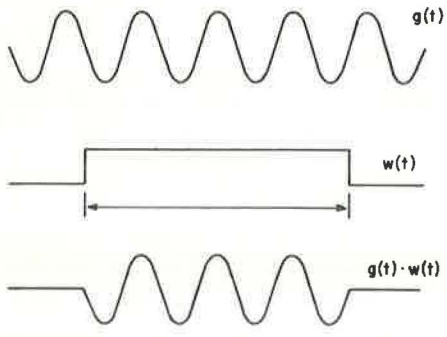

Figure 8. Rectangular data window result when finite data record is used.

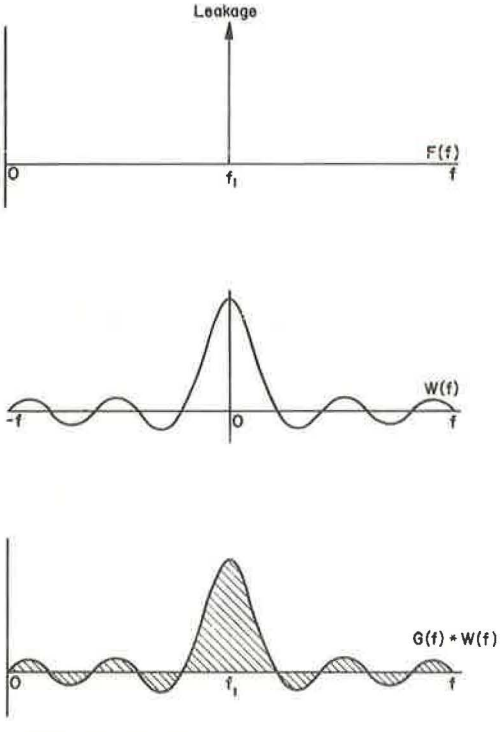

Figure 9. Results of convoluting rectangular data window with sine wave.

Leakage

The problem of leakage occurs because of the use of a road profile signal of finite length. This use may be thought of as multiplying the actual road profile signal by a rectangular data window that limits the infinite profile to finite lengths, as shown in Figure 8. Because multiplication in the time domain is equivalent to convolution in the frequency domain, the Fourier transform of the finite profile signal results in the transformed profile signal being convolved with a $\sin x/x$ function. For example, had the profile signal been a pure cosine wave, its Fourier transform would have been limited to only 1 point on the frequency axis (Fig. 9). However, because of its finite length, which is caused by the rectangular data window, the actual result is as shown in Figure 9. As a result, a loss of energy due to these side lobes occurs (Fig. 9). The problem may be alleviated by using a different type of data window, one that when transformed appears more as a rectangular function (7).

Picket-Fence Effect

Because of the multiplication of the profile signal by a finite-length data window, the effect of the FFT algorithm is similar to the use of a bank of bank-pass filters as shown in Figure 10, depicting the main lobes of the spectral window. The width of each main lobe is inversely proportional to the original profile length. To reduce this ripple distortion requires that the record length analyzed be extended by adding a set of samples identically zero before making the FFT transformation. This procedure causes an overlapping of the Fourier coefficient terms and considerably reduces the amount of ripple, as shown in Figure 10.

Trend Removal

As discussed previously, the filtering in the SD profilometer attenuates the low-frequency and direct-current components from the profile signal and, thus, yields a mean profile signal of approximately zero. It is the fact that this mean may not be identically zero that causes some distortion in the low-frequency spectral estimates. Blackman and Tukey (7) illustrate the effects on the spectral coefficients when this mean is only near zero, and, as noted, the effects can be significant. This is the reason for

their statement that it is almost always wise to use some type of trend-removal function in the spectral analysis.

Degrees of Freedom

As in all statistical analyses, a reasonable number of degrees of freedom should be used when the spectral estimates are computed. The power spectral estimate for a given frequency will vary about the population spectrum according to the chi-square distribution. The number of degrees of freedom, which is a function of the spectral window used, should then be large enough so that usable confidence limits can be obtained. In actual practice, use of 20 or more degrees of freedom has been found desirable for road profile data. The number of degrees of freedom is also extremely important in coherence analysis. Coherence quickly becomes unreliable if the number of degrees of freedom is insufficient and may even be unity if the number of degrees of freedom is too low. Too many degrees of freedom, however, can result in too low coherence values if the spectral estimates are not constant within the spectral data interval (8). [The establishment of confidence intervals on the coherence values can be made by using the tables in the paper by Quinn and Hagen (4) for up to 21 degrees of freedom. The paper by Amos and Koopmans (26) provides additional graphs and tables that can be used for obtaining confidence limits on samples with up to 200 degrees of freedom. Graphs produced by Walker provide coherence distribution data for a large variety of population coherence, degrees of freedom, and confidence limit combinations (10).]

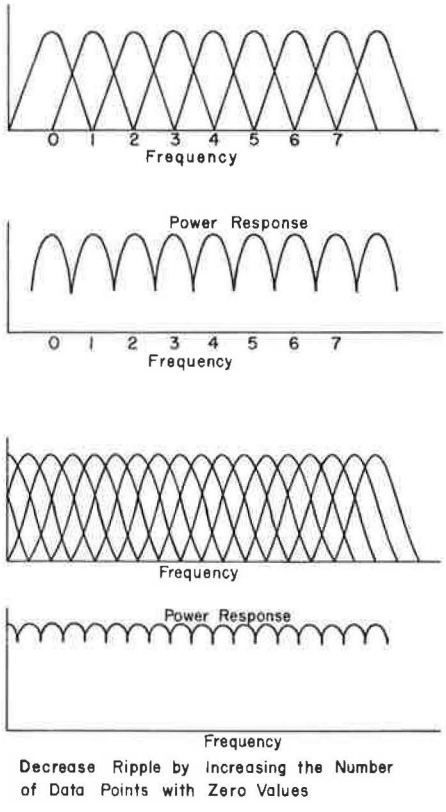

Figure 10. Picket-fence effect.

Prewhitening

Prewhitening, as defined by Blackman and Tukey (7), is the process of prefiltering the profile data so as to make the spectral density more nearly constant. This prefiltering, for example, can be used in the preceding so that more degrees of freedom can be obtained for coherence computation. Prewhitening is discussed in detail by Blackman and Tukey and in many of the listed references.